

1 **TITLE:**

2 Visual projection neurons in the *Drosophila* lobula link feature detection to distinct
3 behavioral programs

4

5 Ming Wu¹, Aljoscha Nern¹, Ryan Williamson, Mai M. Morimoto, Michael B. Reiser,
6 Gwyneth M. Card and Gerald M. Rubin

7 ¹These authors contributed equally.

8

9 **ABSTRACT:**

10 Visual projection neurons (VPNs) provide an anatomical connection between early visual
11 processing and higher brain regions. Here we characterize lobula columnar (LC) cells, a
12 class of *Drosophila* VPNs that project to distinct central brain structures called optic
13 glomeruli. We anatomically describe 22 different LC types and show that, for several
14 types, optogenetic activation in freely moving flies evokes specific behaviors. The
15 activation phenotypes of two LC types closely resemble natural avoidance behaviors
16 triggered by a visual loom. *In vivo* two-photon calcium imaging reveals that these LC
17 types respond to looming stimuli, while another type does not, but instead responds to the
18 motion of a small object. Activation of LC neurons on only one side of the brain can
19 result in attractive or aversive turning behaviors depending on the cell type. Our results
20 indicate that LC neurons convey information on the presence and location of visual
21 features relevant for specific behaviors.

22 **INTRODUCTION**

23

24 Many animals use vision to guide their interactions with the environment. Doing
25 so requires their visual systems to extract information about the presence of ethologically
26 relevant visual features from diverse and dynamic sensory landscapes. Most organisms
27 with elaborated nervous systems compartmentalize this task; in vertebrates and insects,
28 for example, visual processing begins in specialized brain regions of similar general
29 structure, called, respectively, the retina and the optic lobe (Sanes and Zipursky, 2010).
30 The signals computed in these early visual areas are then conveyed to different higher
31 order brain regions by visual projection neurons (VPNs); ultimately these signals must be
32 passed on to the neural circuits that control behaviors.

33

34 While VPNs are anatomically diverse and not necessarily closely related, their
35 unique position as output channels of early visual centers makes these neurons attractive
36 entry points for circuit-level analyses of visual processing. Studies of such neurons, for
37 example of retinal ganglion cells in vertebrates and lobula plate tangential cells in insects,
38 have provided insights into both the computations performed by the early visual system
39 and the visual information that is available to higher brain regions (Borst, 2014; Gollisch
40 and Meister, 2010). However, the relationship between signals encoded by the VPNs and
41 visual behaviors has been difficult to systematically explore in any animal. Compared to
42 photoreceptor neurons, which primarily respond to local luminance changes, VPNs can
43 show much more specialized responses, some of which have been interpreted as encoding
44 visual features directly relevant for specific behaviors, for example the presence of prey

45 (Lettvin et al., 1959) or predators (Zhang et al., 2012). Here we present anatomical,
46 behavioral and physiological analyses of Lobula Columnar (LC) neurons in *Drosophila*
47 that support such a role for this class of VPNs.

48

49 In flies, visual information is first processed in the optic lobes, which are
50 comprised of four neuropils called the lamina, medulla, lobula and lobula plate
51 (Fischbach and Dittrich, 1989; Meinertzhagen and Hanson, 1993). Each neuropil has a
52 repetitive structure of several hundred retinotopically-arranged columns that supports the
53 parallel processing of visual signals from different points in space. Neurons projecting
54 out of the optic lobes originate in the medulla, lobula and lobula plate with the majority
55 from the latter two, deeper neuropil layers. The response properties of several lobula
56 plate VPNs have been characterized in great detail, mainly through studies in larger flies
57 (Borst et al., 2010; Krapp et al., 1998). These lobula plate tangential cells (LPTCs) show
58 strongly directionally selective responses to a variety of motion stimuli and some LPTCs
59 have been proposed to function as matched filters for the complex optic flow patterns
60 associated with a fly's movements (Krapp et al., 1998). Many recent advances have also
61 revealed key components of the upstream circuitry that provides LPTCs with their
62 direction-selective response properties (reviewed in (Borst, 2014)). However, visual
63 processing of stimuli other than wide-field motion is generally much less well understood.
64 For example, flies respond to the movement, shape and position of objects (Card and
65 Dickinson, 2008b; Coen et al., 2016; Egelhaaf, 1985a; Egelhaaf, 1985b; Egelhaaf, 1985c;
66 Ernst and Heisenberg, 1999; Gotz, 1980; Liu et al., 2006; Maimon et al., 2008; Ofstad et
67 al., 2011; Reichardt and Wenking, 1969; Robie et al., 2010; Tang et al., 2004) or to

68 different wavelengths of light (Gao et al., 2008; Karuppudurai et al., 2014; Melnattur et
69 al., 2014). The neural substrates of these behaviors are largely unidentified but have often
70 been proposed to involve neurons in the lobula. A major role of the lobula in visual
71 processing is also indicated by anatomy, since the vast majority of medulla outputs
72 project to the lobula (Fischbach and Dittrich, 1989).

73

74 Of the different classes of VPNs found in the lobula, one group, the LC neurons
75 (Fischbach and Dittrich, 1989; Otsuna and Ito, 2006; Strausfeld and Okamura, 2007), has
76 received particular attention. The LC neurons are the most numerous VPNs of the lobula
77 and, as we show here, can be divided into over twenty distinct types. Anatomical
78 characteristics of typical LC neurons are illustrated in Figure 1. Each LC type comprises
79 multiple neurons of similar morphology whose individual dendritic arbors spread across
80 only part of the array of lobula columns but which, with a few exceptions, cover the
81 entire visual field as a population (Fischbach and Dittrich, 1989; Otsuna and Ito, 2006;
82 Strausfeld and Okamura, 2007) (Figure 1C,F,K). These anatomical properties contrast
83 with those of LPTCs whose large dendritic arbors vary across lobula plate columns but
84 are sufficiently stereotyped to be individually identifiable across animals. In addition to
85 their dendritic arrangements, the second anatomical hallmark of most LC neurons is the
86 convergence of their axons onto cell-type specific target regions in the central brain
87 (Otsuna and Ito, 2006; Strausfeld and Okamura, 2007). These target regions represent
88 distinct neuropil structures often referred to as “optic glomeruli” (Strausfeld, 1976;
89 Strausfeld and Okamura, 2007) (Figure 1A,B,D,E,G-I), named by analogy to the
90 similarly shaped subunits of the antenna lobes, the olfactory glomeruli (Laissue et al.,

91 1999). Similar to olfactory glomeruli, the optic glomeruli are enriched for synaptic sites
92 and can be directly visualized with general neuropil markers (Figure 1D,E) (Ito et al.,
93 2014). The most prominent of these optic glomeruli are found in the ventrolateral central
94 brain, specifically the posterior ventrolateral protocerebrum (PVLP) and the posterior
95 lateral protocerebrum (PLP) (Figure 1B). In addition, a small dorsal brain region with a
96 glomerular structure, the anterior optic tubercle (AOTu) (Figure 1B), is considered a
97 specialized optic glomerulus and also receives LC cell inputs (Otsuna and Ito, 2006;
98 Strausfeld and Okamura, 2007).

99

100 LC neurons have been proposed to encode behaviorally relevant visual features
101 (Strausfeld and Okamura, 2007), a conjecture that is largely based on the striking
102 anatomical reorganization associated with the convergence of their axons into glomeruli.
103 While the dendrites of different LC neuron types are arranged in overlapping retinotopic
104 arrays in the lobula, their synaptic termini in the central brain are grouped into discrete
105 glomeruli, most of which receive input from a single LC neuron type (Otsuna and Ito,
106 2006; Strausfeld and Okamura, 2007). The retinotopic structure of the lobula and other
107 early visual neuropils is thought to facilitate the extraction of visual features from the
108 spatiotemporal patterns of the activity of visual interneurons (ultimately going back to
109 patterns of photoreceptor activity). By contrast, the organization of LC target regions
110 into separate glomeruli, which is similar to the projection pattern of olfactory receptor
111 neurons in the antennal lobe, suggests that different cell types already encode distinct
112 features (such as the presence of specific odorants in the olfactory system) and that
113 spatial information is of secondary importance.

114 Though recent studies have begun to explore functional properties of LC
115 neurons (Aptekar et al., 2015; Mu et al., 2012), the hypothesis that LC neurons are
116 feature responsive cells remains largely untested and little is known about LC neuron
117 function in general. One limitation has been experimental access to defined LC types:
118 although several types of LC neurons have been described in *Drosophila* (Fischbach and
119 Dittrich, 1989; Otsuna and Ito, 2006), specific genetic reagents for the study of these
120 neurons were largely lacking and inputs to several prominent optic glomeruli had not
121 been identified, though candidates for new LC neuron types are, for example,
122 recognizable in images of fly brain clonal units (Ito et al., 2013).

123

124 In parallel to our work, two recently published independent studies (Costa et al.,
125 2016; Panser et al., 2016) have made use of existing image data (such as (Chiang et al.,
126 2011; Jenett et al., 2012)) to reveal additional VPN pathways from the lobula to optic
127 glomeruli. Costa et al report the identification of several new LC neuron types as one of
128 several examples of the application of a new computational method that groups similar
129 neurons using aligned brain images. Their work illustrates the potential power of these
130 computational tools but places less emphasis on the description or interpretation of
131 specific findings regarding VPN neuroanatomy. Panser et al use a different computational
132 method to identify GAL4 driver lines from the Janelia and Vienna Tiles collections
133 (Jenett et al., 2012; Kvon et al., 2014) that appear to include expression in VPN inputs to
134 optic glomeruli and use these lines to generate an anatomical map of these glomeruli.

135

136 In this study, we apply a previously established genetic intersectional approach
137 (Aso et al., 2014a; Tuthill et al., 2013) to generate highly specific split-GAL4 (Luan et al.,
138 2006; Pfeiffer et al., 2010) driver lines that target different LC types. We first use these
139 lines to provide detailed anatomical descriptions of 22 different LC types about half of
140 which had not been previously described by Otsuna and Ito (Otsuna and Ito, 2006). For
141 each type, we examine not only the position and shape of the target glomerulus but also
142 many other anatomical features (such as lateral spread and layer patterns of lobula arbors,
143 cell body positions and cell numbers), significantly extending the analyses in other
144 studies. We find that each LC type is characterized by a distinct layer distribution of
145 dendrites in the lobula and, with a few exceptions, a unique axonal output region in the
146 central brain. Comparison of these output regions with the pattern of optic glomeruli
147 indicates that most prominent glomeruli are the target regions of a specific LC type. Our
148 glomerulus map largely concurs with the results of Panser et al but is based on higher
149 resolution images that allow us to better separate adjacent glomeruli and to define the
150 target regions of two additional LC cell types. We also show that another LC type can be
151 subdivided into four anatomically and genetically defined subtypes. Independent of the
152 overall anatomical transformation associated with the convergence of LC neuron axons
153 into glomeruli (see above), LC neuron axons of a given type might either retain or discard
154 retinotopy within their target glomerulus. Potential retinotopy within optic glomeruli has
155 not been examined in detail and images with sparse labeling of LC neurons have been
156 interpreted as arguing either for or against such axonal retinotopy (Otsuna and Ito, 2006;
157 Panser et al., 2016). To further explore possible retinotopy within individual glomeruli,
158 we used multicolor stochastic labeling of individual LC neurons. In general, we did not

159 observe detectable retinotopy of LC neuron axons within a glomerulus. However, we did
160 identify a few exceptions; in particular, axonal projections of LC neurons to the AOTu
161 retain retinotopy for azimuthal positions, suggesting a specialized role of the AOTu in the
162 processing of spatial information. Stochastic labeling also allowed us to examine
163 additional anatomical features of LC cells such as dendritic arbor size and shape that can
164 not be observed at the population level. We also used our new driver lines to explore
165 behaviors associated with LC neuron activity, by examining the response of freely
166 behaving flies to optogenetic depolarization of individual LC types. In several cases such
167 activation triggers distinct, highly penetrant behavioral responses that resemble natural,
168 visually guided behaviors. In particular, using high-speed videography we show that two
169 of these evoked behaviors, flight-initiating jumping (takeoff) and backward walking,
170 resemble natural avoidance behaviors that can be elicited by a looming visual stimulus.
171 Moreover, the two LC types whose activation evokes these avoidance behaviors respond
172 to looming stimuli as assayed by two-photon calcium imaging. The encoding of looming
173 is not a feature of all LC types, as we found a third LC type to be selectively responsive
174 to small object motion. Finally, we present evidence that activation of LC neurons on
175 only one side of the brain can induce attractive or aversive turning behaviors, depending
176 on the cell type. Taken together, our anatomical and functional data suggest that each LC
177 type conveys information about the presence and at least general location of a
178 behaviorally relevant visual feature. Although details of our data suggest further
179 downstream integration of signals from different LC types, the highly penetrant
180 phenotypes we observe with activation of some LC types are consistent with a simple
181 model for the initiation of several behaviors.

182

183 **RESULTS**

184

185 **Characterization of visual projection neurons that connect the lobula with**
186 **glomerular target regions in the ipsilateral central brain**

187

188 To study and further identify LC neurons, we screened collections of GAL4
189 driver lines (Jenett et al., 2012; Kvon et al., 2014) (Barry J. Dickson, personal
190 communication). We searched for cell types that consisted of many similar cells which as
191 populations covered the entire array of visual columns in the lobula and whose axonal
192 projections converged onto single glomerulus-like regions in the ipsilateral central brain
193 (Figure 1). Other types of lobula VPNs were also identified in the screen but will not be
194 further characterized here. These included a number of additional LC-like cell types
195 which were excluded here because of the different structure or location of their target
196 regions or because their combined dendrites appeared to be restricted to lobula
197 subregions corresponding to only part of the visual field. Some examples of such cells,
198 which include the previously described LC14 (Hassan et al., 2000; Otsuna and Ito, 2006),
199 are shown in Figure 1 – figure supplement 1. In addition to neurons having dendrites in
200 the lobula, we identified columnar VPNs associated with other optic neuropils that also
201 had glomerular target regions (see Figure 1 – figure supplement 1 for an example) but we
202 excluded them from further analysis. For the cell types that met our criteria, we used the
203 split-GAL4 intersectional approach (Luan et al., 2006; Pfeiffer et al., 2010), where GAL4
204 activity is restricted to the overlap in the expression patterns of two GAL4 driver lines, to

205 generate driver lines with predominant or exclusive expression in individual LC types. In
206 combination, the split-GAL4 driver lines reported here have expression in 22 different
207 types of LC neurons. Seven of these LC types (LC4, LC6, LC9-LC13) have been
208 previously described (Fischbach and Dittrich, 1989; Otsuna and Ito, 2006). For
209 consistency, we named new LC types by extending a previously used numbering scheme
210 (Otsuna and Ito, 2006) and coordinated these names with another group that also found,
211 and very recently reported (Panser et al., 2016), several of the new LC neurons described
212 here; except for the cell types shown in Figure 1 – figure supplement 1 (LC14, LC19,
213 LC23), the gaps in the sequence of LC cell type names (LC1-LC3, LC5, LC7 and LC8)
214 are due to the naming scheme and do not correspond to known LC types not covered in
215 this study. Anatomical characteristics of the different LC neuron types are described
216 below; for genotypes of the split-GAL4 driver lines see Materials and Methods. Overall
217 expression patterns of the main split-GAL4 lines used in this study can be found in
218 Figure 2 and Figure 2 – figure supplement 1. Expression patterns of some additional lines
219 for these same cell types are shown in Figure 9 – figure supplement 1 and Figure 10 -
220 figure supplement 1. Confocal stacks of all lines can be downloaded from
221 www.janelia.org/split-GAL4. Details of which split-GAL4 driver lines and other
222 transgenes were used in individual experiments are provided in Materials and Methods.
223

224 We first present detailed anatomical studies of the LC cell types labeled by our
225 split-GAL4 driver lines (Figures 1-7). We then focus on LC neuron function (Figures 8-
226 13). To anatomically characterize LC neuron types and to confirm the identity of the LC
227 neurons labeled by each split-GAL4 driver line, we examined cell shape (Figures 2 and 3;

examples shown in Figure 1D,E,G,I) and the location and shape of target regions in the central brain (Figure 3; visualized with a presynaptic marker [HA-tagged synaptotagmin; syt-smHA]; Figure 1H shows an example) for each LC cell population. We also carried out stochastic labeling experiments to reveal the morphology of individual cells (illustrated in Figure 1J,K) and to explore the arrangements of LC neuron axon terminals relative to the retinotopic positions of their dendrites (Figure 4). Several stereotyped morphological features revealed in these experiments support the classification of LC neurons into the cell types described here: the shape and location of the target glomerulus as well as the size, shape and layer pattern of the lobula arbors; the approximate position of cell bodies; and the path followed by the axons. Anatomical features of LC neurons are summarized in a table in Supplementary file 1A. This table also includes estimates of the approximate number of cells per LC type for most LC types. We describe in detail the distribution and structure of axonal target regions of LC neurons in the central brain (Figure 3) and the layer pattern, size and shape of their dendrites (Figures 5,6 and 7) as these features provide information about the potential synaptic partners of each LC type.

243

244 **LC neurons are the main visual inputs to optic glomeruli**

245

246 We used split-GAL4 driven expression of syt-smHA to visualize presynaptic sites
247 of individual LC neuron populations in the central brain (Figure 1H). To facilitate
248 visualization of combinations of LC cell types, we aligned data collected from confocal
249 stacks of individual driver lines to a standard brain (Aso et al., 2014a). Together, the LC
250 neurons characterized in this study project to 19 distinct target regions in the ipsilateral

251 central brain (Figure 3, Movies 1 and 2). In addition to the shape and location of these
252 target regions, the axonal paths followed by LC neurons are also stereotyped with
253 individual cells of the same type showing a similar projection pattern (Figure 2 and
254 Figure 3A,D,G). To compare LC neuron target areas to the position of optic glomeruli,
255 we focused on the PVLP where several large glomeruli can be readily visualized with
256 general markers of synaptic density (Ito et al., 2014). LC neuron target regions in the
257 PVLP visualized by expression of a presynaptic marker in LC neurons closely matched
258 the glomerular neuropil pattern revealed by anti-Brp staining, which labels presynaptic
259 active zones (Wagh et al., 2006) (Figure 3B,C and Figure 3 – figure supplement 1, Movie
260 1). This result confirmed optic glomeruli as the target regions of these LC neurons and
261 identified LC input neurons for each of several glomeruli whose projection neuron inputs
262 were unknown. In particular, our data show that each of the 12 most prominent glomeruli
263 in the PVLP (or, in one case, the boundary region of PVLP and PLP) (Figure 3B,C,
264 Movie 1) is the target of one columnar VPN type from the lobula. Ten of these glomeruli
265 are the targets of typical LC cell types while two glomeruli receive inputs of neurons with
266 dendrites in both lobula and lobula plate; we refer to these LC-like cells as LPLC1 and
267 LPLC2. Similar cells have been described in other Diptera (Douglass and Strausfeld,
268 1998). Although we visually screened the expression patterns of several thousand GAL4
269 lines, we did not observe additional cases where the terminal fields of a VPN similarly
270 coincided with one of these glomeruli (as defined by anti-Brp labeling), suggesting that
271 LC neurons are the primary inputs to these structures.

272

273 The target regions of most LC cell types in the PVLP were clearly distinct with no
274 or only minimal overlap (Figure 3B,C); some glomeruli appear to overlap in the
275 projection image in Figure 3B but occupy distinct three-dimensional positions (see
276 Movies 1 and 2). In addition to projections to the large PVLP glomeruli, we also
277 characterized several LC neuron types that converged onto more posterior, often smaller
278 regions in the PVLP and PLP (Figure 3D-F, Movies 1 and 2). The target regions of these
279 additional LC cell types appeared more variable in shape and arrangement. Finally,
280 several LC neuron types project to the large subunit of the AOTu (Figure 3G-I); the
281 properties of these LC10 cells are discussed further below. In sum, our results provide a
282 high resolution map of LC neuron target regions and establish a link between the pattern
283 of glomeruli detected with general neuronal markers and the neuron projections of
284 specific LC cell types. With a few exceptions, primarily the AOTu (discussed further
285 below) and the target regions of LC25 and LC22, each glomerulus described here can be
286 uniquely identified as the target region of a single LC neuron type that appears to be the
287 major input to that glomerulus. Although other, non-columnar VPNs may also have some
288 presynaptic sites in or near these optic glomeruli, we did not observe similarly prominent
289 non-LC input neurons to these structures in our GAL4 line screen.

290

291 **Most optic glomeruli do not show obvious internal retinotopy of their LC neuron**
292 **inputs**

293 A prominent feature of LC neurons is the change in the anatomical arrangement
294 of LC neurons as they project from the lobula to the central brain. In the lobula, LC
295 neuron dendrites form parallel retinotopic arrays, whereas their synaptic termini in the

296 central brain are grouped into discrete glomeruli. However, it has not been examined in
297 detail whether any retinotopy is preserved in the glomeruli; that is, whether the positions
298 of the dendrites of individual LC neurons in the lobula and of their presynaptic terminals
299 within their target glomerulus are correlated. To directly compare the relative positions of
300 the dendrites of different LC cells of the same type in the lobula with the arrangement of
301 the presynaptic arbors of the same cells, we examined samples in which several LC cells
302 of the same type were stochastically labeled in distinct colors (Figure 4) using the
303 Multicolor FlpOut (MCFO) technique (Nern et al., 2015). These experiments revealed
304 that most individual LC neurons, with the exceptions discussed below, had branched
305 terminals that appeared to spread throughout their target glomerulus without obvious
306 spatial restriction to subregions or correlation between the distributions of their dendritic
307 arbors in the lobula and their presynaptic arbors in the glomerulus. Figure 4A-C shows
308 examples of this analysis for LC16. Qualitatively, most other LC cell types appeared
309 similar to LC16 in that they lacked any obvious preservation of retinotopy at the
310 glomerulus level; each individual cell's axonal terminal was intermingled with others,
311 featuring pre-synaptic boutons throughout the glomerulus (see Figure 4 – figure
312 supplement 1 for examples of additional LC cell types). Of course, retinotopic patterns in
313 the synaptic connections between these LC neurons and their targets that are not apparent
314 at the resolution examined here may exist. LC9 is an example of a cell type that appeared
315 to retain some retinotopy, though with very low spatial resolution, at the level of the
316 axonal terminals: terminals of single LC9 cells expanded through only part of the
317 glomerulus and their position correlated with the approximate position of the
318 corresponding dendrites in the lobula (Figure 4D-G).

319

320 **The AOTu is innervated by multiple LC cell types that preserve some retinotopy**

321

322 The most striking example of retinotopy within a glomerulus was the arrangement
323 of the terminals of the LC10 neurons that project to the AOTu (Figure 4H-M). LC10 cells
324 have branched terminals similar to other LC neurons but with limited dorso-ventral (DV)
325 spread so that individual cells did not cover the entire AOTu along this axis (Figure 4
326 I,J,L,M). In the AOTu, the relative positions of presynaptic arborizations of LC10 cells
327 along the DV axis of the AOTu largely matched the order of their dendrites along the
328 anterior-posterior (AP) axis of the lobula (Figure 4H,K), though with more overlap
329 between arbors in the AOTu compared to the lobula. By contrast, the DV positions of
330 LC10 dendrites in the lobula were not correlated with arrangements of neuronal processes
331 in the AOTu and the positions of different LC10 terminals largely overlapped along the
332 lateral-medial (LM) and AP axes of the tubercle (Figure 4I,J,L,M). LC10 cells also
333 differed in a second key respect from LC cell types innervating most other optic
334 glomeruli; consistent with previous reports (Otsuna and Ito, 2006), we found that the
335 AOTu is the target of axonal projections of several anatomically distinct LC10 subtypes.
336 Our classification of LC10 cells is mainly based on the size and layer patterns of the
337 lobula arbors of these neurons; these differences, which are predicted to reflect different
338 presynaptic inputs to these cells, are described in detail below (Figure 5F, Figure 7 –
339 figure supplement 1 and Figure 10 – figure supplement 2). Previously reported subtype
340 distinctions (Otsuna and Ito, 2006) were based on differences of the axonal path (dorsal
341 or ventral) within the AOTu, which we also observed but which do not unambiguously

342 identify the subtypes described here, and distinct lateral-medial positions of LC10
343 terminals, which we did not find evidence for; all LC10 types labeled by our driver lines
344 projected to the large medial zone (Ito et al., 2014) of the AOTu (Figure 3G-I), while
345 inputs to the lateral zone, previously interpreted as LC10C cells (Otsuna and Ito, 2006),
346 appear to be projections from the medulla (Otsuna et al., 2014; Panser et al., 2016). We
347 refer to the subtypes defined here as LC10a-LC10d (lowercase letters) to distinguish
348 them from the previously proposed LC10A-LC10C (Otsuna and Ito, 2006). Costa et. al.
349 (Costa et al., 2016) also propose several new LC10 subtypes based on computational
350 clustering of single cell data. These putative cell types are primarily defined by having
351 axonal arbors that are restricted to different positions along the DV axis of the AOTu
352 with corresponding regional patterns of their dendrites along the AP axis of the lobula.
353 Our analyses of retinotopy of LC10 neurons using subtypes specific split-GAL4 lines
354 showed that the axonal terminals of both LC10a (Figure 4H-J) and LC10d (Figure 4K-M)
355 subtypes are retinotopically distributed along the full DV axis of the AOTu, suggesting
356 that different subtypes form independent retinotopic maps that each cover the entire
357 visual field. For this reason, we believe that the clustering method of Costa et al, which
358 relied on the central brain arbors of LC cells, not their layer patterns in the lobula, led to a
359 misclassification of groups of cells of LC10 neurons at different retinotopic positions as
360 distinct cell types. In agreement with this possibility, attempts to identify GAL4 lines
361 with specific expression in such regionally restricted LC10 subtypes were largely
362 unsuccessful (Panser et al., 2016). By contrast, our split-GAL4 driver lines provide
363 genetic support for the LC10 subdivisions we describe here. In sum, within the AOTu the

364 terminals of multiple LC cell types overlap, showing clear retinotopic spatial segregation
365 along one axis.

366

367 **LC neuron processes show cell-type specific innervation patterns of lobula layers**

368

369 Just as the positions of the target glomeruli of LC neurons are indicative of the
370 spatial location of their as yet uncharacterized postsynaptic partners, the distribution of
371 LC neuron arbors across lobula layers can provide clues to the presynaptic inputs to the
372 LC cells. Similar to other optic lobe neuropils, the lobula has a distinctly stratified
373 structure (Fischbach and Dittrich, 1989; Strausfeld, 1976). To compare layer patterns
374 across samples, we used the anti-Brp reference marker (Figure 5A) to both directly
375 identify lobula strata and to enable alignment of different optic lobes to a common
376 reference. In the lobula, anti-Brp staining shows seven bands of alternating labeling
377 intensity (Figure 5A); examination of processes of identified neurons with known
378 positions in the lobula indicated that these anti-Brp strata largely correspond to the
379 previously described (Fischbach and Dittrich, 1989) lobula layers Lo1 to Lo6 (Figure 5A
380 and Figure 5 – figure supplement 1), with Lo5 represented by two anti-Brp bands of
381 different intensity. Comparison of the layer patterns of different LC cell types, each
382 visualized using a specific split-GAL4 driver line, with the anti-Brp label indicated that,
383 for a given type, layer patterns were similar throughout the lobula (Figure 5B,C) but
384 differed for cells of different types (Figure 5B-D). In some cases, differences between
385 layer patterns of different LC cell types, though consistent across samples, were small
386 (for example, between LC6 and LC16, LC4 and LC12 or LC25 and LC26) while other

387 pairs of LC cell types occupied, except for connecting neurites, entirely non-overlapping
388 sets of layers (for example, LC4/LC12/LC18 compared to LC25/LC26). In principle,
389 distinct and apparently uniform layer patterns of LC neuron populations (as shown in
390 Figure 5B-D) could still consist of multiple cell types with distinct arbor stratifications
391 that were not resolved in these images. However, for nearly all LC neuron types, we
392 found that the layer patterns of individual cells that projected to the same target
393 glomerulus were similar to each other and matched the overall layer patterns seen by
394 labeling the entire cell populations using the type-specific split-GAL4 driver lines
395 (compare LC4 and LC15 patterns in Figure 5E and D, respectively; also see Figure 7 -
396 figure supplement 1 for examples of single cell labeling of lobula dendrites for all LC cell
397 types). These results indicate that nearly all optic glomeruli receive input from a single
398 LC neuron type that can be recognized independently by either the dendritic arbor
399 stratification in the lobula or the axonal projection pattern.

400

401 As mentioned above, an exception to this apparent one-to-one correspondence
402 between LC cell types and target glomeruli were LC10 neurons projecting to the AOTu.
403 The majority of our LC10-specific split-GAL4 drivers are expressed in more than one of
404 the four LC10 subtypes. However, we identified several lines with subtype selectivity,
405 including two lines with expression in a single subtype (see Figure 10 – figure
406 supplement 2). This provides genetic support for the treatment of LC10a, LC10b, LC10c
407 and LC10d as distinct, though related, cell types.

408

409 We found that all lobula layers contain processes of at least one LC cell type,
410 although the number of types contributing to each layer varies widely. At one extreme,
411 only LC4 cells have processes in layer Lo1; by contrast, all but three LC (LC4, LC12 and
412 LC18) cell types have processes in layer Lo5. As anatomical overlap between different
413 cells is a necessary condition for synapses between them, the different layer patterns of
414 LC cells can provide clues to their potential connectivity: for example, some LC cell
415 types with Lo5 dendrites might receive inputs from Tm neurons implicated in the
416 processing of spectral information (Gao et al., 2008; Karuppudurai et al., 2014; Lin et al.,
417 2016) (Tm20, shown in Figure 5 – figure supplement 1, is an example). However, since
418 all lobula layers contain terminals of many neurons, connectivity can not be inferred
419 based on layer patterns alone, as not all the neuronal types that arborize in a shared layer
420 will be synaptic partners. In addition, the lobula arbors of some LC neurons may be not
421 only postsynaptic but also make some presynaptic contacts; we found that for several LC
422 cell types the presynaptic marker (syt-smHA) used to visualize the target regions was
423 also detectable, though much more weakly, in one or more lobula layers (Figure 5 -
424 figure supplement 2, Supplementary file 1A), suggesting that some LC neurons are also
425 presynaptic in the lobula.

426

427 **LC neurons show cell-type specific dendritic arbor sizes and shapes**

428

429 Like layer patterns, lateral dendritic spread is also a stereotyped characteristic of
430 LC neurons with functional implications. As populations, the dendrites of each of the LC
431 neuron types form retinotopic arrays that cover the entire lobula (see Figure 1C,F,K).

432 However, the lateral spread of individual LC neuron arbors in the lobula shows
433 considerable cell-type specific variation (Figure 6 and Figure 6 - figure supplement 1).
434 The lateral spread of the lobula arbors of cells of all LC types covered lobula regions
435 corresponding to several of the ~750 visual columns within each eye. The largest arbor
436 spreads were observed for LC11, estimated to be over 60 columns, (Figure 6A and
437 Supplementary file 1A) and LC25, approximately a hundred columns for some cells
438 (Figure 6 – figure supplement 1 and Supplementary file 1A). The smallest arbors were
439 those of LC10a (~10 columns; Figure 6B and Supplementary file 1A). For comparison,
440 some of the medulla inputs to the lobula have lobula arbors corresponding to ~1 visual
441 column (Figure 6D) and some lobula tangential cells span all visual columns of the lobula
442 as single cells (Figure 6E). Since most LC cell types did not show obvious retinotopy
443 within their target glomeruli, we propose that the distinct arbor spreads of different LC
444 cells determine the spatial extent over which their specific response properties are
445 computed, rather than provide retinotopic information at different spatial resolutions.

446

447 Taken together, our estimates of the number of LC cells of each type and their
448 approximate dendritic arbor spread within lobula layers suggest that the dendrites of a
449 given LC type, with the possible exception of the small arbors of LC10a, do not show a
450 strict tiling pattern but rather overlap (Supplementary file 1A). We also directly observed
451 overlap of co-labeled cells in MCFO experiments (some examples can be found in Figure
452 6 - figure supplement 1) for nearly all LC cell types (Supplementary file 1A). Overlap
453 between processes of cells of the same type is also common in the medulla; our previous

454 study (Nern et al., 2015) of Dm neurons using similar methods provides detailed
455 examples of both overlapping and strict tiling patterns of medulla neurons.

456 The morphology of single cells also revealed many additional details of LC
457 neuron arbor structure that appear to be stereotyped within cells of the same type (Figure
458 7, Figure 7 – figure supplements 1, Figure 7 – figure supplements 2 and Supplementary
459 file 1A): For example, the arbor spread, even for a single cell type, can differ between
460 layers (examples are LC11, LC12, LC17 and LC18) and dendritic processes of some cell
461 types appear to point in a specific direction relative to the main neurite (examples include
462 LC26 and LPLC2).

463 In summary, the multicolumnar arbor span (Figure 6 and Figure 6 – figure
464 supplement 1), intricate arbor shapes (Figure 7, Figure 7- figure supplements 1 and 2) and
465 diverse and, in most cases, multistratified layer patterns (Figure 5, Figure 7 – figure
466 supplements 1 and 2) of LC neurons, suggest that these neurons spatially integrate inputs
467 from multiple presynaptic cells of several types. These anatomical characteristics suggest
468 that as a whole, the population of LC cell types has the potential to encode a diversity of
469 visual stimuli, with large differences expected between distinct types.

470

471

472 **Optogenetic activation of LC neurons results in distinct behavioral responses**

473

474 What information do LC neurons provide to the central brain? As discussed in the
475 Introduction, the anatomical reorganization resulting from the convergence of LC axons
476 into largely cell-type specific glomeruli, has led to the speculation (Mu et al., 2012;

477 Strausfeld and Okamura, 2007) that the activity of members of a given LC cell type
478 primarily signals the presence of a particular behaviorally relevant visual feature rather
479 than its precise location. Thus, it is reasonable to expect that strong artificial activation of
480 an individual LC neuronal cell type might elicit a behavioral response that could provide
481 clues to the function of these neurons. To explore this possibility, we conducted an
482 optogenetic activation screen, using our LC cell-type specific split-GAL4 driver lines to
483 genetically target expression of CsChrimson, a red light-activated cation channel
484 (Klapoetke et al., 2014), to specific LC neuron populations.

485

486 We initially focused on 20 split-GAL4 driver lines, each with expression in a
487 different LC neuron type. For LC10 cells, we chose two driver lines that together
488 included all four LC10 subtypes described above. Driver line expression patterns were
489 confirmed by imaging CsChrimson-mVenus expression in flies of the same genotypes
490 used in the behavioral experiments (Figure 2 and Figure 2 – figure supplement 1). We
491 transiently depolarized these cells with a short pulse of red light in the context of two
492 independent, complementary behavioral assays (Figure 8A,B). One assay used a circular
493 arena (100 mm diameter and 3 mm high) (Aso et al., 2014b; Klapoetke et al., 2014), in
494 which groups of about 25 freely walking flies (Figure 8A and Movie 3) were subjected to
495 periodic, repeated light pulses. The second was a single-fly assay (Figure 8B, see
496 Materials and Methods) in which flies were released individually onto a small (5 mm^2)
497 open platform where they were exposed to light activation and their response recorded in
498 two views (side and bottom) at high temporal and spatial resolution, permitting analysis
499 of behaviors with greater detail. All activation experiments were carried out under

500 infrared light to permit video recording while minimizing potential activation of
501 CsChrimson by ambient light.

502

503 An overview of the screen results is presented in Figure 8C, D and in
504 Supplementary file 1B. The table in Supplementary file 1B includes some additional
505 behavioral responses that were below the 25% penetrance threshold used in Figure 8C,D.
506 The red light pulse used for optogenetic activation itself induced weak behavioral
507 responses in flies from a control driver line without detectable expression in the nervous
508 system (the “enhancerless” pBDPGAL4U, (Pfeiffer et al., 2010)). These control
509 responses (also see (Klapoetke et al., 2014)) included a slight increase in forward walking
510 speed or turning. However, we found that red light activation of CsChrimson in LC
511 neurons resulted in several phenotypes that were dramatically different from these
512 baseline responses (Movies 3-6). These phenotypes included larger increases in forward
513 walking speed or turning activity as well as three striking behaviors rarely seen in control
514 flies, which we refer to as jumping, reaching and backward walking.

515

516 We found that the relationship between LC neuron type activated and observed
517 behavior was not one-to-one. In some cases, the same behavior was elicited from
518 activation of different LC cell types. For example, five different cell types (LC4, LC6,
519 LC15, LPLC1 and LPLC2) drove highly penetrant jumping in at least one of the two
520 assays. In other cases, multiple behaviors were observed from activation of a single LC
521 neuron type. For example, LPLC2 activation elicited both jumping and backward
522 walking behaviors with about equal penetrance in the arena assay. Overall, when

523 activated, nearly half of LC neuron types (10/22) drove one of the five behaviors we
524 assessed in a majority of flies tested. Since we did not independently confirm CsChrimson
525 stimulation of LC neurons in a separate assay, we cannot exclude the possibility that the absence
526 of a clear behavioral response of some LC cell types may have been simply due to insufficient
527 activation of these neurons under our experimental conditions.

528

529 The results obtained with the two assays were largely consistent but did show
530 some differences. For example, the jumping phenotype of the LC4 and LPLC1 lines had
531 much higher penetrance in the single-fly assay than in the arena assay whereas the
532 opposite was the case for the forward walking phenotype of the LC24 split-GAL4 driver
533 (Figure 8C,D). We attribute these differences to design differences between the two
534 assays; in particular, the higher intensity and shorter duration of the red light stimulus
535 used in the single-fly assay (50 ms pulse of 3 mW/mm² compared to the 1s pulse of 94
536 uW/mm² stimulus in the arena) and the smaller area of the single-fly assay platform,
537 which limits assessment of walking and turning behaviors.

538

539 The screen results suggest that CsChrimson-mediated acute depolarization of
540 individual LC cell types can induce diverse, cell-type specific behavioral responses. To
541 confirm these phenotypes and pursue a more detailed analysis, we selected three LC
542 neuron driver lines that produced robust and highly penetrant activation phenotypes in
543 both assays: LC6 (jumping), LC10 (reaching) and LC16 (backward walking) (Figure
544 8C,D, Movies 3-6). We used the higher resolution, single-fly assay to further resolve
545 details of LC6 and LC10 phenotypes. LC16 phenotypes, which also include a distinct
546 turning component (Figure 8 – figure supplement 1A-D), were further examined in the

547 larger arena assay.

548

549 To confirm that the jumping, backward walking, and turning phenotypes could
550 not be attributed to the light response or unrelated differences in genetic background, we
551 performed further control experiments with LC6 and LC16 lines. We combined our split-
552 GAL4 driver lines with a *norpA* mutation that renders the fly blind. CsChrimson
553 activation of these lines produced the same behaviors as seen in non-*norpA* flies (Figure 9
554 and Supplementary file 1B), indicating that the behavior is not triggered by the light itself
555 (behavioral penetrance measured in genetically blind flies and experimental lines were
556 not significantly different, binomial test, $p = 0.06$ for jumping, $p = 0.10$ for backward
557 walking and $p = 0.40$ for turning). Additionally, parental lines that do not express
558 CsChrimson as well as flies reared on food without supplemental retinal show little or no
559 jumping, backward walking or turning in response to red light (mean penetrance of 0 %
560 for jumping, 7 % for backward walking and 3 % for turning) (Figure 9, Figure 9 – figure
561 supplement 2 and Supplementary file 1B). We also tested several additional, genetically
562 different, split-GAL4 driver lines with targeted LC6 or LC16 expression (Figure 9 –
563 figure supplement 1) and found that these lines produced the same, highly penetrant
564 jumping or backward walking and turning behaviors (Figure 9, Figure 9 – figure
565 supplement 2 and Supplementary file 1B; 80-100 % for jumping, 89-95 % for backward
566 walking and 29-36 % for turning). These results confirm that the distinct LC6 and LC16
567 phenotypes observed in the screen are due to the experimental activation of these cell
568 types. Furthermore, an independent thermogenetic activation screen of more than 2000
569 lines from the Janelia GAL4 collection also identified the LC6 and LC16 cell types as

570 producing the jumping and backward walking phenotypes through correlation between
571 behavior and anatomy (A. A. Robie and K. Branson, personal communication, September
572 2016). Thus, activation of specific LC neuron types can result in highly penetrant, cell-
573 type specific behavioral responses.

574

575 **LC10 subtypes have different activation behaviors**

576

577 Activation of LC10 can result in a reaching behavior (Figure 10A and Movie 6).
578 However, the two LC10 split-GAL4 driver lines we used in our screen produced different
579 activation phenotypes (Figure 8C,D and Supplementary file 1B). Unlike other LC cell
580 types, LC10 can be divided into four subtypes that each has a distinct layer pattern in the
581 lobula (Figure 5F), while projecting to the same target glomerulus (Figure 3G-I). These
582 different lobula layer patterns suggest different presynaptic inputs and, as a result,
583 different visual response properties of LC10 subtypes that may be associated with
584 different behavioral outputs. To confirm the reaching behavior observed in the screen
585 with additional LC10 driver lines and to look for possible correlations between subtype
586 expression and this behavior, we assayed a panel of 15 LC10 split-GAL4 driver lines
587 (Figure 10; Figure 10 - figure supplement 1). Upon activation, eight LC10 lines showed
588 strong reaching responses (>60 %) and six driver lines showed medium or little reaching
589 (<30 %) (Figure 10B). Consistent with possible functional differences between LC10
590 subtypes in these experiments, we found that the expression patterns of the lines with the
591 strongest reaching behavior appeared to differ from those of the other lines by having
592 denser processes in more distal lobula layers (mainly ~ Lo3 and Lo4) (Figure 10B).

593

594 To determine which of the four LC10 subtypes were included in each of the 15
595 lines used in our behavioral assay, we visualized individual LC10 cells by MCFO
596 labeling (Figure 10C, Figure 10 - figure supplement 2). Although individual LC10 cells
597 showed considerable morphological variability, nearly all labeled LC10 cells in these
598 lines could be readily classified as belonging to one of the four subtypes. This allowed us
599 to determine the presence of LC10a, b, c or d in each driver line. We found LC10a and/or
600 LC10d cells in all lines with strong reaching phenotypes (Figure 10C,D and Figure 10 –
601 figure supplement 2). These lines included one split-GAL4 driver (OL0019B, Figure 10D
602 “a only”) that appeared specific for the LC10a type and another driver (SS03822, Figure
603 10D “d only”) specific for the LC10d type. Control experiments confirmed that the
604 observed reaching behavior did not result from a simple response to light or from
605 unrelated differences in genetic background (Figure 10D and Supplementary file 1B).
606 Thus, activation of LC10a or LC10d neurons alone is sufficient to drive highly penetrant
607 reaching behavior. The lines with weaker reaching phenotypes showed labeling of LC10b
608 and LC10c cells and little or no expression in the other two LC10 subtypes, further
609 suggesting that, unlike LC10a or LC10d, LC10b and LC10c neurons only have a minor,
610 if any, role in generating the reaching behavior.

611

612

613 **LC6 and LC16 activation induce responses that resemble avoidance behaviors**

614

615 The LC10 subtypes examined above have diverse layer patterns in the lobula but
616 project to a common target region (Figure 5F and Figure 3G-I). By contrast, LC6 and
617 LC16 are examples of LC cell types that have very similar arbor stratification in the
618 lobula, but project to distinct optic glomeruli (Figure 11A,B, also see Figure 3, Figure 5
619 and Movies 1 and 2). Despite the similarity in their lobula arbors, LC6 and LC16 show
620 different, highly penetrant, activation-induced behaviors – jumping and backward
621 walking, respectively (Figure 11B and Movie 4-6). The “jumping” phenotype of LC6 is
622 reminiscent of fly takeoff, a behavior that occurs both spontaneously and in response to
623 specific visual stimuli such as a predator-mimicking loom (Card and Dickinson, 2008b).
624 To further explore this similarity, we made use of the single-fly assay that provides a
625 platform in which optogenetically triggered behaviors, such as LC6-mediated jumping,
626 and responses to specific visual stimuli can be directly compared in identical
627 experimental conditions. To visually elicit takeoff behavior, we presented flies with a
628 looming stimulus previously shown to mimic a predator’s approach and trigger fast
629 escape responses (von Reyn et al., 2014). We compared high-speed videos of these flies
630 to similar recordings of the jumping phenotype resulting from optogenetic depolarization
631 of LC6. For the flies that took off in response to the looming stimulus at 90° azimuth
632 (47/174 flies) we observed a consistent, coordinated behavioral sequence that started with
633 the fly beginning to elevate its wings, followed by rapid middle (jumping) leg extension
634 and initiation of flight as previously described (Figure 11C) (Card and Dickinson, 2008b;
635 von Reyn et al., 2014). Flies perform the same sequence when taking off voluntarily,
636 however the elevation of their wings is slower (Card and Dickinson, 2008a), resulting in
637 a significantly longer-duration takeoff sequence than those evoked by looming stimuli.

638 Strikingly, the CsChrimson-mediated LC6 depolarization not only produced a takeoff
639 with this same sequence of events (Figure 11C), but the duration of the takeoff sequence
640 was more similar to that of a looming-evoked takeoff than a voluntary one performed
641 when no stimulus was present (Figure 11D). Thus, LC6 depolarization results in a
642 behavior very closely resembling a looming-evoked escape response.

643

644 In another set of experiments, we found that backward walking is also a possible
645 response to a specific type of looming stimulus. When a fast-approaching looming
646 stimulus was presented in front of the fly at 0° azimuth, many of the flies that did not take
647 off during the observation period instead responded with a backward walking behavior
648 (174/200 flies) similar to that induced by optogenetic depolarization of LC16 (Figure
649 11E). It has been shown that backward walking can also be part of a fly's response to a
650 predator. For example, upon close encounter with a nymphal praying mantis, wild-caught
651 *Drosophila melanogaster* flies have been reported to occasionally respond with a
652 backward walking or “retreat” behavior usually followed by turning (Parigi et al., 2014).
653 We found that looming and LC16 depolarization both caused flies to move backward,
654 and they do so with similar speeds. In contrast, without a visual stimulus, flies on the
655 platform moved less, and their average movements were in a forward direction (Figure
656 11F). These comparisons show that LC6 and LC16 activation phenotypes resemble
657 typical, visually guided behaviors.

658

659 In view of these findings, we performed additional experiments to ask whether
660 silencing of LC6 or LC16 reduces the amount of takeoff or backward walking in response

661 to visual stimuli. We presented the same looming stimuli used in Figure 11 to flies that
662 expressed the inward-rectifying potassium channel Kir2.1 in LC6 or LC16 neurons and to
663 control flies (Figure 11-figure supplement 1). Neither cell type appeared to be essential
664 for the assayed behaviors: No reduction of backward walking compared to controls was
665 observed for LC16 (Figure 11- figure supplement 1C) and a reduced jump frequency
666 when blocking LC6 was apparent only for the fast loom (Figure 11- figure supplement
667 1A). However, no difference in takeoff sequence duration was observed (Figure 11-
668 figure supplement 1B). Because multiple LC neuron types show jumping or backward
669 walking responses to optogenetic stimulation (Figure 8) and non-LC cell types have also
670 been reported to contribute to looming-evoked escape (de Vries and Clandinin, 2012), the
671 simplest explanation of these results is that functional redundancy exists at the level of
672 neurons mediating looming-evoked escape.

673

674

675 **LC neurons selectively encode specific visual features**

676

677 To explore whether LC6 and LC16 encode visual features, such as looming, that
678 are sufficient to evoke jumping and backward walking (Figure 11), we investigated the
679 visual responses of these cell types using *in vivo* two-photon Ca²⁺ imaging from head-
680 fixed flies (Figure 12A). We measured calcium responses of single LC neuron types by
681 imaging from the axons within each glomerulus using an imaging plane selected to obtain
682 the largest slice through the volume of the glomerulus (Figure 12B). In agreement with
683 the anatomical results showing that retinotopy is not simply preserved in the LC6 and

684 LC16 glomeruli (Figure 4 A-C, Figure 4 – supplement 1 A-C), we observed that looming
685 stimuli evoke responses in several axons that span each glomerulus (Figure 12C). We
686 quantified the population response of these axons by integrating the calcium signals
687 within the glomerulus region.

688

689 Calcium signals integrated over each of the LC6 and LC16 glomeruli both show
690 similar increases in response to dark looming disks (Figure 12D, top row). Both cell types
691 appear similarly tuned, responding with larger calcium increments to the slower looming
692 speeds presented (Figure 12 – figure supplement 1, top row). Both cell types are selective
693 to dark looming stimuli as a looming disk that was brighter than the background did not
694 elicit large responses (Figure 12D and Figure 12 - figure supplement 1, middle row).
695 Looming stimuli provide compound visual cues, so to further test for the specificity of
696 these neurons' responses to dark looming objects, we presented a luminance-matched
697 stimulus that darkened over time with the same temporal profile as the dark looming disk,
698 but lacked any coherent edge motion. This stimulus elicited moderate responses in both
699 cell types that were significantly smaller than the dark looming disk (Figure 12D and
700 Figure 12 - figure supplement 1, bottom row; Mann-Whitney test, $p < 0.01$ for both LC6
701 and LC16), indicating their selectivity for stimuli with looming motion.

702

703 To confirm that the similar responses of LC6 and LC16 to looming stimuli were a
704 genuine property of these cells, we performed the identical experiments on an additional
705 LC neuron type. We measured the responses of LC11 (Figure 12B,C), that was selected
706 because its dendrites arborize in lobula layers that are distinct from LC6 and LC16

707 (Figure 5 and Figure 7 - figure supplement 1), and because LC11 was not found to have
708 any strong activation phenotypes across our behavioral assays (Figure 8C,D). LC11 did
709 not show calcium response changes to any of the looming-related stimuli (Figure 12D
710 and Figure 12 - figure supplement 1, black trace). However, we observed large responses
711 from LC11, when we presented simpler moving stimuli that did not contain looming
712 motion. LC11 showed large responses to a small moving object, and more moderate
713 responses to a moving bar spanning our visual display (Figure 12E). In contrast, LC6 and
714 LC16 also showed calcium responses to the small object, but these responses were
715 smaller than those to the loom stimuli, and much smaller than those of LC11 (Figure 12E,
716 Mann-Whitney test, $p < 0.01$ for both LC6 and LC16). Taken together, these results
717 demonstrate that LC6 and LC16 exhibit selectivity for slow, dark looming objects, while
718 LC11 encodes a distinct set of visual features.

719

720 **Behavioral responses to unilateral LC neuron activation**

721

722 Our results support the idea that LC cell types respond to the presence of specific
723 visual features in the environment and that the activation of several LC neuron types can
724 simulate the presence of such features, triggering appropriate behavioral responses.
725 However, during most natural visually guided behaviors, flies respond not only to the
726 general presence of a particular visual feature but also to its location. For example, flies
727 use visual cues to orient toward the far side of a gap when attempting to cross it (Pick and
728 Strauss, 2005) or toward another fly during courtship behavior (Coen et al., 2016). Flies
729 also adjust their takeoff direction relative to the azimuthal orientation of a looming

730 stimulus (Card and Dickinson, 2008b) and show a range of orientation behaviors that
731 depend on the location of objects (Aptekar et al., 2012; Bahl et al., 2013; Heisenberg and
732 Wolf, 1984; Maimon et al., 2008; Reiser and Dickinson, 2010). Such orientation
733 behaviors must depend on neural circuits that convey the spatial location of specific
734 visual features. Indeed, simultaneous activation of most or all LC neurons of a particular
735 type, as in the experiments described above, is probably rather uncommon under natural
736 conditions, and may partially explain why our activation screen revealed robust
737 phenotypes for only half of the LC cell types. Taking LC11 as an illustrative example, if
738 a function of this population is to signal the presence of a small moving object to
739 downstream circuits, then it is not surprising that activating all LC11 neurons
740 simultaneously failed to result in a coherent behavioral response. While our anatomical
741 data suggest that most LC neurons largely discard retinotopic information, the inputs
742 from the fly's two eyes remain distinct.

743 In order to provide optogenetic stimuli that, similar to many naturalistic visual
744 stimuli, differ between the two eyes, we designed a genetic approach to activate LC
745 neurons on only one side of the brain. By using a construct in which GAL4-driven
746 CsChrimson expression requires the prior removal of a transcriptional terminator, we can
747 add temporal control to the cell-type specificity provided by the split-GAL4 driver
748 (Figure 13A, and Materials and Methods). If excision of the transcriptional terminator is
749 induced for a brief time window early in development—after the precursor populations
750 for LC cells in the left and right optic lobes have been established, but before extensive
751 cell proliferation has occurred—animals can be readily obtained in which cells specific to
752 that GAL4 driver on only one side of the animal are labeled. As a stochastic method, this

753 approach also generates flies with bilateral labeling or no labeling (Figure 13B) providing
754 both positive and negative controls of identical genotype and experimental history. To
755 correlate behavioral responses with expression patterns, individual flies were tested in a
756 modified arena (see Materials and Methods) and then retrieved to examine labeling
757 patterns by histology.

758 We applied this method to two LC neuron populations, one of whose activation
759 induces an avoidance response, LC16, and the other an approach by reaching, LC10.
760 Expression patterns were scored as bilateral, unilateral (on the left or right), or no
761 labeling (Figure 13B). The behaviors of flies with either bilateral or no expression were
762 consistent with what we observed in our earlier experiments (Figures 8 and 9). Unlike
763 bilateral activation, unilateral LC16 optogenetic depolarization only rarely resulted in
764 backward walking (Figure 13B), but instead generated strong turning responses (Figure
765 13C and Movie 7). This turning behavior had a strong directional bias with turns
766 predominantly away from the activated side (Figure 13C), suggesting a directional
767 avoidance response. A possible interpretation of these results is that bilateral activation
768 might represent a large object directly ahead, resulting in backward walking, while
769 unilateral activation would mimic an object on one side of the fly, resulting in turning
770 towards the opposite side. Interestingly, unilateral activation of LC10 also caused a
771 strong turning bias, but in the opposite direction; flies predominantly made turns toward
772 the activated side and the most common LC10 activation phenotypes were now turning
773 responses rather than reaching (Figure 13C). Taken together, these data show that (1)
774 bilateral and unilateral activation of LC neurons can have different behavioral
775 consequences and (2) unilateral activation can result in either attractive or aversive

776 turning behaviors, depending on the cell type. These results suggest that LC neurons can
777 convey information on both the nature of a visual feature, by means of the differential
778 activity of different LC cell types, and its location, by the differential activation of the
779 same type in the two optic lobes.

780

781 **Discussion**

782

783 In this report we present anatomical and functional studies of lobula columnar
784 (LC) cells, prominent visual projection neurons from the lobula to target regions in the
785 central brain called optic glomeruli. Comprehensive anatomical analyses of the dendritic
786 arbors and central brain projections of LC neurons support the notion that these cells
787 encode diverse visual stimuli, distinct for each LC cell type, and convey this information
788 to cell-type specific downstream circuits. Precise genetic tools that target individual LC
789 cell types allowed us to explore the behavioral consequences of optogenetic activation of
790 these cell types. We found that activating cells of single LC neuron types was often
791 sufficient to evoke a range of coordinated behaviors in freely behaving flies. Using two-
792 photon calcium imaging from head-fixed flies, we showed that two LC cell types with
793 activation phenotypes similar to avoidance responses, selectively encode visual looming,
794 a stimulus that also evokes similar avoidance behaviors, while a third cell type responded
795 strongly to a small moving object. These results suggest that LC cell types encode visual
796 features that are relevant for specific behaviors. Activation of LC cells in only one brain
797 hemisphere can result in either an attractive or repulsive directional turning response,
798 depending on cell type. Thus which LC neuron channel is activated determines the
799 valence of the behavior, whereas comparison across the brain by two such channels of the
800 same type provides information about the location of relevant visual features.

801

802 **Distinct stratification of LC neuron dendrites and selective visual responses suggest**
803 **LC cells encode diverse, cell-type specific visual stimuli**

804

805 Anatomical properties of LC neurons have been previously described both in
806 *Drosophila* and other Diptera (Fischbach and Dittrich, 1989; Otsuna and Ito, 2006;
807 Strausfeld and Okamura, 2007). Our work extends these studies by providing a
808 comprehensive description of LC neurons in *Drosophila*, including the identification of
809 several previously unreported cell types. Further we combine these anatomical analyses
810 with the generation of highly specific genetic markers (split-GAL4 lines) for each cell
811 type. We found that each of the 22 LC types described here has morphologically distinct
812 dendritic arbors in the lobula with stereotyped arbor stratification, size and shape. As
813 observed in the medulla, where synapse-level connectomics data are available for many
814 cell types (Takemura et al., 2013), different layer patterns and arbor shapes are likely to
815 reflect differences in synaptic connectivity and neuronal computation. Arbors of LC
816 neurons are found in all lobula strata, though with large differences between layers. Only
817 LC4 (and perhaps LPLC1 and LPLC2) cells are potentially postsynaptic to neurons in the
818 most distal lobula layer, Lo1, while other strata such as Lo4 and Lo5B include processes
819 of more than half of the LC types. The presence of at least some LC dendrites in each
820 lobula layer implies that all of the about 50 different interneuron types that convey visual
821 information from the medulla, and to a lesser extent from the lobula plate, to the lobula,
822 are potentially presynaptic to some LC cells, although a far smaller number is likely
823 presynaptic to any single LC cell type. The predicted differences in the synaptic inputs to
824 different LC cell types also suggest that they will differ in their responses to visual
825 stimuli. Thus, individual LC neuron types are expected to encode specific visual stimuli,

826 while the population of all LC cell types together should signal a wide range of
827 behaviorally relevant visual features.

828

829 The visual responses of several LC cell types measured using two-photon calcium
830 imaging (Figure 12) support the expectation that different types selectively respond to
831 different visual features. The three LC neuron types examined preferentially responded to
832 distinct stimuli, with either a dark looming stimulus (LC6 and LC16) or a small moving
833 object (LC11) evoking the strongest measured responses. LC6 and LC16 showed stronger
834 responses to a dark expanding disc than to related stimuli such as an expanding bright
835 disk or a darkening stimulus that lacks the expanding motion. The reduction in the LC6
836 and LC16 responses when the edge motion is removed from the stimulus is precisely
837 what is expected of loom-sensitive neurons and is reminiscent of behavioral studies in
838 houseflies showing that darkening contrast combined with edge motion is the most
839 effective stimulus for triggering takeoffs (Holmqvist and Srinivasan, 1991). Consistent
840 with their similar responses in the imaging experiments, LC6 and LC16 have very similar
841 lobula layer patterns while LC11 has a different arbor stratification indicating that LC11
842 receives inputs from a different set of medulla cell types than LC6 and LC16.

843

844 It is likely that the selectivity for visual stimuli observed in LC neuron responses
845 is both a property of the stimulus selectivity of their inputs—some selectivity was seen
846 while imaging in the dendrites of a few LC cell types (Aptekar et al., 2015)—and specific
847 computations implemented by individual LC neuron types. In addition, cells post-
848 synaptic to the LC cells may integrate the responses of several individual LC neurons of

849 the same type to provide more robust detection of specific visual features. For example,
850 while LC6 and LC16 cells as populations are strongly excited by dark looming stimuli,
851 we currently do not know whether individual LC6 and LC16 neurons, which have
852 dendritic extents well below the maximum size of our looming stimuli, and also well
853 below the size known to elicit maximal behavioral responses (von Reyn et al., 2014),
854 show the same response properties. Our anatomical data and genetic reagents provide a
855 starting point for the additional functional and ultra-structural studies that will be required
856 to elucidate the circuit mechanisms that produce the response properties of these and
857 other LC cell types.

858

859 **LC neuron convergence and the signaling of positional information**

860

861 The suggestion that LC cells are feature-responsive neurons has been partly based
862 on the apparent dramatic reduction in retinotopy between LC neuron dendrites, which
863 have a retinotopic arrangement in the lobula, and their axons, which appear to discard this
864 spatial information as they converge onto target glomeruli (Mu et al., 2012; Strausfeld
865 and Okamura, 2007; Strausfeld et al., 2007). We extended previous analyses of LC
866 neuron arbor convergence by directly visualizing multiple single LC cells in a glomerulus
867 in the same fly (Figure 4). These experiments revealed no detectable retinotopy of LC
868 cell processes in most glomeruli even at this cellular level of resolution. It is possible that
869 the responses of individual LC cells carry information about retinotopic position; given
870 the comparatively small size of LC dendrites (the lateral spread of even the largest LC
871 cells covers less than 20% of visual columns) and the retinotopic distribution of these

872 dendrites in the lobula it would be surprising if they did not. Such retinotopic responses
873 could for example be relevant for those LC cell types that appear to have presynaptic
874 sites in the lobula and are thus likely to provide input to retinotopically organized circuits.
875 However, with the caveat that we did not examine synapse-level connectivity, for most
876 LCs the available anatomical information appears to support the view that much
877 retinotopic information is discarded at the glomerulus level. Consistent with this
878 anatomical observation, the calcium imaging experiments from single LC cell types
879 revealed visual responses to localized stimuli that could be measured throughout a cross-
880 section of the glomerulus without clear retinotopic arrangement of the responding axons
881 (Figure 12B,C). Because of the columnar nature and apparently restricted visual field of
882 the dendrites of LC neurons, the features computed by individual LC neurons are likely
883 to be well defined in subregions of the eye, with perhaps downstream circuits required to
884 integrate these locally-extracted features, as discussed above for looming. We currently
885 have little insight into how these computations are initiated in the optic glomeruli and this
886 remains an exciting area for future investigation.

887

888 Unlike the other LC neurons, we found that LC10, and to a lesser extent LC9,
889 cells retain some retinotopic information in the arrangement of their axon terminals
890 indicating that the loss of retinotopy is not a necessary consequence of axonal
891 convergence onto a glomerular target region. More specifically, we observed that the
892 order of LC10 axonal terminals in the AOTu along the DV axis matches the sequence of
893 AP positions of the corresponding dendrites in the lobula. This organization could
894 facilitate synaptic interactions of LC10 cells corresponding to different azimuthal

895 positions in the visual field with distinct target cells. Consistent with a possible general
896 role of the AOTu in processing or relaying of retinotopic information, retinotopic
897 responses have been recently been observed in the dendrites of central complex neurons
898 (Seelig and Jayaraman, 2013) that, mainly based on work in other insects (Pfeiffer and
899 Homberg, 2014; Pfeiffer et al., 2005), are thought to be synaptic targets of output neurons
900 of the lateral zone of the AOTu (Ito et al., 2014).

901

902 We found that, independent of the presence or absence of retinotopy at the
903 glomerulus level, positional information can be extracted from differential activity of LC
904 cells between the two optic lobes. We directly demonstrated this capability by genetically
905 restricting optogenetic LC neuron activation to only one optic lobe. This unilateral
906 activation evoked directional turning responses relative to the activated brain side. Thus,
907 LC neuron signaling appears to convey information on both different visual features and
908 their location. This may further extend the similarities to the antennal lobes where
909 differences in odorant receptor neuron activity between the left and right antennal lobes
910 may contribute to odorant tracking (Gaudry et al., 2013).

911

912 **Optogenetic activation of LC neurons can induce naturalistic behaviors**

913

914 We found that activation of different types of LC neurons can induce distinct
915 behaviors including jumping, reaching, wing extension, forward walking, backward
916 walking and turning. While specific activation phenotypes have been reported for a
917 variety of cell types and behaviors, many of these studies have focused on command-like

918 neurons thought to orchestrate specific motor programs (Bidaye et al., 2014; Flood et al.,
919 2013; Lima and Miesenbock, 2005; von Philipsborn et al., 2011; von Reyn et al., 2014).
920 By contrast, the activation phenotypes we report here result from the optogenetic
921 stimulation of different types of related visual projection neurons. A plausible
922 interpretation of these results is that activation of LC neurons can mimic the presence of
923 the visual features that these neurons normally respond to and thus elicits behavioral
924 responses associated with these fictive stimuli. This possibility is supported by several
925 lines of evidence from our studies of LC6 and LC16. First, optogenetic depolarization of
926 each of these cell types evokes a specific behavioral response – backward walking for
927 LC16 and jumping for LC6 – that resembles a similar natural avoidance or escape
928 behavior (Parigi et al., 2014; von Reyn et al., 2014). Second, backward walking and
929 jumping can both also be elicited by presentation of a predator-mimicking visual loom
930 (Card and Dickinson, 2008b)(and this study) and, third, in calcium imaging experiments
931 both LC16 and LC6 showed a preferential response to a similar looming stimulus
932 compared to a number of related stimuli. Although we did not explore LC10 response
933 properties, we note that LC10-activation phenotypes also show similarities to natural
934 behaviors: movements resembling the directed foreleg extension displayed during
935 activation-evoked reaching occur, for example, during gap-climbing behavior (Pick and
936 Strauss, 2005) and in aggressive fly-fly interactions (Chen et al., 2002).

937

938 Overall, the LC neuron activation phenotypes we observed suggest that the
939 encoding of visual information at the level of LC neurons is sufficiently specialized to
940 contribute to distinct behavioral responses in a cell-type dependent fashion. However,

941 patterns of LC neuron activation that produce more refined fictive stimuli than we
942 employed in the current work will be required to fully explore the LC neuron behavioral
943 repertoire. Likewise, more comprehensive physiological studies of the response
944 properties of the LC cell types will be needed.

945

946 **Further integration and processing of LC neuron signals by downstream circuits is**
947 **likely to be required to activate specific behaviors under natural conditions**

948

949 How does LC cell activation evoke specific behavioral responses? In the simplest
950 scenario, LC neuron depolarization could directly activate a single postsynaptic premotor
951 descending interneuron that would then in turn trigger the observed behavior. This
952 appears plausible in some cases: for example, activation of LC4 neurons (called ColA
953 cells in larger flies) might evoke a jumping response via activation of the Giant Fiber
954 (GF) cells, a pair of large descending neurons known to be postsynaptic to ColA
955 (Strausfeld and Bassemir, 1983) and LC4 (K. von Reyn and G.M. Card, personal
956 communication, September 2016) and which have a known role in escape behavior (von
957 Reyn et al., 2014; Wyman et al., 1984). For other LC cell types, there is currently no
958 evidence suggesting a direct connection to descending neurons. For example, candidate
959 descending neurons for the LC16 backward walking response, the moon-walker
960 descending interneurons (Bidaye et al., 2014), do not have dendrites in or near the LC16
961 glomerulus. Responses to diverse visual stimuli, some of which may derive from LC
962 neuron activity, have also been observed in higher order brain centers without direct

963 connections to LC neurons such as the central complex (Seelig and Jayaraman, 2013;
964 Weir and Dickinson, 2015).

965 Our activation experiments also provide several indications that the signaling
966 downstream of LC neurons is likely to be more complex; for example, activation of a
967 single LC cell type can give rise to multiple behaviors such as reaching, wing extension
968 and turning for LC10, or backward walking and turning for LC16. Changes of the spatial
969 pattern of LC neuron activation, as in our stochastic labeling experiments, can further
970 modify activation phenotypes. For example, unilateral LC16 activation primarily evokes
971 turning away from the location of LC16 activation, not backward walking, suggesting
972 that relative differences in LC16 activity between the two eyes can guide the direction of
973 motor output through downstream signaling. Furthermore, several different LC neuron
974 types may contribute to the same or similar behaviors, as suggested by the jumping
975 phenotypes of LC4, LC6, LC15, LPLC1 and LPLC2. Presumably, visual signals and
976 other information downstream of LC neurons are integrated to select appropriate
977 behavioral actions. Such additional processing is also suggested by cases of neurons with
978 overlapping response properties but distinct activation phenotypes such as LC6 and LC16.
979 We also note that some responses to LC neuron activation appear to be context dependent;
980 for example, we observed reduced forward walking for several LC cell types on the
981 platform of the single-fly assay that is much smaller than the arena used in the arena
982 assay (Figure 8 – figure supplement 1E and F, Supplementary file 1B).

983

984 In addition, we only examined the behavior of standing or walking flies and LC
985 neuron signaling might have different consequences depending on the behavioral state.

986 For example, looming stimuli can also elicit avoidance responses in flying flies (Muijres
987 et al., 2014; Tammero and Dickinson, 2002), but these responses differ from the takeoff
988 or retreat behaviors of walking animals. Therefore, while LC cell activity appears to
989 convey visual information that is specialized for sets of related behavioral responses, LC
990 neurons do not appear to instruct a single behavioral output.

991

992 **Several types of LC neurons may contribute to avoidance and escape circuits**

993

994 The most common activation phenotypes observed in our screen were apparent
995 avoidance responses. Furthermore, in addition to the LC cells studied here, other VPNs
996 may also contribute to avoidance behaviors (de Vries and Clandinin, 2012). This
997 predominance of avoidance phenotypes is perhaps not unexpected. Since escape
998 responses have to be fast and reliably executed under many different conditions, neurons
999 that signal features that can evoke escape may be particularly likely to show phenotypes
1000 in an activation screen. Given the importance of predator avoidance for fly survival, it
1001 appears plausible that a considerable fraction of visual output neurons might be utilized
1002 for the detection of visual threats ranging from looming to small objects (Card, 2012;
1003 Maimon et al., 2008). Furthermore, it is likely that CsChrimson-mediated depolarization
1004 of an entire population of LC neurons is more similar to the pattern of neuronal activity
1005 induced by an imminent collision, and thus responses of many individual loom-sensitive
1006 neurons, so it is not surprising that our activation screen revealed at least two looming-
1007 sensitive neuron types.

1008

1009 The escape-inducing neurons we identified could provide inputs to different
1010 escape response pathways, such as long- and short-mode escape (von Reyn et al., 2014),
1011 or act as multiple inputs to the same downstream circuits. Interestingly, neurons with
1012 avoidance-like activation phenotypes project to two separate groups of adjacent
1013 glomeruli, one in the dorsal PVLP (LC6, LC16 and also LC15) and one more ventral and
1014 medial (LC4, LPLC1 and LPLC2). This spatial organization may facilitate synaptic
1015 interactions of functionally related LC neuron types with common downstream pathways
1016 for a specific behavior. The second group is close to dendritic branches of the GF, large
1017 descending neurons required for short-mode responses in *Drosophila* and a postsynaptic
1018 partner of LC4/ColA (Strausfeld and Bassemir, 1983)(K. von Reyn and G.M. Card,
1019 personal communication, September 2016) and possibly also the two LPLC cell types.
1020 LC6 terminals do not overlap with GF dendrites and LC6 cells may play a role in the GF-
1021 independent escape pathways that have been proposed in both *Drosophila* (Fotowat et al.,
1022 2009; von Reyn et al., 2014) and housefly (Holmqvist, 1994). Parallel neuronal pathways
1023 involved in escape behaviors have been identified or postulated in both vertebrates and
1024 invertebrates (Burrows and Rowell, 1973; Fotowat and Gabbiani, 2011; Fotowat et al.,
1025 2011; Munch et al., 2009; Yilmaz and Meister, 2013), but a contribution of several
1026 identified visual projection neurons to such pathways, as suggested by our activation
1027 screen, has not been previously reported. Different visual output neurons with distinct
1028 tuning of their response properties to looming parameters such as speed, size, luminance
1029 change or edge detection might have evolved to ensure robust responses to avoid
1030 predators or collisions. It is, however, currently not known whether LPLC1, LPLC2, LC4
1031 and LC15 are indeed sensitive to looming stimuli and if so, whether their response details

1032 differ from LC16, LC6 and each other. Nevertheless, the identification of these neurons
1033 opens the possibility to examine the potential contribution of several visual pathways to
1034 avoidance behaviors.

1035

1036 LC neurons are a subset of the about a hundred VPN cell types that relay the
1037 output of optic lobe circuits to targets in the central brain. Our data strongly support
1038 existing proposals for LC cell types as feature-detecting neurons, which have been
1039 mainly based on the distinct anatomical properties of LC cells (Strausfeld and Okamura,
1040 2007). While these anatomical features distinguish LC neurons from many other VPNs,
1041 association of VPN pathways with specific behaviors is not unique to LC cell types. The
1042 notion that individual neuronal pathways are tuned for specific behavioral requirements is
1043 a prominent theme in invertebrate neuroethology, with these neurons described as
1044 ‘matched filters’ for behaviorally relevant features of the external world (Warrant, 2016;
1045 Wehner, 1987). A number of previously studied VPN pathways, outside of the LC
1046 subgroup, have been described as encoding specific behaviorally related visual stimuli. In
1047 particular, very similar to our results for LC6 and LC16, a group of tangential cells of the
1048 lobula and lobula plate (Foma-1 neurons) were found to respond to looming visual
1049 stimuli and, upon optogenetic activation, trigger escape responses (de Vries and
1050 Clandinin, 2012). And perhaps most famously, the long-studied LPTCs, such as the HS
1051 and VS cells, integrate local motion signals so as to preferentially respond to global optic
1052 flow patterns that are remarkably similar to visual motion encountered during specific
1053 behavioral movements (Hausen, 1976, 1982a, b; Krapp et al., 1998). Both our results and
1054 these findings are consistent with the idea that, at the outputs of the fly visual system, we

1055 find VPN pathways whose encoding properties are already well matched to particular fly
1056 behaviors or groups of behaviors. Matching the response properties of these deep sensory
1057 circuits to behavioral needs may be a general evolutionary solution to the challenge of
1058 dealing with the complexity of the visual world with limited resources.

1059

1060

1061 **Concluding Remarks**

1062

1063 LC neurons have long been recognized as a potential entry point for the circuit-
1064 level study of visual responses outside of the canonical motion detection pathways. We
1065 provide a comprehensive anatomical description of LC cell types and genetic reagents to
1066 facilitate such further investigations. We also show that activation of several LC cell
1067 types results in avoidance behaviors and that some of these same LC types respond to
1068 stimuli that can elicit such behaviors. Other LC neurons appear to mediate attractive
1069 behavioral responses. Our work provides a starting point for exploring the circuit
1070 mechanisms both upstream and downstream of LC neurons.

1071

1072

1073 **Legends**

1074

1075 Figure 1. Introduction to lobula columnar (LC) neurons. Schematics (A-C) and confocal
1076 images (D-K) show the lobula and adjacent parts of the visual system. (A,D,G,H)
1077 Horizontal sections. (B,E,I,J) Anterior views. (C,F,K) Cross-section views of the lobula.
1078 Some subregions of the optic lobe (Me, Medulla; Lp, Lobula plate; Lo, Lobula) and
1079 central brain (AOTu, Anterior Optic Tuber; PVLP, Posterior Ventrolateral
1080 Protocerebrum; PLP, Posterior Lateral Protocerebrum) are indicated in selected panels.
1081 Dendrites of individual LC neurons (red and blue cells in the schematics and red, blue
1082 and green cells in J,K) span only part of the visual field. As populations, the neurons of a
1083 given LC cell type cover most or all of the lobula (F), though LC neurons with regionally
1084 restricted lobula arbors also exist (e.g. LC14 (Otsuna and Ito, 2006), see Figure 1- figure
1085 supplement 1). LC neurons receive feed forward visual inputs from photoreceptors in the
1086 retina via a series of optic lobe interneurons (a few lamina neurons, in brown, and
1087 transmedullary neurons [Tm], in green are illustrated as examples in [A]). This places LC
1088 neurons at least 2-3 synapses downstream of the photoreceptors. The majority of LC
1089 neurons projects to distinct target regions in the central brain called optic glomeruli; some
1090 of these are illustrated in (A) and (B) and also visible as distinct structures in the anti-Brp
1091 pattern in the images in (D) and (E). Most optic glomeruli are located in the PVLP and
1092 the adjacent more posterior PLP. The more dorsal AOTu [illustrated in (B)] is considered
1093 a specialized optic glomerulus. For a more detailed map of optic glomeruli see Figure 3.
1094 Confocal images show either populations of neurons (D-I) or individual cells labeled
1095 using Multicolor FlpOut (MCFO) (Nern et al., 2015) (J,K). LC cell types shown are

1096 LC17 (D,G,H) and LC16 (E,F,I-K). Population labeling (D-I) was with split-GAL4
1097 driven expression of a membrane marker (green; myr::smFLAG, using pJFRC225-
1098 5XUAS-IVS-myr::smFLAG in *VK00005*) with a presynaptic marker also shown
1099 [magenta; synaptotagmin-HA, using pJFRC51-3XUAS-IVS-syt::smHA in *su(Hw)attP1*]
1100 in (D,E) and by itself in (H). A neuropil marker (anti-Brp) is included in grey in (D-F,K)
1101 and neuropil regions are also in grey in the schematics. Images in (D,E,G-J) were
1102 generated using brains that were computationally aligned to a template brain using the
1103 anti-Brp pattern as reference. The anti-Brp pattern in (D,E) is that of the standard brain
1104 used for alignment. Images in (D-K) show projection images of different views of three-
1105 dimensional image stacks; these were generated in either Fiji (<http://fiji.sc/>) (D,E,G-J) or
1106 Vaa3D (Peng et al., 2010) (F,K). Scale bars represent 20 μ m.

1107

1108 Figure 1- figure supplement 1. Examples of additional LC cell types and similar neurons.
1109 These cell types were not selected for further analyses in this study since they did not
1110 project to glomerular target regions in the ventrolateral central brain, covered only part of
1111 the lobula as cell populations or are VPNs of a different optic lobe region. (A,B) LC14
1112 cells, which project to the contralateral lobula, have been previously described (Hassan et
1113 al., 2000; Otsuna and Ito, 2006). LC14 is the name used by Otsuna and Ito; some closely
1114 related cells, here named LC14b, project to the contralateral medulla in addition to the
1115 lobula (Hassan et al., 2000; Langen et al., 2013). LC19 (C) and LC23 (D) are newly
1116 identified cell types that project to the contralateral (LC19) or both the ipsi- and
1117 contralateral (LC23) central brain. LC19 and LC23 neurons have cell bodies in the cell
1118 body rind between optic lobe and central brain near the dorsal tip of the lobula neuropile.

1119 LC19 arbors in the lobula are located mainly in layers Lo5 and Lo6, those of LC23
1120 neurons primarily in layers Lo2 and Lo4 (see Figure 5 – figure supplement 1 for details
1121 of lobula stratification). LC19 processes are present across the entire lobula; those of
1122 LC23 appear to cover only the anterior, not the posterior lobula. Images show projection
1123 views (generated in Vaa3D) of MCFO labeled neurons together with the anti-Brp
1124 neuropil marker (grey). (E) An example of a columnar lobula plate VPN (LPC1) also
1125 identified by others (Panser et al., 2016). LPC1 cells have cell bodies in the lobula plate
1126 cortex. Their processes in the lobula plate are mainly in lobula plate layer Lp2. (A), (B)
1127 and (C) show multiple cells; (D) and (E) segmented single cells. Scale bar represents 50
1128 μ m.

1129

1130 Figure 2. Expression patterns of LC neuron split-GAL4 lines. Split-GAL4 driven -
1131 expression of 20xUAS-CsChrimson-mVenus (insertion in *attP18*; visualized using anti-
1132 GFP antibody labeling; green) and a neuropil marker (anti-Brp, magenta) are shown.
1133 Genotypes are identical to those used in the behavioral experiments in Figure 8. Some
1134 adjustments of brightness and contrast of individual samples were made. For each driver
1135 line (but not across different lines), adjustments and microscope settings were identical
1136 for the brain shown in this Figure and the corresponding ventral nerve cord (VNC) shown
1137 in Figure 2 – figure supplement 1. Images in this and other Figures with CsChrimson
1138 expression patterns are representative of 2-5 brains and 2-3 VNCs imaged for each split-
1139 GAL4 line. Scale bar represents 50 μ m. Original confocal stacks are available from
1140 www.janelia.org/split-GAL4.

1141

1142 Figure 2 - figure supplement 1. VNC expression patterns of the corresponding brains
1143 shown in Figure 2. Imaging parameters and brightness or contrast adjustments were
1144 identical for each brain/VNC pair. Scale bar represents 50 μ m. Original confocal stacks
1145 are available from www.janelia.org/split-GAL4.

1146

1147 Figure 3. LC neuron terminals in the central brain are organized into distinct neuropil
1148 structures. (A) Illustration of the projection patterns of 12 LC cell types that project to
1149 major optic glomeruli in the PVLP (or in the PVLP/PLP boundary region). Image is a
1150 substack maximum intensity projection of a composite image stack generated from 12
1151 computationally aligned image stacks (one for each cell type). Images were manually
1152 segmented to exclude background and some off-target cell types. Unedited pre-alignment
1153 stacks are available from www.janelia.org/split-GAL4. For details of genotypes see
1154 Supplementary File 1D. (B,C) Target regions of the LC neurons shown in (A) match the
1155 optic glomeruli pattern in the PVLP. Target regions of different LC cell types were
1156 labeled by split-GAL4 driven expression of a presynaptic marker (pJFRC51-3XUAS-
1157 IVS-syt::smHA in *su(Hw)attP1*, detected using anti-HA antibody labeling). Images for
1158 different cell types were edited and combined as described above. The anti-Brp pattern of
1159 the standard brain used for alignment is shown in grey. (C) Pattern of optic glomeruli
1160 revealed by anti-Brp labeling. Image is the same as the anti-Brp channel of the overlay
1161 shown in (B). Note the close correspondence of the presynaptic terminals of LC cell
1162 populations and optic glomeruli. Asterisk marks a large synapse rich (based on anti-Brp

labeling) glomerular structure in the PLP that appears to be the target of several columnar VPNs that were not included here since we considered them to be primarily associated with the lobula plate, not the lobula (though some have lobula branches). As an example, one cell of one such type (LPC1) is shown in Figure 1- figure supplement 1E. LPC1 was also identified by (Panser et al., 2016). (D-F) Overlays generated as in (A) and (B) showing the projection patterns (D) and target regions (E,F) of additional LC neurons with terminals in the posterior PVLP and in the PLP. LC24, LC25 and LC26 projected to locations close to those of LC15, LC6 and LC16 but slightly more posterior and might also slightly overlap with each other. In particular, LC25 was unusual in that its terminals spread along the surface of, and perhaps partly overlapped with, the LC15 target region and other adjacent glomeruli (E and Figure 3 – figure supplement 1). Similarly, part of the boundary of the LC22 target region, as visualized by synaptic marker expression in LC22 cells, was less well defined than the boundaries of most other glomeruli (F). The LC22 glomerulus also appears to overlap with the target region of a second columnar VPN: stochastic labeling experiments revealed an additional LPLC-like cell type (distinct from LPLC1 and LPLC2 and tentatively named LPLC4 in agreement with (Panser et al., 2016)) that projects to the same approximate location as LC22. While we have yet to generate specific split-GAL4 drivers for this additional LPLC cell type and therefore did not further characterize these neurons here, their overlap with LC22 terminals was directly confirmed by co-labeling of single cells of both types in the same specimen (Figure 3 – figure supplement 2). (G-I) LC10 neurons project to the large subunit of the AOTu. Overlays (generated as described above) showing cell shapes (G) and presynaptic sites (H) of LC10 cells labeled by two different split-GAL4 driver lines. LC10 neurons

1186 showed two distinct general projection paths with axons entering the large subunit of the
1187 AOTu from both dorsally and ventrally (magenta cells) or only from ventrally (green
1188 cells), in agreement with previous findings suggesting the existence of LC10 subtypes
1189 (Otsuna and Ito, 2006). (I) Anti-Brp reference pattern alone. The LC10 terminals are in a
1190 distinct large subcompartment (white bracket) of the AOTu. The AOTu also includes
1191 smaller subunits adjacent to this LC10 target region. Scale bars represent 30 μ m (A,G,I),
1192 20 μ m (B,E) or 50 μ m (D).

1193

1194 Figure 3 – figure supplement 1. Presynaptic marker expression in individual LC cell
1195 types. Single confocal sections are shown. Images were rotated to show similar views.
1196 The anti-Brp reference pattern (grey) and the presynaptic marker (syt-smHA, magenta)
1197 are shown. The white appearance of the LC12 glomerulus is due to cross-talk between
1198 different labeling channels that occurred in some samples (see Materials and Methods).
1199 Genotypes are the same as in the images used for the overlays in Figure 3. Many LC
1200 types also show some syt-smHA labeling in the lobula; examples of this are shown in
1201 Figure 5 - figure supplement 2 and additional cases included in Supplementary file 1A.
1202 Scale bar represents 20 μ m.

1203 Figure 3 – figure supplement 2. A second type of columnar VPN projects to the LC22
1204 target region. Main image and inset show two views along approximately orthogonal
1205 axes of MCFO labeled LC22 (green) and LPLC4 (magenta) cells generated using a
1206 GAL4 driver line (R11C10) with expression in both cell types. The layer pattern of
1207 LPLC4 dendrites is different from both LPLC1 and LPLC2 (see Figure 5 and Figure 7 –

1208 figure supplement 2). Images show reoriented substack projection views generated using
1209 Vaa3D. Scale bar represents 20 μ m.

1210

1211 Figure 4. Multicolor stochastic labeling reveals differences in the arrangement of the
1212 terminal arbors of different LC types within their target glomerulus. (A-C) LC16. (A)
1213 Position of the dendrites of three LC16 cells in the lobula in a layer cross-section view.
1214 Each cell occupies a distinct position along the long (DV) and short (AP) axes of the
1215 lobula (axes shown as dotted white lines). By contrast, within the target glomerulus (B,C;
1216 two roughly orthogonal views are shown) the arbors of the same cells are intermingled
1217 without an obvious correlation to the retinotopic pattern in the lobula. Most other LC
1218 types appeared similar to LC16; additional examples are shown in Figure 4 – figure
1219 supplement 1. (D-G) LC9. Most LC9 cells have presynaptic arbors that spread through
1220 more than one half of the glomerulus but do not fill it completely (F,G). Comparison of
1221 the approximate positions of arbors of individual LC9 cells in the glomerulus (F,G) with
1222 the AP positions of their dendrites in the lobula (D,E) suggests some retinotopy within
1223 the glomerulus, though with very low spatial resolution: For example, out of 57
1224 examined LC9 cells, all of the cells (27/27) with axon terminals in the anterior-ventral tip
1225 of the glomerulus (such as the green cell in (F) and both cells in (G)) also had dendrites in
1226 the posterior half of the lobula while this was the case for only a few of the remaining
1227 LC9 cells (6/30). (H-M) LC10. The relative order of LC10a (H-J) and LC10d (K-M)
1228 terminals along the DV axis of the AOTu (shown in two orthogonal views, I,J for LC10a
1229 and L,M for LC10d) matches the order along the AP axis of the lobula (H for LC10a and
1230 K for LC10d). Individual cells were labeled using MCFO. Reconstructed views of

1231 reoriented subtstacks generated in Vaa3D are shown. For both LC10a and LC10d, similar
1232 results were observed for LC10 cells from five optic lobes, each with at least three
1233 labeled cells. Analyses of MCFO-labeled LC10b (36 cells from 18 brains) and LC10c (33
1234 cells from 17 brains) single cells also showed an approximate correspondence between
1235 AP positions of dendrites in the lobula and DV positions of axonal arbors in the AOTu.
1236 LC10b cells also showed considerable variation in their lateral-medial spread within the
1237 medial zone of the AOTu but further analyses will be required to explore possible
1238 correlations between these differences and arbor positions in the lobula. Scale bars
1239 represent 20 μ m (A,D,E,H,K) or 10 μ m (C,F,G,I,L).

1240 Figure 4 - figure supplement 1. Terminal arbor arrangements of additional LC cell types.
1241 (A-C) LC6, (D-F) LC11, (G-I) LC13, (J-L) LC12, (M-O) LC18, (P-R) LPLC2.
1242 Substantial overlap of the arbors of co-labeled single cells in their target regions was also
1243 observed for the remaining LC cell types (at least two brains with two or more labeled
1244 cells were examined for each cell type). While there are occasional differences between
1245 the spread of single cells of the same type within their target glomerulus (e.g. the LC6
1246 cells in (B) do not all extend to the lateral tip of the glomerulus), we did not find obvious
1247 correlations between such differences and these cell's retinotopic positions in the lobula.
1248 Lobula cross-section views and two orthogonal views of the target glomerulus are
1249 displayed as in Figure 4. Scale bars represent 20 μ m (A) or 10 μ m (C).

1250

1251 Figure 5. Layer specific arborizations of LC neurons in the lobula. (A) Anti-Brp neuropil
1252 marker shows bands of different intensity in the lobula that can serve as approximate

1253 markers of layer boundaries. The image is a maximum intensity projection through 10
1254 adjacent sections (0.38 μ m spacing) of the reference channel of the standard brain used
1255 for alignments. Approximate layer boundaries are indicated. Layer boundaries were
1256 defined by positions of known cell types and closely match the anti-Brp pattern (see
1257 Figure 5 – figure supplement 1). Lo5 was divided into two sublayers based on the anti-
1258 Brp pattern. Further subdivisions of strata based on positions of arbors of different cell
1259 types would be possible but were not applied here. (B,C) Layer patterns of LC6 (B) and
1260 LC12 (C). Split-GAL4 expression of a membrane marker is shown in green. Images were
1261 aligned to a standard brain using the anti-Brp pattern (shown in grey). Images are
1262 maximum intensity projections through the same series of sections of brains aligned to
1263 the same template as in (A). Approximate layer boundaries are marked with white lines.
1264 (D) Layer patterns of the remaining LC cell types (except LC10 neurons). Projections
1265 were generated as in (B,C) but are shown without the anti-Brp pattern. All layers, but
1266 only a portion of the lobula are shown. Schematics in (B-F) indicate innervated layers as
1267 filled circles; black circles represent more extensive arborizations than grey circles. Note
1268 that these simplified schematics do not capture some details of the layer patterns (such as
1269 sublayer patterns). Additional description of layer patterns can be found in
1270 Supplementary file 1A. (E) Single cell layer patterns are consistent with layer patterns
1271 seen at the population level. LC4 and LC15 are shown as examples. Additional single cell
1272 images can be found in Figure 7 – figure supplement 1. (F) Layer patterns of LC10
1273 subtypes. LC10b and LC10d cells have similar layer patterns but differ in other aspects
1274 such as arbor size (LC10b arbors in the lobula are larger). Additional examples of MCFO
1275 labeled LC10 cells of different subtypes can be found in Figure 7 – figure supplement 1

1276 and Figure 10 - figure supplement 2. Images in (E,F) were manually matched to the layer
1277 markers using the anti-Brp pattern. Scale of some images was slightly adjusted to
1278 compensate for varying depth of the lobula. Scale bars represent 20 μ m (A, also applies
1279 to B and C) or 10 μ m (D,E; scale bar in E also applies to F).

1280 Figure 5 - figure supplement 1. Layer positions of arbors of known cell types. Lobula
1281 terminals of MCFO labeled T5, Tm9, Tm4, Tm3 and Tm20 cells (Fischbach and Dittrich,
1282 1989) are shown. Anti-Brp pattern is in grey. Layer boundaries are marked with white
1283 lines. Golgi studies (Fischbach and Dittrich, 1989) have described T5 and Tm9 in Lo1,
1284 Tm4 and Tm3 proximal terminals in Lo4 near the boundary of Lo5, and Tm20 terminals
1285 in Lo5 near the boundary of Lo6. Tm4 and Tm3 also have apparent presynaptic
1286 varicosities in Lo2 (both) and Lo1 (Tm4). These cell types therefore can be used to
1287 identify the approximate boundaries of all six lobula strata. Further division of Lo5 into
1288 two sublayers is suggested by the anti-Brp pattern and supported by the differential
1289 presence of arbors of several neuronal cell types in these sublayers (compare for example,
1290 LC20 and LC25 in Figure 5D). Images show reoriented substack projection views
1291 generated using Vaa3D. Scale bar represents 10 μ m.

1292

1293 Figure 5 - figure supplement 2. Potential presynaptic sites of LC neurons in the lobula.
1294 In addition to the target glomerulus in the central brain (see Figure 3 and Figure 3 –
1295 figure supplement 1), split-GAL4 driven pJFRC51-3XUAS-IVS-syt::smHA in
1296 *su(Hw)attP1* expression also resulted in labeling in the lobula in several LC cell types.
1297 Single confocal sections with anti-Brp in grey, syt-smHA in magenta and/or a membrane

1298 marker (pJFRC225-5XUAS-IVS-myr::smFLAG in *VK00005*) in green are shown for
1299 each cell type as indicated in (A). Although the interpretation of such fainter syt-smHA
1300 labeling patterns is not always straightforward, they strongly suggest that at least some
1301 LC neurons (including cell types not shown in this Figure) also have presynaptic sites
1302 within the lobula. Additional details on syt-HA labeling in the lobula are provided in
1303 Supplementary file 1A. Strong syt-smHA labeling in layer Lo6 in (E) appears to be
1304 mainly due to LC10b cells (compare with (C) for LC10d cells alone), though a lobula
1305 intrinsic neuron type weakly labeled by the split-GAL4 driver line used might also
1306 contribute to the pattern. Scale bar represents 20 μ m.

1307

1308 Figure 6. Column spread of LC neurons and other cell types in the lobula in cross-
1309 section views. Cells were labeled using MCFO. Cross-section views of the lobula were
1310 generated using Vaa3D. The AP and DV axes of the lobula are indicated. Anti-Brp
1311 reference marker is shown in grey. LC neuron arbor sizes and shapes in the lobula are
1312 diverse across different cell types but similar within each type. LC cell types shown are
1313 LC11 (A), LC10a (B) and LC22 (C). The remaining LC cell types are shown in Figure 6
1314 – figure supplement 1. MCFO labeled cells of a columnar medulla neuron type (Tm3)
1315 present in each of ~ 750 visual columns (D) and a lobula tangential cell (LT) that spans
1316 the entire lobula (E) are shown for comparison. All LC arbors are multicolumnar with
1317 estimated sizes from about 10 (LC10a) to over 60 (LC11) visual columns. LC22 cells
1318 were similar in size to LC11 along the long (DV) but not the short (AP) axis of the lobula.
1319 (F) Schematic summary of the column spread of different cell types in the lobula. Scale
1320 bar represents 20 μ m.

1321

1322 Figure 6 – figure supplement 1. Layer cross-section views of lobula arbors of the LC
1323 neuron types not shown in Figure 6. Cross-section views of LC cells of the indicated
1324 types were generated as described in the Figure 6 legend. Asterisks in the LC10b and
1325 LC21 panels mark two MCFO labeled cells (LC10c and LC11, respectively) that do not
1326 belong to the indicated cell type. LO and LP in the LPLC panels indicate cross-section
1327 views of the lobula and lobula plate, respectively. Scale bar in the LC4 panel represents
1328 20 μ m; images of other cell types are shown at very similar scale.

1329

1330 Figure 7. Single cell shapes of LC neurons. Maximum intensity projection images of
1331 MCFO labeled single cells were manually segmented to exclude other labeled cells or
1332 background signal and converted to inverted grayscale images. Cells are shown in a
1333 similar orientation (with dorsal approximately up and lateral approximately to the left)
1334 and at the same scale. Scale bar represents 50 μ m.

1335 Figure 7 – figure supplement 1. Layer patterns of single cells of 22 LC neuron types.
1336 Images are reoriented views (generated using Vaa3D) of MCFO labeled LC neurons.
1337 Anti-Brp neuropil marker is in grey. For each cell type, two different views, along the AP
1338 and along the DV axes of the lobula, respectively, are shown. The two panels for a cell
1339 type can either show the same specimen in two views or two different specimens. Scale
1340 bars in the LC4 panels represent 20 μ m; images of other cell types are shown at very
1341 similar scale.

1342

1343 Figure 7 – figure supplement 2. Single cell labeling of LPLC arbors in lobula and lobula
1344 plate. (A) LPLC1. (B) LPLC2. (C) LPLC4. Numbers indicate the four LP layers
1345 (Fischbach and Dittrich, 1989). Similar to lobula layers, the LP layers can be identified
1346 by changes in the intensity of anti-Brp labeling: Each LP layer shows a band of strong
1347 anti-Brp signal flanked by weaker labeling. All three LPLC cell types have processes in
1348 all lobula plate layers and several layers of the lobula but differ in details of arbor
1349 structure and layer patterns. For example, lobula layers of LPLC4 (mainly Lo2, Lo4 and
1350 Lo6) are different from both LPLC1 (Lo2-Lo4 and Lo5B) and LPLC2 (Lo4 and Lo5B).
1351 The presence of processes in multiple lobula plate layers, as shown by all LPLC types,
1352 could support responses to stimuli that combine different directions of motion, such as a
1353 visual loom (Schilling and Borst, 2015). Scale bars represent 20 μ m.

1354

1355 Figure 8. Optogenetic activation of LC neurons induces distinct behavioral responses that
1356 differ between LC cell types. (A) A representative video image of group of freely
1357 walking flies in the circular arena assay. (B) Representative video images of a freely
1358 behaving fly on a small glass platform in the single-fly assay. A side view (upper part of
1359 the panel) and a bottom view (lower part) of the fly are simultaneously recorded on a
1360 single high-speed video camera with the aid of two small prisms (see Materials and
1361 Methods). (C,D) The results of CsChrimson activation of different LC cell types in the
1362 arena (C) and the single-fly (D) assays are summarized in a grayscale intensity map. Each
1363 column represents a distinct behavior and each row represents a different split-GAL4
1364 driver line with predominant expression in the indicated cell type. Shading represents the
1365 behavioral penetrance (percentage of trials or flies of a specific genotype in which a

1366 given behavior was observed, see Supplementary file 1B for the names of the GAL4 lines
1367 used and penetrance values). In both assays, the occurrences of reaching and jumping
1368 behaviors were annotated manually, while locomotor behaviors including forward
1369 walking, backward walking and turning were determined based on velocity and angular
1370 speed derived from automated fly tracking (see Figure 8 – figure supplement 1, and
1371 Materials and Methods). For locomotor behaviors we set a conservative threshold of two
1372 standard deviations away from the mean to be considered an activation phenotype (Figure
1373 8 – figure supplement 1E,F). In this way, we determined the behavioral penetrance for
1374 five phenotypes - reaching, jumping, forward walking, backward walking and turning - in
1375 both the arena and the single-fly assays. In the single-fly assay, the high jumping
1376 penetrance of four LC cell types (LC4, LC6, LPLC1 and LPLC2) resulted in too few flies
1377 (<=12) available for analyses of walking and turning behaviors (indicated with a '\').

1378

1379 Figure 8 – figure supplement 1. Quantification of locomotor behaviors and determination
1380 of behavioral penetrance. (A) A representative tracking of a fly with LC16 activation in
1381 the arena assay. Arrows indicate the start and end positions. Fly's trajectory is denoted in
1382 red (during stimulation, 1 s) or in white (before and after stimulation, 1 s each). (B)
1383 Time-series plot of velocity and angular speed of pBDPGAL4U control (black, trial
1384 count = 109, fly count = 23) and LC16 activated (red, trial count = 65, fly count = 14)
1385 flies. Solid and dashed lines indicate median and inner-quartile range, respectively. Grey
1386 rectangles in this and other panels signify optogenetic stimulation with red light. (C,D)
1387 Notched box plots showing the distribution of mean velocity (C) and angular speed (D),
1388 before, during, and after optogenetic stimulation, of pBDPGAL4U control (black) and

1389 LC16 activated (red) flies. The increased translational velocity of LC16 flies compared to
1390 controls prior to Chrimson stimulation appears to be due to reduced walking of the
1391 control flies after repeated red light stimulation: The data in (B-D) are averages from
1392 multiple trials (trials 1 to trial 5) with the maximum light stimulus from experiments with
1393 increasing intensities (i.e. the same flies were stimulated repeatedly within an experiment
1394 with a series of light intensities; see Materials and Methods). To examine whether the
1395 apparent higher basal locomotion of LC16 flies during pre-stimulation light off was a
1396 response to prior stimulations, we compared trial 1 data to trial 5 data from the
1397 experiments in Figure 9, because in these experiments only the maximum light stimulus
1398 was used (data for different LC16 split- GAL4 lines and for the different control flies
1399 shown in Figure 9 were pooled). Data for trial 1 showed no pre-stimulus difference
1400 between LC16 and control flies ($p = 0.88$, by Wilcox rank sum test), while locomotion
1401 was reduced for the controls in trial 5 ($p < 0.01$). (E,F) Jitter plots showing the
1402 distribution of mean velocity and angular speed during optogenetic stimulation of control
1403 and LC neuron driver lines in the arena (E) and single-fly (F) assays. Each dot represents
1404 an individual trial. A conservative threshold is set at the 97.7th percentile of the
1405 pBDPGAL4U control distribution, indicated by dashed red lines. Grey and black dots
1406 represent trials within and outside of the normal range, respectively. For walking, trials
1407 above the top red line are counted as displaying a forward walking phenotype and trials
1408 below the bottom red line are counted as displaying a backward walking phenotype. For
1409 turning, trials above the red line are counted as displaying a turning phenotype.

1410

1411 Figure 8 – figure supplement 2. Variability of LC16 backward walking behavior across
1412 trials and across flies. In the circular arena experiments, each fly was repeatedly tested in
1413 a series of trials (see Materials and Methods). For most analyses, we pooled data across
1414 all flies and trials (as shown in the left panel for walking behavior after optogenetic
1415 stimulation of different LC neuron types; these are the same data plotted as separate data
1416 point for each trial in Figure 8 – figures supplement 1). To further explore sources of
1417 variability in these experiments, using LC16 activation induced backward walking as an
1418 example, we reanalyzed the data by pooling results for either all flies of the same trial
1419 (per trial) or all trials of the same fly (per fly). This revealed different degrees of
1420 variability both across flies within the same trial and across trials for the same fly.
1421 Nonetheless, this variability does not change our conclusion that LC16 activation results
1422 in a strong backward walking response.

1423

1424

1425 Figure 9. Experiments with additional LC6 and LC16 driver lines confirm the activation
1426 phenotypes of these cell types. (A,B) Behavioral penetrance for different controls and
1427 multiple split-GAL4 driver lines for (A) jumping (flies that jumped within 200 ms of
1428 stimulation onset) with LC6 controls based on the OL0077B driver line and (B)
1429 backward walking and turning with LC16 controls based on the OL0046B driver line.
1430 Each dot represents an experiment done with a different genotype: orange, LC neuron
1431 activation in blind norpA flies that also carry an LC6 (A) or LC16 (B) split-GAL4 line;
1432 green, pBDPGAL4U control in blind norpA flies; blue, flies reared on food without

1433 supplemental retinal; red, split-GAL4 DBD or AD halves; grey, genetically distinct split-
1434 GAL4 driver lines with targeted expression in LC6 (A) or LC16 (B). Horizontal and
1435 vertical lines indicate mean and standard deviation, respectively, for the control group
1436 and split-GAL4 group. Genotypes of the driver lines, behavioral penetrance and total trial
1437 and fly counts are listed in Supplementary file 1B. Expression patterns of the split-GAL4
1438 driver lines used are shown in Figure 9 – figure supplement 1.

1439

1440 Figure 9 – figure supplement 1. Expression patterns of multiple split-GAL4 driver lines
1441 for LC6 and LC16. Brain (A,B) and VNC (C,D) expression patterns of split-GAL4
1442 drivers for LC6 (A,C) and LC16 (B,D). Split-GAL4 driven expression of 20xUAS-
1443 CsChrimson-mVenus (insertion in *attP18*; visualized using anti-GFP antibody labeling;
1444 green) and a neuropil marker (anti-Brp, magenta) are shown. Imaging parameters and
1445 brightness or contrast adjustments were identical within each brain/VNC pair but not
1446 across all images. OL0077B and OL0046B images are the same as those shown in Figure
1447 2. Scale bar represents 50 μ m. Original confocal stacks are available from
1448 www.janelia.org/split-GAL4.

1449

1450 Figure 9 – figure supplement 2. Quantification of LC16 activation induced locomotor
1451 behaviors and determination of behavioral penetrance. Jitter plots show the distribution of
1452 mean velocity and angular speed during optogenetic stimulation of multiple LC16 split-
1453 GAL4 driver lines and control lines. Color codes are the same as in Figure 9. Penetrance
1454 determined as in Figure 8 – figure supplement 1E.

1455

1456

1457 Figure 10. Reaching behavior resulting from activation of LC10 subtypes. (A)
1458 Representative video images of a fly exhibiting reaching behavior in the single-fly assay.
1459 Time stamps indicate milliseconds (ms) after the start of reaching. (B) Comparison of
1460 lobula layer patterns and penetrance of reaching upon optogenetic activation for 15 LC10
1461 split-GAL4 lines. The images show reconstructed views of CsChrimson expression in the
1462 lobula (generated using Vaa3D and manually aligned using the anti-Brp reference
1463 marker). Approximate layer positions are indicated on the left. Scale bar represents 10
1464 μ m. CsChrimson expression using two additional LC10 driver lines (SS00941 and
1465 SS00942) resulted in unexpected uncoordinated behaviors in response to optogenetic
1466 activation that precluded analyses of reaching behavior. These lines, which are related as
1467 they only differ from each other in the insertion site of the AD hemidriver (see
1468 Supplementary file 1B), were therefore excluded from further analyses. (C) Single cell
1469 labeling reveals subtype expression patterns of LC10 driver lines. Overall lobula
1470 expression of an LC10 split-GAL4 line (SS02664) (top panel; displayed as in B) and
1471 examples of MCFO labeled single cells from this line (bottom panels) are shown. LC10
1472 subtypes (indicated below the images) of single cells were assigned based on layer
1473 patterns, arbor sizes and shape as follows: LC10c cells mainly arborize in layer Lo5B
1474 with some processes in the adjacent layers. LC10a cells also have arbors in Lo5B, but
1475 differ from LC10c by having additional processes in the more distal layers Lo2, Lo3 and
1476 Lo4. LC10b and LC10d differ from LC10a and LC10c by having major arbors in Lo6
1477 and only few processes in Lo5B. Their distal arbors reach Lo4. LC10b cells are wider

1478 than LC10d cells and show many small varicosities (presumably presynaptic sites;
1479 compare Figure 5- figure supplement 2E) in Lo6. LC10 neurons also differ in their
1480 axonal paths in the AOTu: LC10a and LC10d axons run both dorsally and ventrally, and
1481 LC10b and LC10c only ventrally (Figure 3G; also see Figure 10 – figure supplements 1).
1482 Scale bars represent 10 μ m. (D) Reaching penetrance observed upon activation of the
1483 LC10 split-GAL4 drivers and various control lines in the single-fly assay. Split-GAL4
1484 drivers are grouped by expression patterns in the LC10 subtypes: either subtype a and/or
1485 d, or neither a nor d. Driver lines were included in the “a and/or d” category if two or
1486 more cells of these types were identified in MCFO experiments (see Figure 10 – figure
1487 supplement 2). Colors representing various controls and split-GAL4 driver lines are the
1488 same as those in Figure 9.

1489

1490 Figure 10 – figure supplement 1. Expression patterns of LC10 split-GAL4 driver lines.
1491 Brain (A) and VNC (B) expression patterns using 20xUAS-CsChrimson-mVenus in
1492 *attP18* visualized with an anti-GFP antibody (green) and a neuropil marker (anti-Brp,
1493 magenta) are shown. While some driver lines also had expression in a few non-LC10
1494 cells, none of these additional neurons was consistently present in lines with the reaching
1495 behavior. Imaging parameters and brightness or contrast adjustments were identical for
1496 each brain/VNC pair but not across all images. OL0020B and OL0023B images are the
1497 same as those shown in Figure 2. Scale bar represents 50 μ m. Original confocal stacks
1498 are available from www.janelia.org/split-GAL4.

1499

1500 Figure 10 – figure supplement 2. Stochastic single cell labeling reveals LC10 subtype
1501 expression patterns of the LC10 split-GAL4 driver lines. (A) Examples (10 per driver line)
1502 of MCFO-labeled LC10 cells from five different lines. Subtype classification is indicated
1503 for each cell (white lowercase letters). Anti-Brp pattern (used to facilitate comparison of
1504 layer positions across specimens) is shown in grey; views were generated using Vaa3D.
1505 Layer patterns of these projection images were manually aligned using the anti-Brp
1506 marker. To do so, the scale of some images was slightly adjusted to compensate for the
1507 non-uniform depth of the lobula. Approximate layer positions are indicated in the bottom
1508 right panel. Scale bar represents 10 μ m. (B) Summary of LC10 MCFO results. For each
1509 driver line, the number of MCFO-labeled LC10 cells of each subtype was determined for
1510 the indicated number of fly brain samples. Some LC10 cells that were located at an edge
1511 of the lobula neuropil or overlapped with other labeled cells and thus could not be
1512 identified were excluded from the counts. Total cells refer to the number of all LC10 cells
1513 that were assigned a subtype. Subtypes that were only seen as single labeled cell are in
1514 parentheses in the summary.

1515

1516 Figure 11. LC6 and LC16 activation behaviors resemble avoidance responses evoked by
1517 visual looming. (A) LC6 and LC16 project to adjacent, non-overlapping target glomeruli.
1518 The image was generated using a 3D image rendering software (FluoRender) (Wan et al.,
1519 2012) on aligned confocal images. (B) LC6 and LC16 have similar layer patterns in the
1520 lobula. An overlay of substack projections of aligned image stacks is shown. Anti-Brp
1521 reference marker is in grey. (C) Representative video images from the single-fly assay
1522 showing that a looming stimulus and LC6 activation evoke very similar coordinated

1523 behavioral sequences, which include wing elevation, middle leg extension and initiation
1524 of flight. Time stamp is set at 0 ms for the frame of takeoff. Negative and positive values
1525 are for frames before and after takeoff, respectively. (D) Notched box plots showing the
1526 duration of the takeoff sequence measured as the time from the first moment of wing
1527 movement to the last moment of tarsal contact with the ground after the stimulus (Mann-
1528 Whitney test, $p = 0.29$ between looming and LC6 activation, and $p < 0.001$ between LC6
1529 activation and no stimulus). (E) Representative video images from the single-fly assay
1530 showing that a looming stimulus and LC16 activation evoke very similar backward
1531 walking behaviors. Time stamp is set at 0 ms for the start of backward walking. (F) Total
1532 distance flies walked on the platform of the single-fly assay. Positive and negative values
1533 are for forward and backward walking, respectively (Mann-Whitney test, $p = 0.71$
1534 between looming and LC16 activation, and $p < 0.001$ between LC16 activation and no
1535 stimulus). Scale bars represent 50 μm (A) or 20 μm (B).

1536 Figure 11 – figure supplement 1. Behavioral consequences of silencing LC6 and LC16 by
1537 Kir2.1 expression. Split-GAL4 driver lines OL0077B (LC6, A-B) or OL0046B (LC16, C)
1538 were crossed to flies with pJFRC49-10XUAS-IVS-eGFPKir2.1 in a DL strain
1539 background. pBDPGAL4U crossed to the same effector or DL flies were used as
1540 controls. (A,B) Looming stimuli were presented at an elevation of 45°, an azimuth of 90°,
1541 and an l/v of 20 (as in Figure 11C,D). In addition, a slow stimulus was presented using
1542 an l/v of 160 since calcium imaging suggests LC6 is tuned to slower looms (Figure 12 –
1543 figure supplement 1). Confidence intervals were determined using the Clopper-Pearson
1544 method. Fly counts for each experiment from left to right are 170, 117, 141, and 89. (C)
1545 Looming stimuli were presented as in Figure 11E-F, specifically chosen to induce

1546 backward walking. Total distance flies walked on the platform of the single-fly assay.

1547 Fly counts from left to right are 396, 43, and 40.

1548 Figure 12. LC16 and LC6, but not LC11, respond to visual looming stimuli with robust

1549 calcium increases. (A) Visual stimuli evoked calcium responses of LC neurons were

1550 imaged in head-fixed flies. (B) The axon terminals of LC cells bundle to form cell-type

1551 specific glomeruli (subset shown in C). We imaged from a single glomerulus by using

1552 spilt-GAL4 lines labeling individual cell-types (LC16, LC6 or LC11). Representative

1553 regions for calcium imaging experiments are marked with the yellow dashed rectangles.

1554 Exemplary responses of LC16, LC6 and LC11 to a slow dark looming disk are shown (C;

1555 each single frame taken from peak response of an individual fly, distinct genotypes were

1556 used to image from each glomerulus). (D) LC16, LC6 and LC11 responses to looming

1557 visual stimuli are shown for three variants of the stimulus (from top to bottom: dark

1558 looming disk, bright looming disk, luminance-matched) expanding at r/v= 550ms (n=5

1559 per genotype). Error bars indicate mean \pm SEM. Statistics were performed on mean $\Delta F/F$

1560 during a time window in which the response peaks (2 s before and after the looming

1561 stimulus stops expanding). (E) As a comparison to looming stimuli, we also presented

1562 moving object stimuli that contain local motion that is distinct from looming. LC11

1563 responds strongly to the motion of the small ($9^\circ \times 9^\circ$) spot, but not the long bar ($9^\circ \times 72^\circ$)

1564 moving object. The objects moved at $22.5^\circ/\text{s}$, starting 18° left of the visual midline and

1565 stopping 108° to the right of the midline. Statistics were performed on mean $\Delta F/F$ during

1566 the whole stimulus epoch.

1567

1568 Figure 12 – figure supplement 1. LC16 and LC6 are tuned to slower looming speeds.

1569 Stimulus evoked calcium responses to different loom speeds. The responses are mean

1570 $\Delta F/F$ during a time window in which the response peaks (2 s before and after the looming

1571 stimulus stops expanding). Stimuli from top to bottom rows: dark looming disk, bright

1572 looming disk, luminance-matched.

1573

1574 Figure 13. Behavioral responses to unilateral LC neuron stimulation differ from bilateral

1575 activation behaviors and are directional. (A) Schematic illustration of a genetic method

1576 for stochastic labeling and activation of LC neurons. A “stop-cassette” reporter

1577 (pJFRC300-20XUAS-FRT>-dSTOP-FRT>-CsChrimson-mVenus in *attP18*) was used for

1578 Flp-recombinase mediated control of CsChrimson expression. This reporter/effectector

1579 construct (small schematic in the right brain hemisphere of the larval brains in the

1580 illustration) is based on the “Flp-out” design (Struhl and Basler, 1993). It contains 20

1581 Upstream Activating Sequences (UAS) and a core promoter (grey rectangle) for GAL4-

1582 activated expression, a transcriptional terminator (white rectangle with a red prohibition

1583 sign) flanked by Flp-recombinase target (FRT) sites (black triangles), and a CsChrimson-

1584 mVenus fusion gene (green rectangle). Heat shock induces expression of the Flp-

1585 recombinase which can excise the transcriptional terminator, allowing expression of

1586 CsChrimson-mVenus under the control of a split-GAL4 driver (not shown). By

1587 expressing a limiting amount of Flp-recombinase early in development (1st instar larval

1588 stage), stochastic stop-cassette excision occurs in LC precursor cells, generating adults in

1589 which most or all neurons of one LC neuron type (determined by the split-GAL4 driver)

1590 express CsChrimson-mVenus in either no, one, or two optic lobes. (B) Strong backward
1591 walking behavior requires bilateral LC16 activation. Notched box plots showing the
1592 distribution of mean velocity for bilateral LC16 activation (trial count = 101, fly count =
1593 10), unilateral LC16 activation (trial count = 75, fly count = 7) and no labeling controls
1594 (trial count = 114, fly count = 11). Behavioral responses of individual flies were assayed
1595 and their brains were subsequently dissected to determine expression patterns. Unilateral
1596 LC16 activation produced far less backward walking than bilateral activation (Mann-
1597 Whitney test, $p < 0.001$). (C) Unilateral activation of LC16 and LC10 induces aversive
1598 and attractive turning, respectively. Notched box plots showing the distribution of mean
1599 angular velocity for different labeling categories of LC16 and LC10: For LC16, trial and
1600 fly counts are the same as in (B). For LC10, bilateral (trial count = 91, fly count = 8),
1601 unilateral (trial count = 268, fly count = 24) and no labeling (trial count = 281, fly count
1602 = 22). For unilateral activation, behavioral data from animals with labeling only on the
1603 left brain hemisphere were reversed and combined with those from animals with labeling
1604 only on the right brain hemisphere. In addition to flies with clear bilateral or unilateral
1605 expression, 18 flies in the LC10 stochastic activation experiments had expression in both
1606 brain halves but showed differences in the apparent number of labeled LC10 cells
1607 between the hemispheres. Because of the wide range of these labeling differences we did
1608 not include these flies in the above analysis. However, the behavioral results for this
1609 group also showed a turning bias towards the side with stronger labeling (see Figure 13 –
1610 figure supplement 1), suggesting that even small differences of LC10 activation between
1611 the two hemispheres may be sufficient to induce ipsilateral turning.

1612

1613 Figure 13 – figure supplement 1. Turning behavior of LC10 flies with bilateral labeling
1614 that is stronger in one brain hemisphere (trial count = 212, fly count = 18). Data for flies
1615 with uniform bilateral expression or no labeling are the same as in the main Figure and
1616 included for comparison.

1617

1618 Movie 1. Composite of aligned images showing a series of sections through the
1619 ventrolateral central brain with the target regions of 18 LC (or LPLC) neurons visualized
1620 by presynaptic marker expression. Original images, composite image assembly and color
1621 scheme are as in Figure 3. The anti-Brp reference pattern (grey) of the template brain
1622 used for alignment is shown both together with the labeled LC terminals (left panel) and
1623 individually (right panel). Terminals of LC10 cell types in the AOTu are not included in
1624 the movie. We believe the slight overlap seen between LC12 and LC18 and between
1625 LC24 and LC26 is due to imperfect alignment, rather than true overlap.

1626 Movie 2. Three-dimensional rendering of the target regions of LC (or LPLC) neurons in
1627 the ventrolateral central brain shown in Figure 3 and Movie 1. Image assembly and color
1628 scheme are as described for Figure 3. Anti-Brp reference pattern is in grey. Terminals of
1629 LC10 cell types in the AOTu are not included. The movie was generated using Vaa3D.

1630

1631 Movie 3. An example of an LC neuron activation phenotype (backward walking and
1632 turning) in the arena assay. A representative video showing groups of freely walking flies
1633 tested in the circular arena. The video is shown at 0.4x actual speed and the red indicators
1634 at the corners indicate the timing of optogenetic activation (1 s). This example shows a

1635 highly penetrant backward walking and turning phenotype resulting from LC16

1636 activation.

1637 Movie 4. Examples of distinct LC neuron activation phenotypes in the arena assay. One

1638 representative fly for each phenotype is shown before, during and after optogenetic

1639 stimulation (1 s each, 3 s in total). Flies' centers of mass are tracked and their trajectories

1640 are represented with blue (before and after stimulation) or red (during stimulation) dotted

1641 lines. The video is shown at 0.4x actual speed.

1642 Movie 5. Examples of distinct LC neuron activation phenotypes in the arena assay. 10

1643 representative flies for each phenotype are shown for the duration of optogenetic

1644 stimulation (1 s). Flies' centers of mass are tracked for the duration of stimulation and

1645 their trajectories are represented with red dotted lines. Many flies with the reaching

1646 behavior also extended one or both wings in response to CsChrimson activation, though

1647 we did not further characterize this aspect of the behavior in this study. The video is

1648 shown at 0.2x actual speed.

1649 Movie 6. Examples of distinct CsChrimson activation phenotypes in the single-fly assay.

1650 10 representative flies of each genotype are shown during the 50 ms optogenetic

1651 stimulation and for the following 450 ms. Jumping and reaching phenotypes are shown in

1652 the side view whereas forward walking, backward walking and turning phenotypes are

1653 shown in the bottom view. The pBDPGAL4U control flies are shown in both the side and

1654 bottom views. In the bottom view, a red horizontal line through flies' center of mass is

1655 used to help visualize forward walking, backward walking and turning behaviors.

1656 Movie 7. Examples of phenotypes upon bilateral and unilateral activation of LC16 in the
1657 stochastic activation experiment. A representative fly for bilateral and unilateral LC16
1658 activation is shown before, during and after optogenetic stimulation (1 s each, 3 s in total).
1659 Flies' centers of mass are tracked and their trajectories are represented with blue (before
1660 and after stimulation) or red (during stimulation) dotted lines. The video is shown at 0.4x
1661 actual speed.

1662

1663 Supplementary File 1A. Summary of the anatomical properties of the 22 LC neuron types
1664 described in detail in this study. Cell numbers and lateral arbor spreads are listed as mean
1665 \pm SD. Column coverage was estimated using arbor spread measurements. Further details
1666 are provided in the Materials and Methods.

1667 Supplementary File 1B. Details of the behavioral experiments in Figures 8-13. This table
1668 includes information on split-GAL4 hemidrivers (the AD and DBD halves), behavioral
1669 penetrance for each of the five examined phenotypes, and trial and fly counts, from both
1670 the arena and single-fly assays. While the raw data counts within each assay are the same,
1671 a small number of trials could not be scored by either manual annotation or automatic
1672 tracking; as a result there are some small differences in the number of quantified data
1673 points for the two scoring methods. Use of fly culture media different from standard
1674 cornmeal molasses food with supplemental retinal is indicated as follows: ret-: standard
1675 cornmeal molasses food without supplemental retinal. Vit-: Vitamin A-deficient food
1676 based on grape juice recipe (see Materials and Methods) with supplemental retinal. Vit-,

1677 ret-: Vitamin A-deficient food without supplemental retinal. *norpA* indicates flies that are
1678 rendered blind by a null mutation in the *norpA* gene, *norpA*[36].

1679 Supplementary File 1C. Split-GAL4 driver lines for the LC neuron types described in this
1680 study. Split-GAL4 line names in bold indicate drivers used in behavioral experiments.

1681 Supplementary File 1D. Details of the fly lines used to generate the data for the anatomy
1682 Figures and Movies 1 and 2.

1683

1684 **Materials and Methods**

1685

1686

1687 **Fly stocks and rearing conditions**

1688

1689 Split-GAL4 transgenes were selected based on GAL4-line expression patterns
1690 (Jenett et al., 2012; Kvon et al., 2014) (Barry J. Dickson, personal communication) and
1691 constructed as previously described (Pfeiffer et al., 2010). Tables with details of
1692 genotypes are included as Supplementary files 1B, 1C and 1D. Supplementary file 1B
1693 summarizes genotypes and results of behavioral experiments. Supplementary file 1C lists
1694 all LC cell types described here and the driver lines for each type; Supplementary file 1D
1695 provides details of the genetic reagents used for each panel of the anatomy Figures and
1696 for Movies 1 and 2. With a few exceptions indicated in Supplementary files 1B and 1C,
1697 all split-GAL4 AD transgenes are inserted in *attP40* and all DBD transgenes in *attP2*.

1698

1699 *Drosophila melanogaster* were reared on standard cornmeal/molasses food at
1700 25 °C and 50 % humidity unless otherwise indicated. For optogenetic activation
1701 experiments in the arena and stochastic activation experiment, flies were reared on
1702 standard food supplemented with retinal (0.2 mM all-trans-retinal prior to eclosion and
1703 then 0.4 mM post eclosion) at 22 °C and 60 % humidity in darkness. For optogenetic
1704 activation experiments in the single-fly assay, flies were reared on standard food
1705 supplemented with retinal (0.4 mM all-trans-retinal throughout) at 22 °C and 60 %

1706 humidity in darkness. Flies of both sexes were used for behavioral experiments unless
1707 otherwise indicated. All anatomical analyses were done with female flies.

1708

1709 Vitamin A-deficient food was described previously (Nichols and Pak, 1985).

1710 Briefly, per 500 ml of food: 270 ml H₂O, 230 ml grape juice (Welch's), 11 g Bacto agar
1711 (Difco), 30 g glucose, 10 g sucrose, 5 g fructose, 10 g yeast (Fleischmann's dry), 10 ml 1
1712 M NaOH, 2 ml propionic acid and 0.2 ml phosphoric acid.

1713

1714 In addition to the split-GAL4 lines (see Supplementary files 1B, 1C and 1D), the
1715 following fly strains were used: (1) 20XUAS-CsChrimson-mVenus in *attP18* (Klapoetke
1716 et al., 2014); (2) pBPDGAL4U in *attP2*, an enhancerless GAL4 driver (Pfeiffer et al.,
1717 2010); used as a control driver in behavioral assays; (3) hs-FLP-PESTOpt in *attP3* (Nern
1718 et al., 2015); (4) pJFRC300-20XUAS-FRT>-dSTOP-FRT>-CsChrimson-mVenus in
1719 *attP18*; created by transferring the stop cassette from pJFRC177-10XUAS-FRT>-
1720 dSTOP-FRT>-myr::GFP (Nern et al., 2011) into UAS-CsChrimson-mVenus; (5) MCFO-
1721 1 (Nern et al., 2015); (6) MCFO-7 (Nern et al., 2015); (7) pJFRC200-10XUAS-IVS-
1722 myr::smGFP-HA in *attP18*, pJFRC216-13XLexAop2-IVS-myrm::smGFP-V5 in
1723 *su(Hw)attP8* (HA_V5) (Nern et al., 2015); (8) pJFRC7-20XUAS-IVS-GCaMP6m in
1724 VK00005 (Chen et al., 2013) in DL background; (9) w⁺; pJFRC51-3XUAS-IVS-
1725 syt::smHA in *su(Hw)attP1*, pJFRC225-5XUAS-IVS-myrm::smFLAG in VK00005 (Nern et
1726 al., 2015); (10) *norpA*[36] (de Vries and Clandinin, 2012); (11) w⁺ DL; DL; pJFRC49-
1727 10XUAS-IVS-eGFPKir2.1 in *attP2* (DL) (DL denotes chromosomes derived from the

1728 DL fly strain)(von Reyn et al., 2014); (12) DL (wild-type strain from M.H. Dickinson,
1729 University of Washington).

1730

1731

1732 **Immunohistochemistry and imaging**

1733

1734 For screening of split-GAL4 combinations, we adapted a protocol previously
1735 applied to large-scale characterization of GAL4 expression patterns of larval fly brains
1736 (Li et al., 2014). Brains of adult flies carrying the split-GAL4 hemidriver combination of
1737 interest and a UAS reporter (pJFRC200-10XUAS-IVS-myr::smGFP-HA in *attP18*) were
1738 dissected in insect cell culture medium, incubated ~ 12-24 h at 4 °C in 10 µl 1% (w/v)
1739 paraformaldehyde in the same medium in 60-well or 72-well Terasaki plates, washed
1740 with PBS and subsequently attached to Poly-L-Lysine coated coverslips while immersed
1741 in PBS. Further processing was in Copeland jars in a total volume of ~ 10 ml. This
1742 included the following steps: 2 x 5 min in PBT (PBS + 0.5 % Triton X-100), 1 h in PBT
1743 with 0.5 % Normal Goat Serum (PBT-NGS), overnight at 4 °C in PBT-NGS with
1744 primary antibodies (rabbit anti-GFP 1:1000, mouse anti-Brp or mAb Nc82 (Wagh et al.,
1745 2006) 1:50), 2 x 5 min in PBT, 1 h in PBT-NGS, overnight at 4 °C in PBT-NGS with
1746 secondary antibodies, 2 x 5 min in PBT and 1x 5 min in PBS. Brains were then post-fixed
1747 for 4 h with 4 % (w/v) PFA in PBS, further rinsed with PBS and subsequently dehydrated
1748 and mounted in DPX as described (Nern et al., 2015). A detailed updated version of this
1749 screening protocol is available online ([https://www.janelia.org/project-](https://www.janelia.org/project-team/flylight/protocols)
1750 [team/flylight/protocols](#) under “IHC - Adult Split Screen”).

1751

1752 We used two sets of markers to visualize split-GAL4 expression patterns.

1753 20XUAS-CsChrimson-mVenus in *attP18* (Klapoetke et al., 2014) was used to reveal the
1754 overall expression patterns of split-GAL4 lines used in behavioral experiments with this
1755 effector. For most other anatomical analyses (except stochastic labeling), a combination
1756 of pJFRC51-3XUAS-IVS-Syt::smHA in *su(Hw)attP1* and pJFRC225-5XUAS-IVS-
1757 myr::smFLAG in *VK00005* (Nern et al., 2015) was used. Immunolabeling of fly brains to
1758 detect these markers together with anti-Brp as a neuropil label was performed as
1759 described (Aso et al., 2014a). Brains were mounted in DPX. Detailed protocols can be
1760 found online (<https://www.janelia.org/project-team/flylight/protocols> under “IHC - Anti-
1761 GFP”, “IHC - Polarity Sequential” and “DPX mounting”).

1762 Stochastic labeling of LC neurons in multiple colors was performed using

1763 Multicolor FlpOut (MCFO) (Nern et al., 2015). MCFO fly stocks used for specific
1764 experiments are listed in Supplementary File 1D. MCFO samples were processed for
1765 immunolabeling of three epitope-tagged marker proteins (smGFP-HA, smGFP-V5 and
1766 smGFP-FLAG (Viswanathan et al., 2015)) together with the anti-Brp reference pattern
1767 and mounted in DPX as described (Nern et al., 2015). Detailed protocols can be found
1768 online (<https://www.janelia.org/project-team/flylight/protocols> under “IHC - MCFO”).

1769 Images were acquired on Zeiss LSM 710 or 780 confocal microscopes with 20x
1770 0.8 NA or 63x 1.4 NA objectives at 0.62 μm x 0.62 μm x 1 μm (20x) or 0.19 μm x 0.19
1771 μm (in a few cases 0.38 μm x 0.38 μm) x 0.38 μm (63x) voxel size. In some images (e.g.
1772 panel A of Figure 3 - figure supplement 1), signal from Alexa647 or DyLight649 dyes
1773 was also detected in the reference pattern (Alexa488) channel. This crosstalk appears to

1774 be mainly due to altered spectral properties of these dyes in the DPX mounting medium
1775 rather than microscope set-up or antibody cross-reaction. Four channel MCFO images
1776 (HA, V5, FLAG plus anti-Brp) were acquired as two separate stacks which were
1777 combined post-imaging. For 63x images, brain regions larger than a single field of view
1778 were imaged as up to five overlapping tiles; multiple tiles were combined (“stitched”).
1779 Brain alignment to a template brain was achieved as described (Aso et al., 2014a); to
1780 facilitate alignment of 63x tiles, most samples imaged as 63x were also imaged as whole
1781 brains at 20x. Initial image processing steps applied to most or all images (such as
1782 stitching and alignment) were as previously described (Aso et al., 2014a). Alignment
1783 quality showed some variation between specimens and within subregions of the same
1784 specimen; samples with acceptable alignment quality in the relevant brain regions were
1785 identified by visual inspection of an overlay of the aligned anti-Brp patterns of the sample
1786 and the template brains. Some processed (e.g. aligned or stitched) images used for
1787 anatomical analyses were stored using a “visually lossless” compression (h5j format).
1788 This compression did not appear to have a detectable effect on the neuroanatomical
1789 features that were characterized using these images.

1790 Fiji (<http://fiji.sc>) and Vaa3D (Peng et al., 2010) were used for most analyses and
1791 processing of individual images. To generate specific views from three dimensional
1792 image stacks, appropriately oriented substack views were generated using the
1793 Neuronannotator mode of Vaa3D and exported as TIFF format screenshots. The scale of
1794 these images was calibrated using the known dimensions and pixel resolution of the
1795 starting image and the pixel resolution and zoom of the exported image. In some cases,
1796 multiple Figure panels (in either the same Figure or different Figures) show different

1797 views of the same cells that were generated from the same image stack (using Vaa3D) to
1798 illustrate distinct anatomical features. To display images in similar orientations within a
1799 figure, some images were rotated or mirrored. To fill in empty space outside the original
1800 field of view in some panels with rotated images, canvas size was increased and space
1801 outside the original image filled in with zero pixels using Fiji. Some images (for example
1802 in the overlays in Figure 3) were manually segmented to remove background or labeled
1803 cells or structures other than those of interest; instances of such processing are
1804 specifically noted in the respective figure legends. Overlays of aligned images were
1805 assembled in Fiji with the exception of Figure 11A for which aligned images of LC6 and
1806 LC16 were segmented and overlaid using FluoRender (Wan et al., 2012), as previously
1807 described (Aso et al., 2014a). Figures were assembled using Adobe InDesign with some
1808 schematics generated in Adobe Illustrator.

1809 All reported anatomical features were confirmed with multiple specimens. For
1810 analyses of glomerulus shape and location and overall lobula layer patterns, at least three
1811 brains per cell type were imaged at high resolution (63x) with pJFRC51-3XUAS-IVS-
1812 Syt::smHA in *su(Hw)attP1* and pJFRC225-5XUAS-IVS-myr::smFLAG in *VK00005* as
1813 reporters (see above). For the illustrations in Figure 3 and Figure 5, individual aligned
1814 brains were selected based on alignment quality in the regions of interest; however the
1815 features shown were also examined in unaligned samples and for at least two additional
1816 brains. The number of MCFO labeled single cells that were imaged and examined at high
1817 resolution varied: The lowest numbers was for LC26 (7 cells); the highest numbers were
1818 for LC10 subtypes (see Figure 10 – figure supplement 2B). Estimates of cell numbers in
1819 Supplementary file 1A are based on manual counts using high resolution (63x) confocal

1820 stacks of the indicated split-GAL4 driver lines with pJFRC225-5XUAS-IVS-
1821 myr::smFLAG in *VK00005* as reporter (see above). Numbers are averages of counts of
1822 cells from three or more optic lobes. Lateral arbor spreads of LC neurons within lobula
1823 layers were estimated using substack projection images similar to those shown in Figure
1824 7 – figure supplement 1. A segmented line was drawn along the part of a lobula layer
1825 covered by a cell’s arbors and the length of this line (measured using Fiji) divided by the
1826 maximum length of the entire layer determined in the same way. Arbor spreads were
1827 measured along both the AP and DV axes of the lobula. To estimate visual column
1828 coverage from these numbers, we assumed a circular eye of ~ 750 ommatidia, a uniform
1829 distribution of the corresponding visual columns across the lobula (i.e. ~ 31 columns
1830 along each lobula axis) and treated LC neuron arbors within each layer as planar and
1831 ellipse-shaped. All of these simplifications, which are approximations of described
1832 features of the visual system (Wolff and Ready, 1993) (Meinertzhagen and Hanson,
1833 1993), limit the precision of these estimates, with larger overestimates expected for large
1834 arbors.

1835

1836 **Optogenetic activation behavioral assays**

1837

1838 *Circular arena assay.* Groups of approximately 25 flies (3 to 10 d post-eclosion)
1839 were tested at 25 °C and 50 % relative humidity in a dark chamber. Optogenetic
1840 activation experiments were performed in a 100 mm diameter and 3 mm high circular
1841 arena as previously described (Aso et al., 2014b; Klapoetke et al., 2014). For activation
1842 of neurons expressing CsChrimson, the arena was uniformly illuminated with 617 nm

1843 LEDs (Red-Orange LUXEON Rebel LED - 122 lm; Luxeon Star LEDs) at increasing
1844 intensities: 5, 10, 20, 49 and 94 $\mu\text{W}/\text{mm}^2$. Overall, higher light intensities appeared to
1845 produce more penetrant but otherwise qualitatively similar behavioral responses. Data
1846 collected with the maximum light stimulus ($94 \mu\text{W}/\text{mm}^2$) were therefore used for all
1847 detailed analyses. For each intensity, five to six 1-s trials were performed. The inter-
1848 stimulus interval was 9 s between trials of the same intensity and 20 s between trials of
1849 different intensities. Videos were recorded under reflected IR light using a camera
1850 (ROHS 1.3 MP B&W Flea3 USB 3.0 Camera; POINT GREY) with an 800 nm long pass
1851 filter (B&W filter; Schneider Optics) at 50 frames per second, 1024 x 1024 pixel
1852 resolution.

1853

1854

1855

1856 *Single-fly assay.* Flies were automatically released one at a time onto a small glass
1857 platform (5 mm by 5 mm) using a custom-built system. Further details of this system
1858 will be described elsewhere. Two small prisms, one placed in front of the glass platform
1859 and one below it, allowed a side view and a bottom view of the fly to be simultaneously
1860 recorded on a single high-speed video camera (Photron, SA-4 and SA-X). A 10 Hz video
1861 feed was processed in real time and used to coordinate stimulus presentation via software
1862 (https://github.com/wryanw/single_fly_tracking_and_analysis) written in MATLAB
1863 (Mathworks, inc. Natick, MA). For optogenetic activation, four 608 nm LEDs were
1864 turned on for 50 ms with 3 mW total intensity beginning when the fly was still and
1865 centered on the platform. For looming stimulus experiments, a dark disc on a light

1866 background was projected on a screen above the platform with a non-linear expansion
1867 rate that mimicked that of an object approaching the fly with constant velocity (see (von
1868 Reyn et al., 2014)). Video frames of the fly behavior were recorded at a rate of 6000
1869 frames per second and a spatial resolution of 3 pixels per mm for the duration of each
1870 stimulus plus 500 ms after for optogenetic experiments and 150 ms after for looming
1871 experiments. For the looming-evoked jumping experiments, the looming stimulus was
1872 presented at an azimuth of 90°, which elicits jumping more frequently than any other
1873 azimuth (data not shown). For backward walking, the stimulus was presented at 0°,
1874 which elicits that behavior better than the 90° azimuth stimulus used to elicit
1875 jumping. Both stimuli were presented at an elevation of 45° above the horizon. All
1876 experiments were conducted at 23 °C and 50 % humidity. Data was acquired in 20-min
1877 sessions on four independent apparatuses simultaneously, during which time about 20
1878 videos could be collected per apparatus. Videos were used in subsequent analyses only
1879 when one fly was present for the duration of the experiment (90 % of videos).

1880

1881 *Stochastic labeling and activation assay.* Crosses of 40-50 pairs of males and
1882 females were set up in egg-laying cages on grape juice plates (containing 30 % agar)
1883 supplemented with a drop of yeast paste. First instar larvae hatched within a 3-h period
1884 were collected with a brush, seeded in standard cornmeal/molasses food supplemented
1885 with retinal and were immediately subject to heat shock at 37 °C for 90-120 min to
1886 induce stochastic, recombinase-mediated excision of transcriptional-terminating cassettes
1887 in the 20XUAS-FRT>STOP>FRT-CsChrimson-mVenus in *attP18* transgene. Flies were
1888 then reared at 22 °C at 60 % relative humidity in darkness. The activation behaviors of

1889 individual 4-10 d post-eclosion flies were tested at 25 °C at 50 % relative humidity in a
1890 32-mm diameter bowl arena with a top dome (6 mm maximum height) that had been
1891 coated with Sigmacote (Sigma).

1892

1893 Bowl arenas were illuminated with 617 nm LEDs at 94 uW/mm² and fifteen 1-s
1894 trials with an inter-stimulus interval of 9 s were performed for each fly. Trials in which
1895 flies showed startle response or stayed on the ceiling (two trials per fly on average) were
1896 excluded from further analysis. Video recording and fly tracking were performed in the
1897 same way as described for the circular arena assay. After assaying, flies were retrieved
1898 and their brains were dissected and stained to assess CsChrimson-mVenus expression.
1899 Behavioral data were categorized by expression patterns (bilateral, unilateral on the right,
1900 unilateral on the left, or no labeling). In the LC10 experiments, some of the assayed flies
1901 showed bilateral CsChrimson expression but with more labeling on one side compared to
1902 the other. These flies were placed in their own category and behavioral data for this group
1903 analyzed separately. For unilateral labeling, trajectories for left activation were inverted
1904 and combined with right activation data. Flies of both sexes were used in the LC16
1905 experiments and only female flies were used in the LC10 experiments.

1906

1907

1908 **Behavioral data analysis and statistics**

1909

1910 Fly tracking videos were analyzed using either manual human annotation or software
1911 (https://github.com/wryanw/bowl_assay_tracking_and_analysis) written in

1912 MATLAB. The automated tracking identifies the center of mass of each fly and
1913 determines the fly's azimuthal orientation for every frame using a template-matching
1914 algorithm. The center of mass is determined in 2 dimensions in the arena assay and 3
1915 dimensions in the single-fly assay, with 95 % of the data having an error of less than 5
1916 pixels. Position and orientation information for each fly was converted to velocity (to
1917 measure forward and backward walking) using a smoothing filter or angular
1918 velocity/speed (to measure turning) using a sliding Savitzky-Golay filter (Orfanidis,
1919 1996). Forward and backward walking velocity was determined relative to the orientation
1920 of the fly, along its path of movement. For the arena assay, mean velocities were
1921 calculated for the full 1 s of optogenetic activation. For the single-fly assay, mean
1922 velocities for motion and turning were calculated for the first 350 ms after the onset of
1923 light stimulation during which most flies remained in the field of view on the assay's
1924 small platform. Reaching and jumping were elicited later than 350 ms in some cases, so a
1925 500 ms cutoff was used for these behaviors. These average motion and turning values for
1926 individual flies were used to generate the distributions seen in Figure 8 – figure
1927 supplement 1 and Figure 9 – figure supplement 2. For assessing behavioral phenotype
1928 penetrance, we used thresholds that required turning rates for experimental data to be
1929 beyond the 97.7th percentile of control data and walking velocity to be outside of the
1930 2.3rd percentile (negative values, backward walking) or the 97.7th percentile (positive
1931 values, forward walking) to be scored as positive. These percentiles roughly correspond
1932 to two standard deviations away from the mean in a normal distribution; we use
1933 percentiles because the distributions are non-normal. The thresholds were determined
1934 independently for the arena and the single-fly assays and are indicated by horizontal red

1935 lines in Figure 8 – figure supplement 1 and Figure 9 – figure supplement 2. The
1936 thresholds were used to convert mean velocities into true/false values for forward
1937 walking, backward walking and turning. Jumping and reaching were scored
1938 manually. Jumping in the arena assay was defined as events in which a fly's legs all left
1939 the ground, usually accompanied by the initiation of wing flapping and change in fly
1940 shape. Jumping in the single-fly assay was defined as a fly leaving the platform due to a
1941 sudden leg extension. Reaching in the arena assay was defined as when the fly pitches its
1942 body back and reaches with a forward and upward extension of the forelegs, while
1943 staying in the same location. Reaching in the single-fly assay was defined as a head-up
1944 elevation of the long body axis, with both front legs leaving the platform and at least one
1945 leg elevating above a horizontal plane at the level of the dorsal tip of the head. For box
1946 plots, the dividing line in the box indicates the median, the boxes contain the inner
1947 quartile range, the notches give the 95 % confidence interval, the lines extending beyond
1948 the box include 95 % of the data, and the dots beyond those lines are outliers.

1949

1950

1951 **Ca²⁺ imaging, data analysis, and visual stimuli**

1952

1953 All flies used for calcium imaging experiments were reared under standard
1954 conditions (25 °C, 60 % humidity, 12 h light/12 h dark, standard cornmeal/molasses
1955 food), and all imaging experiments were performed on females 3-6 d post-eclosion. To
1956 image from individual lobula columnar cell-types, split-GAL4 driver lines (LC6:
1957 OL0070B, LC16: OL0046B, LC11: OL0015B) were crossed to pJFRC7-20XUAS-IVS-

1958 GCaMP6m in *VK00005* (DL background) effector line. The imaging preparation was
1959 almost identical to that described in (Strother et al., 2014). Briefly, flies were cold
1960 anesthetized and tethered to a fine wire at the thorax using UV-curing adhesive. The two
1961 most anterior legs (T1) were severed and glued down along with the proboscis to prevent
1962 grooming of the eyes and to immobilize the head. Tethered flies were glued by the head
1963 capsule into the fly holder and after addition of saline to the bath, the cuticle at the back
1964 of the head was dissected away to expose the brain. Muscles 1 and 16 were severed to
1965 reduce motion of the brain within the head capsule, and the post-ocular air sac on the
1966 imaged side was removed to expose the optic glomeruli.

1967

1968 The optic glomeruli were imaged using a two-photon microscope (Bruker/Prairie
1969 Ultima IV) with near-infrared excitation (930 nm, Coherent Chameleon Ultra II) and a
1970 60x objective (Nikon CFI APO 60XW). The excitation power was never greater than 20
1971 mW at the sample. Imaging parameters varied slightly between experiments but were
1972 within a small range of our typical acquisition parameters: 128 x 90 pixel resolution, and
1973 10 Hz frame rate (10.0-10.5 Hz). LC cell axon calcium data were collected from single
1974 planes selected to capture a consistently large slice of each glomerulus.

1975

1976 Flies were placed in the center of a modular LED display (Reiser and Dickinson,
1977 2008) on which visual stimuli were presented. The display was configured to cover 60 %
1978 of a cylinder, with LEDs subtending 72° in elevation and 216° in azimuth (maximum
1979 pixel size of 2.25°) as seen by the fly in the center of the cylinder. The display consists of
1980 574 nm peak output LEDs (Betlux ultra-green 8x8 LED matrices, #BL-M12A881UG-XX)

1981 covered with a gel filter (LEE #135 Deep Golden Amber) to greatly reduce stimulus
1982 emission at wavelengths that overlap with those of GCaMP emission.

1983

1984 The stimuli were generated using custom MATLAB scripts
1985 (<https://github.com/mmmorimoto/visual-stimuli>). The dark loom stimulus consisted of a
1986 series of 35 disk sizes, with the edge pixel intensity interpolated to approximate a circle
1987 on the LED screen. The luminance-matched stimulus was created using the dark looming
1988 disk stimulus, spatially scrambling the location of dark pixels of each frame only within
1989 the area of the final size of the disk. The time series of looming stimuli sizes were
1990 presented based on the classic parameterization for looming stimuli assuming a constant
1991 velocity of approach. The speed of the loom is represented by a single parameter (r/v)
1992 that describes the ratio of the stimulus radius to its approach speed (Gabbiani et al., 1999).
1993 All looming stimuli appear as 4.5° spots and increase to a maximum diameter of 54°. The
1994 experimental protocol consisted of 3 repetitions of each stimulus type presented using a
1995 randomized block trial structure.

1996

1997 Data analysis was performed with software written in MATLAB. Motion
1998 compensation was performed by cross-correlating each frame to a reference image, using
1999 software written by James Strother
2000 (https://bitbucket.org/jastrother/neuron_image_analysis). The fluorescence signal is
2001 determined within hand-drawn regions of interest selected to tightly enclose the entire
2002 slice of each glomerulus captured within the imaging plane. $\Delta F/F$ is calculated as the
2003 ratio of $(F - F_0) / F_0$, where F is the instantaneous fluorescence signal and F_0 is calculated

2004 as the 10th percentile of the fluorescence signal within a sliding 300 frame window. For
2005 combining responses of individual flies across animals, we normalized the ΔF/F
2006 responses from each individual fly to the 98th percentile of the ΔF/F across all visual
2007 stimuli within one experiment. All responses are the mean of the mean response (across
2008 repeated stimulus presentations) of each of 5 flies. Error bars indicate mean ± SEM. All
2009 significance results presented for Ca²⁺ imaging were determined with the Mann-Whitney
2010 test.

2011

2012

2013

2014 **Acknowledgements**

2015 We thank the Janelia FlyLight Project Team and Teri Ngo for help with brain dissections,
2016 histology and confocal imaging and Janelia Scientific Computing for image processing
2017 and data analysis tools. Heather Dionne made the pJFRC300 construct. Yoshi Aso shared
2018 an early version of the arena assay and Steve Sawtelle, Igor Negashov and Jinyang Liu
2019 made improvements to this apparatus. Ji-Young Kim provided the arena used for the
2020 stochastic activation experiments. We also thank William Rowell for technical assistance,
2021 James Strother for the Ca²⁺ imaging software, Tom Clandinin for the *norpA* flies,
2022 Zhiyong Liu, Rajyashree Sen, Yoshi Aso and Wyatt Korff for advice, Kei Ito, Alice
2023 Robie, Kristin Branson, Ines Ribeiro and Barry Dickson for communicating unpublished
2024 results, Axel Borst for comments on the manuscript, Andrew Straw and colleagues for
2025 agreeing to a shared nomenclature for the LC cell types and Crystal Di Pietro for
2026 administrative assistance.

2027

2028 **References**

- 2029 Aptekar, J.W., Keles, M.F., Lu, P.M., Zolotova, N.M., and Frye, M.A. (2015). Neurons forming
2030 optic glomeruli compute figure-ground discriminations in *Drosophila*. *The Journal of*
2031 *neuroscience : the official journal of the Society for Neuroscience* **35**, 7587-7599.
- 2032 Aptekar, J.W., Shoemaker, P.A., and Frye, M.A. (2012). Figure tracking by flies is supported by
2033 parallel visual streams. *Current biology : CB* **22**, 482-487.
- 2034 Aso, Y., Hattori, D., Yu, Y., Johnston, R.M., Iyer, N.A., Ngo, T.T., Dionne, H., Abbott, L., Axel, R.,
2035 Tanimoto, H., *et al.* (2014a). The neuronal architecture of the mushroom body provides a logic
2036 for associative learning. *eLife* **3**.
- 2037 Aso, Y., Sitaraman, D., Ichinose, T., Kaun, K.R., Vogt, K., Belliart-Guerin, G., Placais, P.Y., Robie,
2038 A.A., Yamagata, N., Schnaitmann, C., *et al.* (2014b). Mushroom body output neurons encode
2039 valence and guide memory-based action selection in *Drosophila*. *eLife* **3**.
- 2040 Bahl, A., Ammer, G., Schilling, T., and Borst, A. (2013). Object tracking in motion-blind flies.
2041 *Nature neuroscience* **16**, 730-738.
- 2042 Bidaye, S.S., Machacek, C., Wu, Y., and Dickson, B.J. (2014). Neuronal control of *Drosophila*
2043 walking direction. *Science* **344**, 97-101.
- 2044 Borst, A. (2014). Fly visual course control: behaviour, algorithms and circuits. *Nature reviews*
2045 *Neuroscience* **15**, 590-599.
- 2046 Borst, A., Haag, J., and Reiff, D.F. (2010). Fly motion vision. *Annu Rev Neurosci* **33**, 49-70.
- 2047 Burrows, M., and Rowell, C.H.F. (1973). Connections between Descending Visual Interneurons
2048 and Metathoracic Motoneurons in Locust. *J Comp Physiol* **85**, 221-234.
- 2049 Card, G., and Dickinson, M. (2008a). Performance trade-offs in the flight initiation of *Drosophila*.
2050 *The Journal of experimental biology* **211**, 341-353.
- 2051 Card, G., and Dickinson, M.H. (2008b). Visually mediated motor planning in the escape response
2052 of *Drosophila*. *Current biology : CB* **18**, 1300-1307.
- 2053 Card, G.M. (2012). Escape behaviors in insects. *Current opinion in neurobiology* **22**, 180-186.
- 2054 Chen, S., Lee, A.Y., Bowens, N.M., Huber, R., and Kravitz, E.A. (2002). Fighting fruit flies: a model
2055 system for the study of aggression. *Proc Natl Acad Sci U S A* **99**, 5664-5668.
- 2056 Chen, T.W., Wardill, T.J., Sun, Y., Pulver, S.R., Renninger, S.L., Baohan, A., Schreiter, E.R., Kerr,
2057 R.A., Orger, M.B., Jayaraman, V., *et al.* (2013). Ultrasensitive fluorescent proteins for imaging
2058 neuronal activity. *Nature* **499**, 295-300.
- 2059 Chiang, A.S., Lin, C.Y., Chuang, C.C., Chang, H.M., Hsieh, C.H., Yeh, C.W., Shih, C.T., Wu, J.J.,
2060 Wang, G.T., Chen, Y.C., *et al.* (2011). Three-dimensional reconstruction of brain-wide wiring
2061 networks in *Drosophila* at single-cell resolution. *Current biology : CB* **21**, 1-11.
- 2062 Coen, P., Xie, M., Clemens, J., and Murthy, M. (2016). Sensorimotor Transformations Underlying
2063 Variability in Song Intensity during *Drosophila* Courtship. *Neuron* **89**, 629-644.
- 2064 Costa, M., Manton, J.D., Ostrovsky, A.D., Prohaska, S., and Jefferis, G.S. (2016). NBLAST: Rapid,
2065 Sensitive Comparison of Neuronal Structure and Construction of Neuron Family Databases.
2066 *Neuron* **91**, 293-311.
- 2067 de Vries, S.E., and Clandinin, T.R. (2012). Loom-sensitive neurons link computation to action in
2068 the *Drosophila* visual system. *Current biology : CB* **22**, 353-362.

- 2069 Douglass, J.K., and Strausfeld, N.J. (1998). Functionally and anatomically segregated visual
2070 pathways in the lobula complex of a calliphorid fly. *The Journal of comparative neurology* 396,
2071 84-104.
- 2072 Egelhaaf, M. (1985a). On the neuronal basis of figure-ground discrimination by relative motion
2073 in the visual system of the fly. I. Behavioural constraints imposed on the neuronal network and
2074 the role of the optomotor system. *Biol Cybern* 52, 123-140.
- 2075 Egelhaaf, M. (1985b). On the neuronal basis of figure-ground discrimination by relative motion
2076 in the visual system of the fly. II. Figure-detection cells, a new class of visual interneurones. *Biol*
2077 *Cybern* 52, 195-209.
- 2078 Egelhaaf, M. (1985c). On the neuronal basis of figure-ground discrimination by relative motion
2079 in the visual system of the fly. III. Possible input circuitries and behavioural significance of the
2080 FD-cells. *Biol Cybern* 52, 267-280.
- 2081 Ernst, R., and Heisenberg, M. (1999). The memory template in *Drosophila* pattern vision at the
2082 flight simulator. *Vision Res* 39, 3920-3933.
- 2083 Fischbach, K.F., and Dittrich, A.P.M. (1989). The optic lobe of *Drosophila melanogaster*. I. A Golgi
2084 analysis of wild-type structure. *Cell and Tissue Research* 258, 441-475.
- 2085 Flood, T.F., Iguchi, S., Gorczyca, M., White, B., Ito, K., and Yoshihara, M. (2013). A single pair of
2086 interneurons commands the *Drosophila* feeding motor program. *Nature* 499, 83-87.
- 2087 Fotowat, H., Fayyazuddin, A., Bellen, H.J., and Gabbiani, F. (2009). A novel neuronal pathway for
2088 visually guided escape in *Drosophila melanogaster*. *J Neurophysiol* 102, 875-885.
- 2089 Fotowat, H., and Gabbiani, F. (2011). Collision detection as a model for sensory-motor
2090 integration. *Annu Rev Neurosci* 34, 1-19.
- 2091 Fotowat, H., Harrison, R.R., and Gabbiani, F. (2011). Multiplexing of motor information in the
2092 discharge of a collision detecting neuron during escape behaviors. *Neuron* 69, 147-158.
- 2093 Gabbiani, F., Krapp, H.G., and Laurent, G. (1999). Computation of object approach by a wide-
2094 field, motion-sensitive neuron. *The Journal of neuroscience : the official journal of the Society*
2095 for Neuroscience
- 2096 Gao, S., Takemura, S.Y., Ting, C.Y., Huang, S., Lu, Z., Luan, H., Rister, J., Thum, A.S., Yang, M.,
2097 Hong, S.T., et al. (2008). The neural substrate of spectral preference in *Drosophila*. *Neuron* 60,
2098 328-342.
- 2099 Gaudry, Q., Hong, E.J., Kain, J., de Bivort, B.L., and Wilson, R.I. (2013). Asymmetric
2100 neurotransmitter release enables rapid odour lateralization in *Drosophila*. *Nature* 493, 424-428.
- 2101 Gollisch, T., and Meister, M. (2010). Eye smarter than scientists believed: neural computations in
2102 circuits of the retina. *Neuron* 65, 150-164.
- 2103 Gotz, K.G. (1980). Visual guidance in *Drosophila*. *Basic Life Sci* 16, 391-407.
- 2104 Hassan, B.A., Birmingham, N.A., He, Y., Sun, Y., Jan, Y.N., Zoghbi, H.Y., and Bellen, H.J. (2000).
2105 atonal regulates neurite arborization but does not act as a proneural gene in the *Drosophila*
2106 brain. *Neuron* 25, 549-561.
- 2107 Hausen, K. (1976). Functional Characterization and Anatomical Identification of Motion Sensitive
2108 Neurons in Lobula Plate of Blowfly *Calliphora-Erythrocephala*. *Z Naturforsch C* 31, 629-&.
- 2109 Hausen, K. (1982a). Motion Sensitive Interneurons in the Optomotor System of the Fly .1. The
2110 Horizontal Cells - Structure and Signals. *Biol Cybern* 45, 143-156.
- 2111 Hausen, K. (1982b). Motion Sensitive Interneurons in the Optomotor System of the Fly .2. The
2112 Horizontal Cells - Receptive-Field Organization and Response Characteristics. *Biol Cybern* 46, 67-
2113 79.
- 2114 Heisenberg, M., and Wolf, R. (1984). Vision in *Drosophila*. *Genetics of Microbehavior*, Vol 12
2115 (Springer Berlin Heidelberg).

- 2116 Holmqvist, M.H. (1994). A visually elicited escape response in the fly that does not use the giant
2117 fiber pathway. *Vis Neurosci* 11, 1149-1161.
- 2118 Holmqvist, M.H., and Srinivasan, M.V. (1991). A visually evoked escape response of the housefly.
2119 *Journal of comparative physiology A, Sensory, neural, and behavioral physiology* 169, 451-459.
- 2120 Ito, K., Shinomiya, K., Ito, M., Armstrong, J.D., Boyan, G., Hartenstein, V., Harzsch, S., Heisenberg,
2121 M., Homberg, U., Jenett, A., et al. (2014). A systematic nomenclature for the insect brain.
2122 *Neuron* 81, 755-765.
- 2123 Ito, M., Masuda, N., Shinomiya, K., Endo, K., and Ito, K. (2013). Systematic analysis of neural
2124 projections reveals clonal composition of the Drosophila brain. *Current biology : CB* 23, 644-655.
- 2125 Jenett, A., Rubin, G.M., Ngo, T.T., Shepherd, D., Murphy, C., Dionne, H., Pfeiffer, B.D., Cavallaro,
2126 A., Hall, D., Jeter, J., et al. (2012). A GAL4-driver line resource for Drosophila neurobiology. *Cell*
2127 *reports* 2, 991-1001.
- 2128 Karuppudurai, T., Lin, T.Y., Ting, C.Y., Pursley, R., Melnattur, K.V., Diao, F., White, B.H.,
2129 Macpherson, L.J., Gallio, M., Pohida, T., et al. (2014). A hard-wired glutamatergic circuit pools
2130 and relays UV signals to mediate spectral preference in Drosophila. *Neuron* 81, 603-615.
- 2131 Klapoetke, N.C., Murata, Y., Kim, S.S., Pulver, S.R., Birdsey-Benson, A., Cho, Y.K., Morimoto, T.K.,
2132 Chuong, A.S., Carpenter, E.J., Tian, Z., et al. (2014). Independent optical excitation of distinct
2133 neural populations. *Nature methods* 11, 338-346.
- 2134 Krapp, H.G., Hengstenberg, B., and Hengstenberg, R. (1998). Dendritic structure and receptive-
2135 field organization of optic flow processing interneurons in the fly. *J Neurophysiol* 79, 1902-1917.
- 2136 Kvon, E.Z., Kazmar, T., Stampfel, G., Yanez-Cuna, J.O., Pagani, M., Schernhuber, K., Dickson, B.J.,
2137 and Stark, A. (2014). Genome-scale functional characterization of Drosophila developmental
2138 enhancers *in vivo*. *Nature* 512, 91-95.
- 2139 Laissue, P.P., Reiter, C., Hiesinger, P.R., Halter, S., Fischbach, K.F., and Stocker, R.F. (1999).
2140 Three-dimensional reconstruction of the antennal lobe in *Drosophila melanogaster*. *The Journal*
2141 *of comparative neurology* 405, 543-552.
- 2142 Langen, M., Koch, M., Yan, J., De Geest, N., Erfurth, M.L., Pfeiffer, B.D., Schmucker, D., Moreau,
2143 Y., and Hassan, B.A. (2013). Mutual inhibition among postmitotic neurons regulates robustness
2144 of brain wiring in Drosophila. *eLife* 2, e00337.
- 2145 Lettvin, J.Y., Maturana, H.R., McCulloch, W.S., and Pitts, W.H. (1959). What the frog's eye tells
2146 the frog's brain. *Proc Inst Radio Engrs* 47, 1940-1951.
- 2147 Li, H.H., Kroll, J.R., Lennox, S.M., Ogundeyi, O., Jeter, J., Depasquale, G., and Truman, J.W. (2014).
2148 A GAL4 driver resource for developmental and behavioral studies on the larval CNS of
2149 *Drosophila*. *Cell reports* 8, 897-908.
- 2150 Lima, S.Q., and Miesenbock, G. (2005). Remote control of behavior through genetically targeted
2151 photostimulation of neurons. *Cell* 121, 141-152.
- 2152 Lin, T.Y., Luo, J., Shinomiya, K., Ting, C.Y., Lu, Z., Meinertzhagen, I.A., and Lee, C.H. (2016).
2153 Mapping chromatic pathways in the Drosophila visual system. *The Journal of comparative*
2154 *neurology* 524, 213-227.
- 2155 Liu, G., Seiler, H., Wen, A., Zars, T., Ito, K., Wolf, R., Heisenberg, M., and Liu, L. (2006). Distinct
2156 memory traces for two visual features in the Drosophila brain. *Nature* 439, 551-556.
- 2157 Luan, H., Peabody, N.C., Vinson, C.R., and White, B.H. (2006). Refined spatial manipulation of
2158 neuronal function by combinatorial restriction of transgene expression. *Neuron* 52, 425-436.
- 2159 Maimon, G., Straw, A.D., and Dickinson, M.H. (2008). A simple vision-based algorithm for
2160 decision making in flying Drosophila. *Current biology : CB* 18, 464-470.
- 2161 Meinertzhagen, I.A., and Hanson, T.E. (1993). The development of the optic lobe. In *The*
2162 *Development of Drosophila melanogaster*, M. Bate, and A.M. Arias, eds. (Plainview, N.Y.: Cold
2163 Spring Harbor Laboratory Press), pp. 1363-1491.

- 2164 Melnattur, K.V., Pursley, R., Lin, T.Y., Ting, C.Y., Smith, P.D., Pohida, T., and Lee, C.H. (2014).
2165 Multiple redundant medulla projection neurons mediate color vision in *Drosophila*. *Journal of*
2166 *neurogenetics* *28*, 374-388.
- 2167 Mu, L., Ito, K., Bacon, J.P., and Strausfeld, N.J. (2012). Optic glomeruli and their inputs in
2168 *Drosophila* share an organizational ground pattern with the antennal lobes. *The Journal of*
2169 *neuroscience : the official journal of the Society for Neuroscience* *32*, 6061-6071.
- 2170 Muijres, F.T., Elzinga, M.J., Melis, J.M., and Dickinson, M.H. (2014). Flies evade looming targets
2171 by executing rapid visually directed banked turns. *Science* *344*, 172-177.
- 2172 Munch, T.A., da Silveira, R.A., Siegert, S., Viney, T.J., Awatramani, G.B., and Roska, B. (2009).
2173 Approach sensitivity in the retina processed by a multifunctional neural circuit. *Nature*
2174 *neuroscience* *12*, 1308-1316.
- 2175 Nern, A., Pfeiffer, B.D., and Rubin, G.M. (2015). Optimized tools for multicolor stochastic labeling
2176 reveal diverse stereotyped cell arrangements in the fly visual system. *Proc Natl Acad Sci U S A*
2177 *112*, E2967-2976.
- 2178 Nern, A., Pfeiffer, B.D., Svoboda, K., and Rubin, G.M. (2011). Multiple new site-specific
2179 recombinases for use in manipulating animal genomes. *Proc Natl Acad Sci U S A* *108*, 14198-
2180 14203.
- 2181 Nichols, R., and Pak, W.L. (1985). A simple medium for vitamin A deprivation of *Drosophila*
2182 *melanogaster*. *Drosophila Information Service* *61*, 195-196.
- 2183 Ofstad, T.A., Zuker, C.S., and Reiser, M.B. (2011). Visual place learning in *Drosophila*
2184 *melanogaster*. *Nature* *474*, 204-207.
- 2185 Orfanidis, S.J. (1996). In *Introduction to signal processing* (Englewood Cliffs, N.J.: Prentice Hall).
- 2186 Otsuna, H., and Ito, K. (2006). Systematic analysis of the visual projection neurons of *Drosophila*
2187 *melanogaster*. I. Lobula-specific pathways. *The Journal of comparative neurology* *497*, 928-958.
- 2188 Otsuna, H., Shinomiya, K., and Ito, K. (2014). Parallel neural pathways in higher visual centers of
2189 the *Drosophila* brain that mediate wavelength-specific behavior. *Front Neural Circuits* *8*, 8.
- 2190 Panser, K., Tirian, L., Schulze, F., Villalba, S., Jefferis, G.S., Buhler, K., and Straw, A.D. (2016).
2191 Automatic Segmentation of *Drosophila* Neural Compartments Using GAL4 Expression Data
2192 Reveals Novel Visual Pathways. *Current biology : CB*.
- 2193 Parigi, A., Porter, C., Cermak, M., Pitchers, W.R., and Dworkin, I. (2014). How predator hunting-
2194 modes affect prey behaviour: Capture deterrence in *Drosophila melanogaster*. *bioRxiv*.
- 2195 Peng, H., Ruan, Z., Long, F., Simpson, J.H., and Myers, E.W. (2010). V3D enables real-time 3D
2196 visualization and quantitative analysis of large-scale biological image data sets. *Nature*
2197 *biotechnology* *28*, 348-353.
- 2198 Pfeiffer, B.D., Ngo, T.T., Hibbard, K.L., Murphy, C., Jenett, A., Truman, J.W., and Rubin, G.M.
2199 (2010). Refinement of tools for targeted gene expression in *Drosophila*. *Genetics* *186*, 735-755.
- 2200 Pfeiffer, K., and Homberg, U. (2014). Organization and functional roles of the central complex in
2201 the insect brain. *Annual review of entomology* *59*, 165-184.
- 2202 Pfeiffer, K., Kinoshita, M., and Homberg, U. (2005). Polarization-sensitive and light-sensitive
2203 neurons in two parallel pathways passing through the anterior optic tubercle in the locust brain.
2204 *J Neurophysiol* *94*, 3903-3915.
- 2205 Pick, S., and Strauss, R. (2005). Goal-driven behavioral adaptations in gap-climbing *Drosophila*.
2206 *Current biology : CB* *15*, 1473-1478.
- 2207 Reichardt, W., and Wenking, H. (1969). Optical detection and fixation of objects by fixed flying
2208 flies. *Naturwissenschaften* *56*, 424-425.
- 2209 Reiser, M.B., and Dickinson, M.H. (2008). A modular display system for insect behavioral
2210 neuroscience. *J Neurosci Methods* *167*, 127-139.

- 2211 Reiser, M.B., and Dickinson, M.H. (2010). Drosophila fly straight by fixating objects in the face of
2212 expanding optic flow. *The Journal of experimental biology* **213**, 1771-1781.
- 2213 Robie, A.A., Straw, A.D., and Dickinson, M.H. (2010). Object preference by walking fruit flies,
2214 *Drosophila melanogaster*, is mediated by vision and graviperception. *The Journal of*
2215 *experimental biology* **213**, 2494-2506.
- 2216 Sanes, J.R., and Zipursky, S.L. (2010). Design principles of insect and vertebrate visual systems.
2217 *Neuron* **66**, 15-36.
- 2218 Schilling, T., and Borst, A. (2015). Local motion detectors are required for the computation of
2219 expansion flow-fields. *Biology open* **4**, 1105-1108.
- 2220 Seelig, J.D., and Jayaraman, V. (2013). Feature detection and orientation tuning in the
2221 *Drosophila* central complex. *Nature* **503**, 262-266.
- 2222 Strausfeld, N.J. (1976). *Atlas of an insect brain* (Springer Berlin Heidelberg).
- 2223 Strausfeld, N.J., and Bassemir, U.K. (1983). Cobalt-coupled neurons of a giant fibre system in
2224 Diptera. *J Neurocytol* **12**, 971-991.
- 2225 Strausfeld, N.J., and Okamura, J.Y. (2007). Visual system of calliphorid flies: organization of optic
2226 glomeruli and their lobula complex efferents. *The Journal of comparative neurology* **500**, 166-
2227 188.
- 2228 Strausfeld, N.J., Sinakevitch, I., and Okamura, J.Y. (2007). Organization of local interneurons in
2229 optic glomeruli of the dipterous visual system and comparisons with the antennal lobes. *Dev*
2230 *Neurobiol* **67**, 1267-1288.
- 2231 Strother, J.A., Nern, A., and Reiser, M.B. (2014). Direct observation of ON and OFF pathways in
2232 the *Drosophila* visual system. *Current biology : CB* **24**, 976-983.
- 2233 Struhl, G., and Basler, K. (1993). Organizing activity of wingless protein in *Drosophila*. *Cell* **72**,
2234 527-540.
- 2235 Takemura, S.Y., Bharioke, A., Lu, Z., Nern, A., Vitaladevuni, S., Rivlin, P.K., Katz, W.T., Olbris, D.J.,
2236 Plaza, S.M., Winston, P., et al. (2013). A visual motion detection circuit suggested by *Drosophila*
2237 connectomics. *Nature* **500**, 175-181.
- 2238 Tammero, L.F., and Dickinson, M.H. (2002). Collision-avoidance and landing responses are
2239 mediated by separate pathways in the fruit fly, *Drosophila melanogaster*. *The Journal of*
2240 *experimental biology* **205**, 2785-2798.
- 2241 Tang, S., Wolf, R., Xu, S., and Heisenberg, M. (2004). Visual pattern recognition in *Drosophila* is
2242 invariant for retinal position. *Science* **305**, 1020-1022.
- 2243 Tuthill, J.C., Nern, A., Holtz, S.L., Rubin, G.M., and Reiser, M.B. (2013). Contributions of the 12
2244 neuron classes in the fly lamina to motion vision. *Neuron* **79**, 128-140.
- 2245 Viswanathan, S., Williams, M.E., Bloss, E.B., Stasevich, T.J., Speer, C.M., Nern, A., Pfeiffer, B.D.,
2246 Hooks, B.M., Li, W.P., English, B.P., et al. (2015). High-performance probes for light and electron
2247 microscopy. *Nature methods* **12**, 568-576.
- 2248 von Philipsborn, A.C., Liu, T., Yu, J.Y., Masser, C., Bidaye, S.S., and Dickson, B.J. (2011). Neuronal
2249 control of *Drosophila* courtship song. *Neuron* **69**, 509-522.
- 2250 von Reyn, C.R., Breads, P., Peek, M.Y., Zheng, G.Z., Williamson, W.R., Yee, A.L., Leonardo, A., and
2251 Card, G.M. (2014). A spike-timing mechanism for action selection. *Nature neuroscience* **17**, 962-
2252 970.
- 2253 Wagh, D.A., Rasse, T.M., Asan, E., Hofbauer, A., Schwenkert, I., Durrbeck, H., Buchner, S.,
2254 Dabauvalle, M.C., Schmidt, M., Qin, G., et al. (2006). Bruchpilot, a protein with homology to
2255 ELKS/CAST, is required for structural integrity and function of synaptic active zones in *Drosophila*.
2256 *Neuron* **49**, 833-844.

- 2257 Wan, Y., Otsuna, H., Chien, C.B., and Hansen, C. (2012). FluoRender: An Application of 2D Image
2258 Space Methods for 3D and 4D Confocal Microscopy Data Visualization in Neurobiology Research.
2259 IEEE Pac Vis Symp, 201-208.
- 2260 Warrant, E.J. (2016). Sensory matched filters. *Current biology : CB* 26, R976-R980.
- 2261 Wehner, R. (1987). Matched-Filters - Neural Models of the External World. *Journal of*
2262 *Comparative Physiology a-Neuroethology Sensory Neural and Behavioral Physiology* 161, 511-
2263 531.
- 2264 Weir, P.T., and Dickinson, M.H. (2015). Functional divisions for visual processing in the central
2265 brain of flying Drosophila. *Proc Natl Acad Sci U S A* 112, E5523-5532.
- 2266 Wolff, T., and Ready, D.F. (1993). Pattern formation in the Drosophila retina. *In: The*
2267 *development of Drosophila melanogaster. eds Bate M, Martinez-Arias A (Cold Spring Harbor Lab*
2268 *Press, Plainview, NY).*
- 2269 Wyman, R.J., Thomas, J.B., Salkoff, L., and King, D.G. (1984). The *Drosophila* giant fiber system.
2270 *In: Neural Mechanisms of Startle Behavior, edited by Robert C. Eaton. New York: Plenum Press,*
2271 *1984, 133-161.*
- 2272 Yilmaz, M., and Meister, M. (2013). Rapid innate defensive responses of mice to looming visual
2273 stimuli. *Current biology : CB* 23, 2011-2015.
- 2274 Zhang, Y., Kim, I.J., Sanes, J.R., and Meister, M. (2012). The most numerous ganglion cell type of
2275 the mouse retina is a selective feature detector. *Proc Natl Acad Sci U S A* 109, E2391-2398.

2276

2277

Figure 1

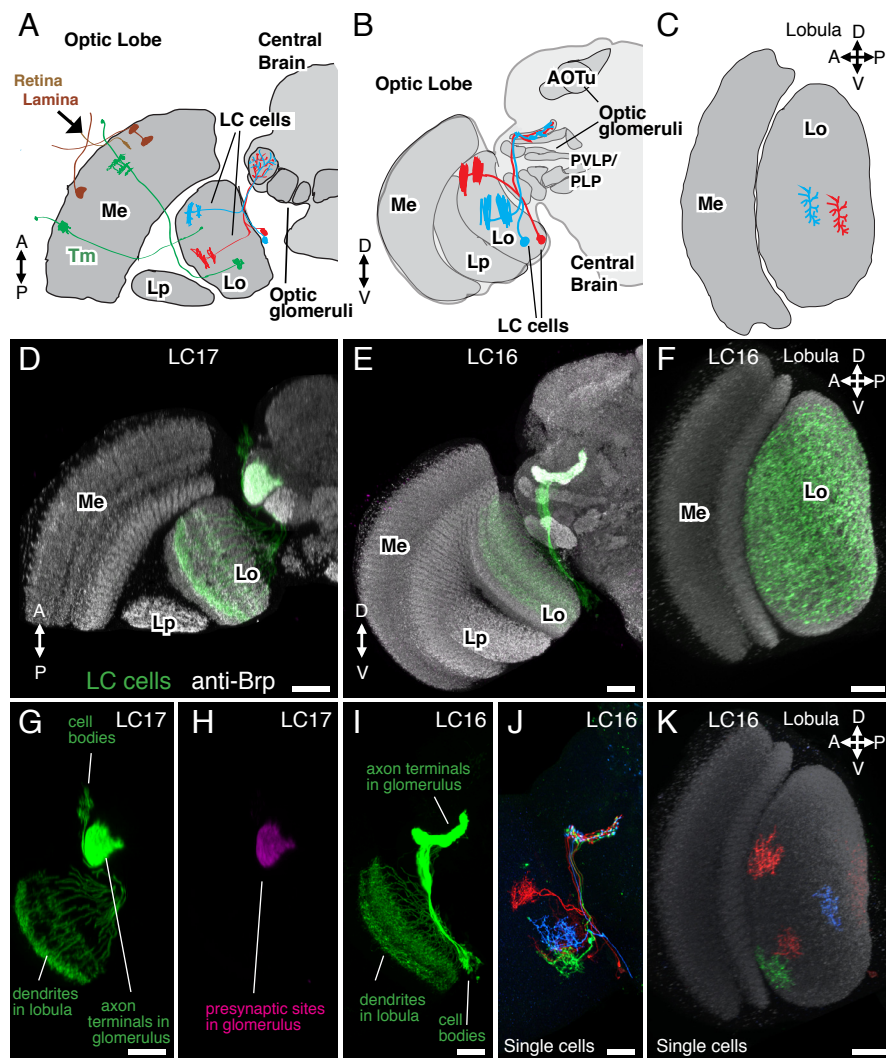


Figure 1 - figure supplement 1

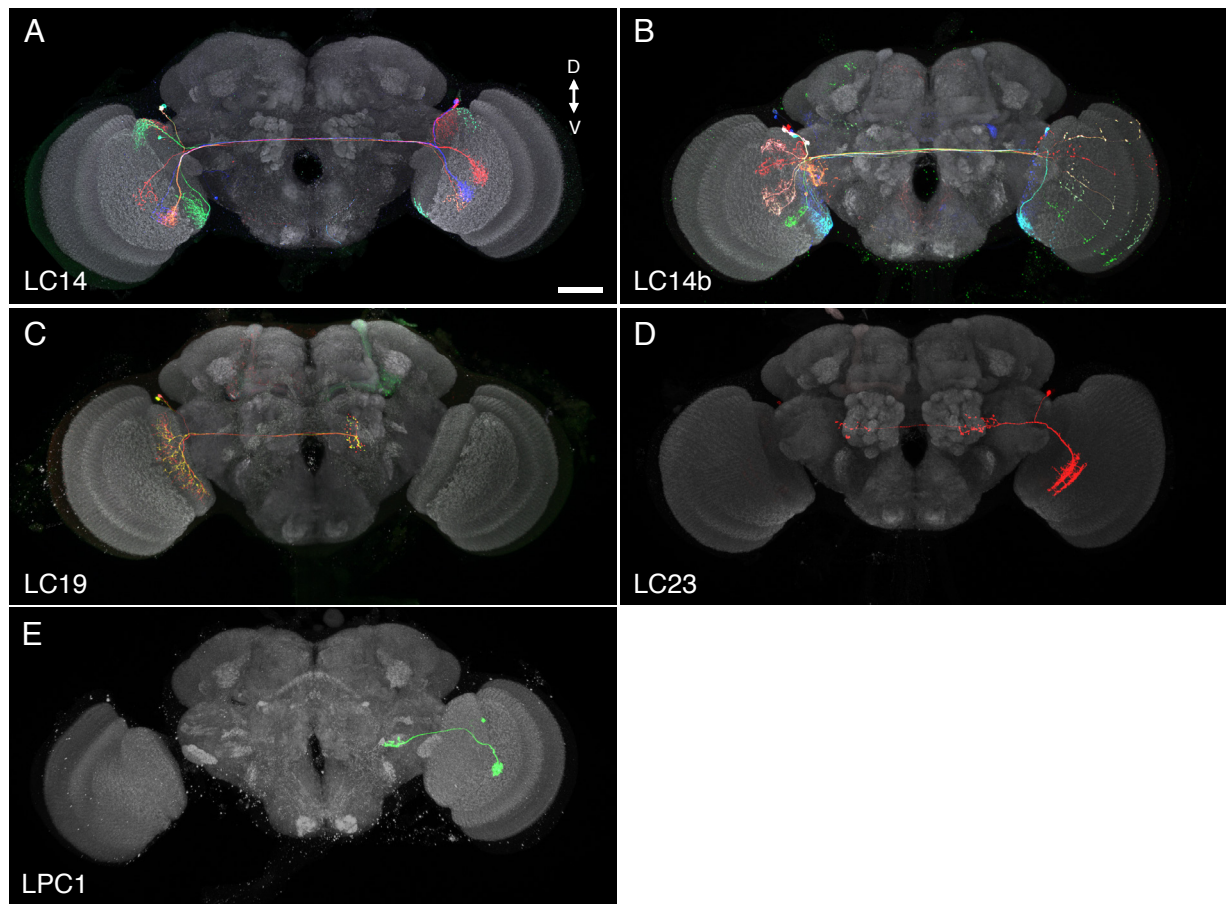


Figure 2

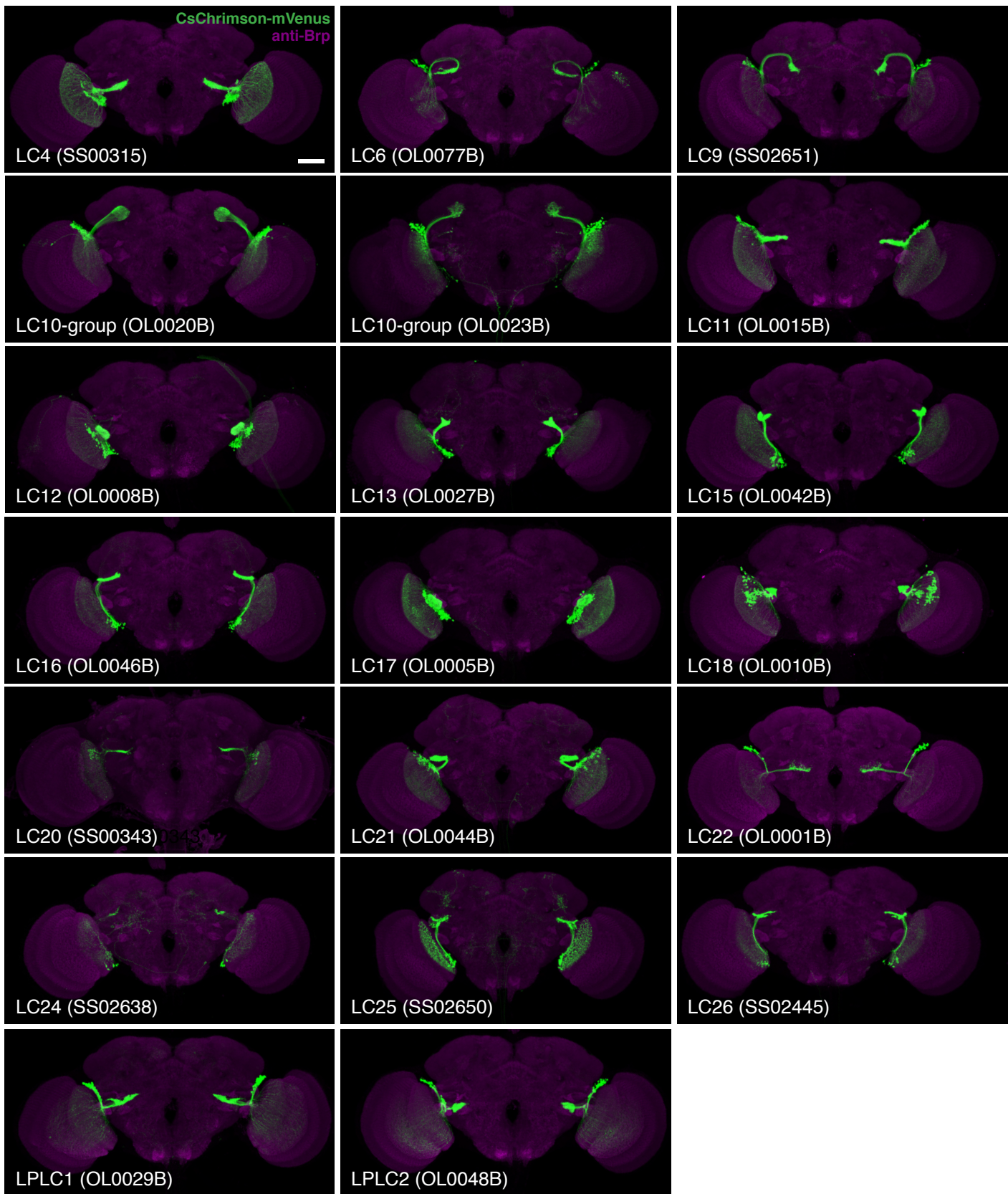


Figure 2 - figure supplement 1

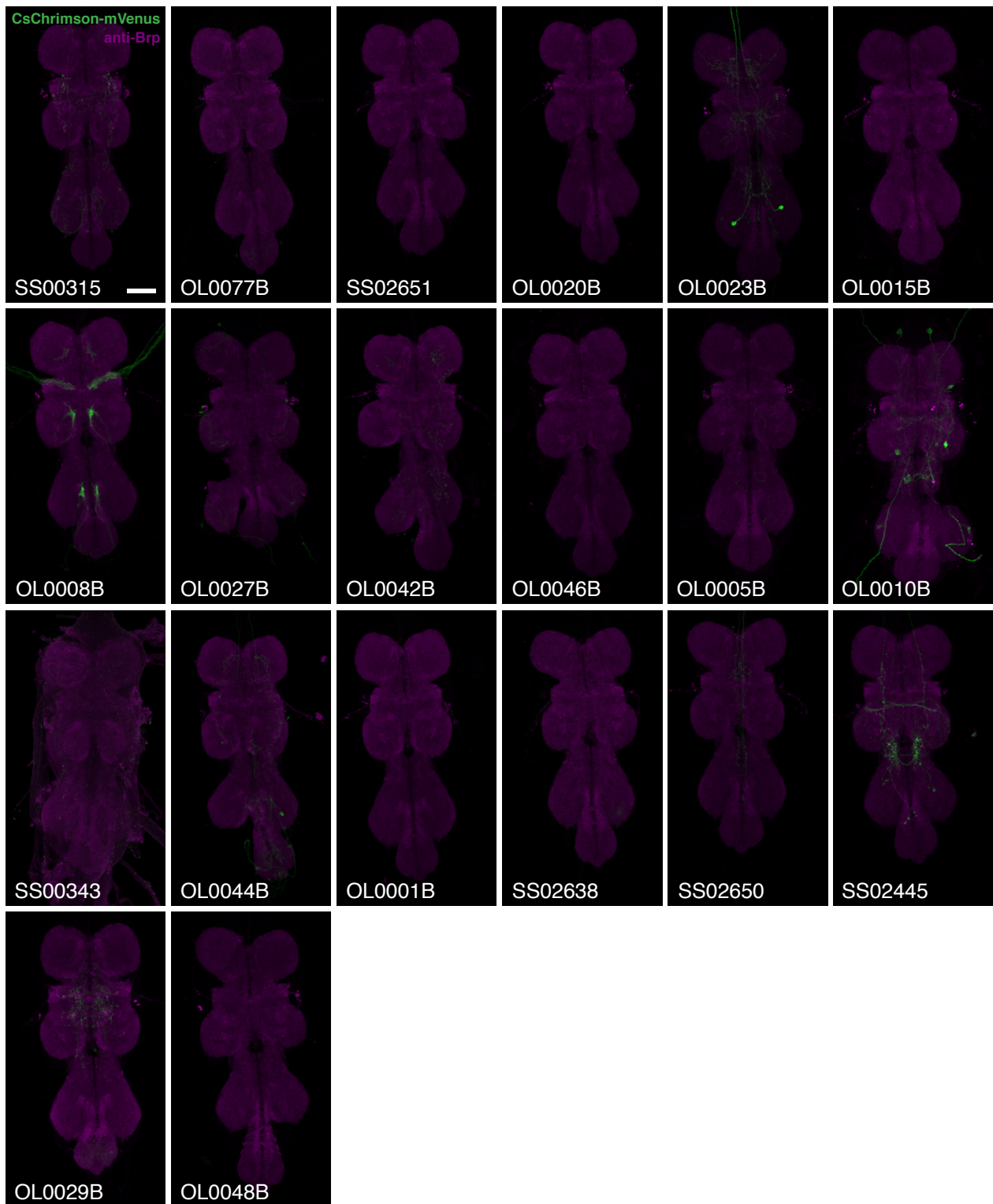


Figure 3

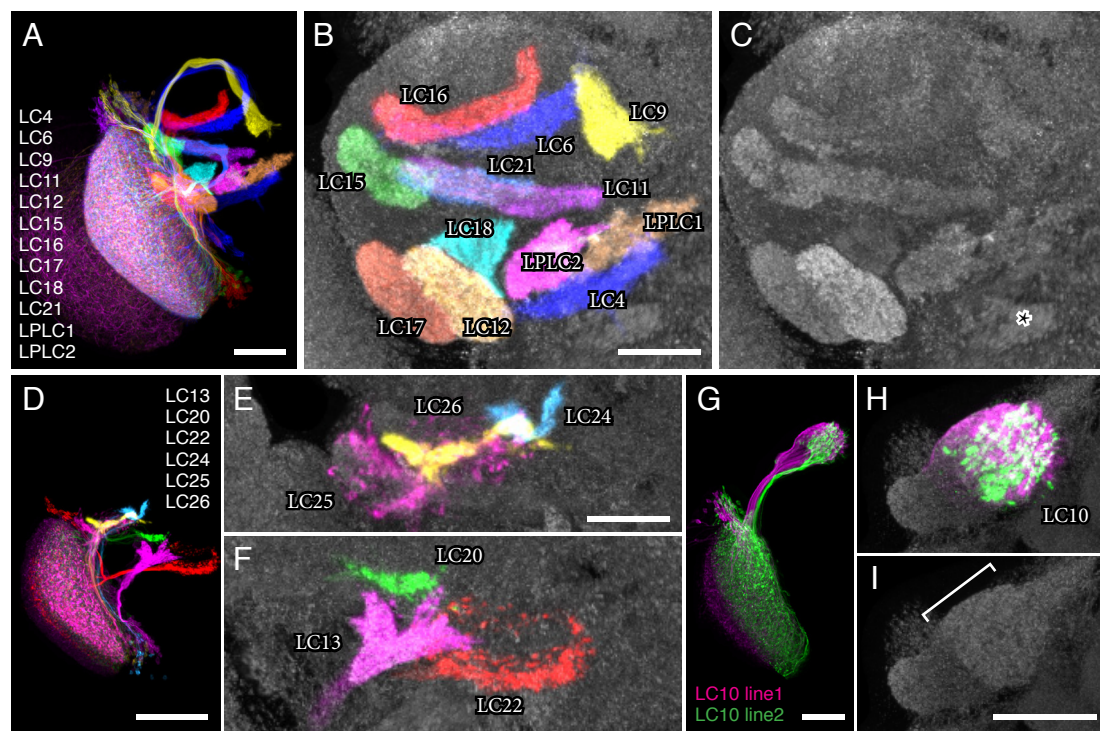


Figure 3 - figure supplement 1

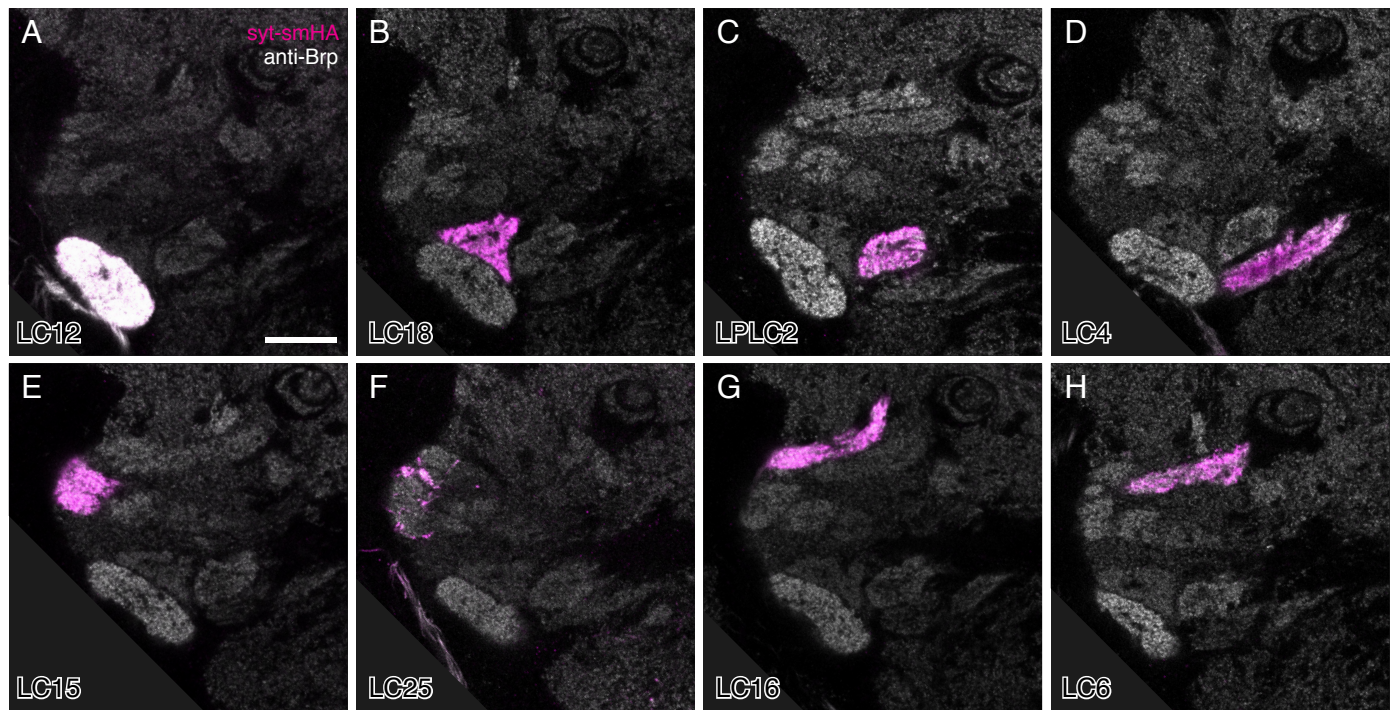


Figure 3 - figure supplement 2

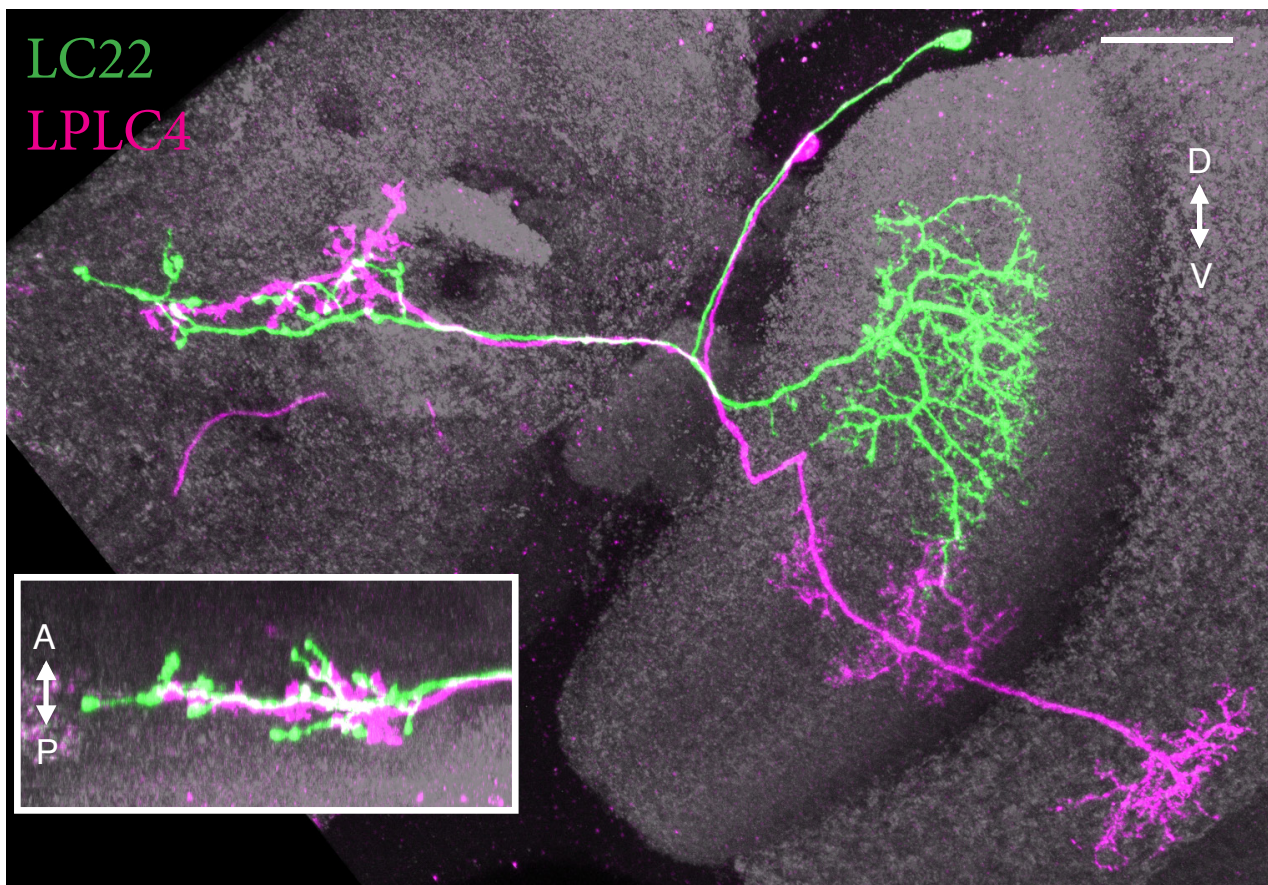


Figure 4

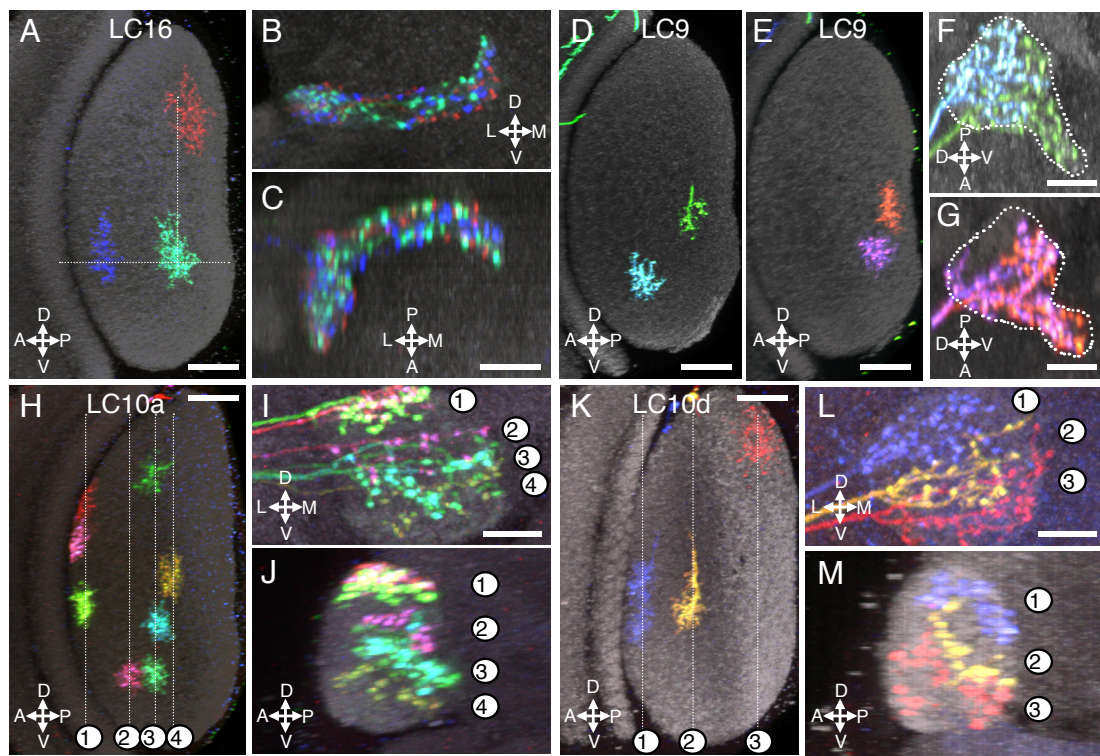


Figure 4 - figure supplement 1

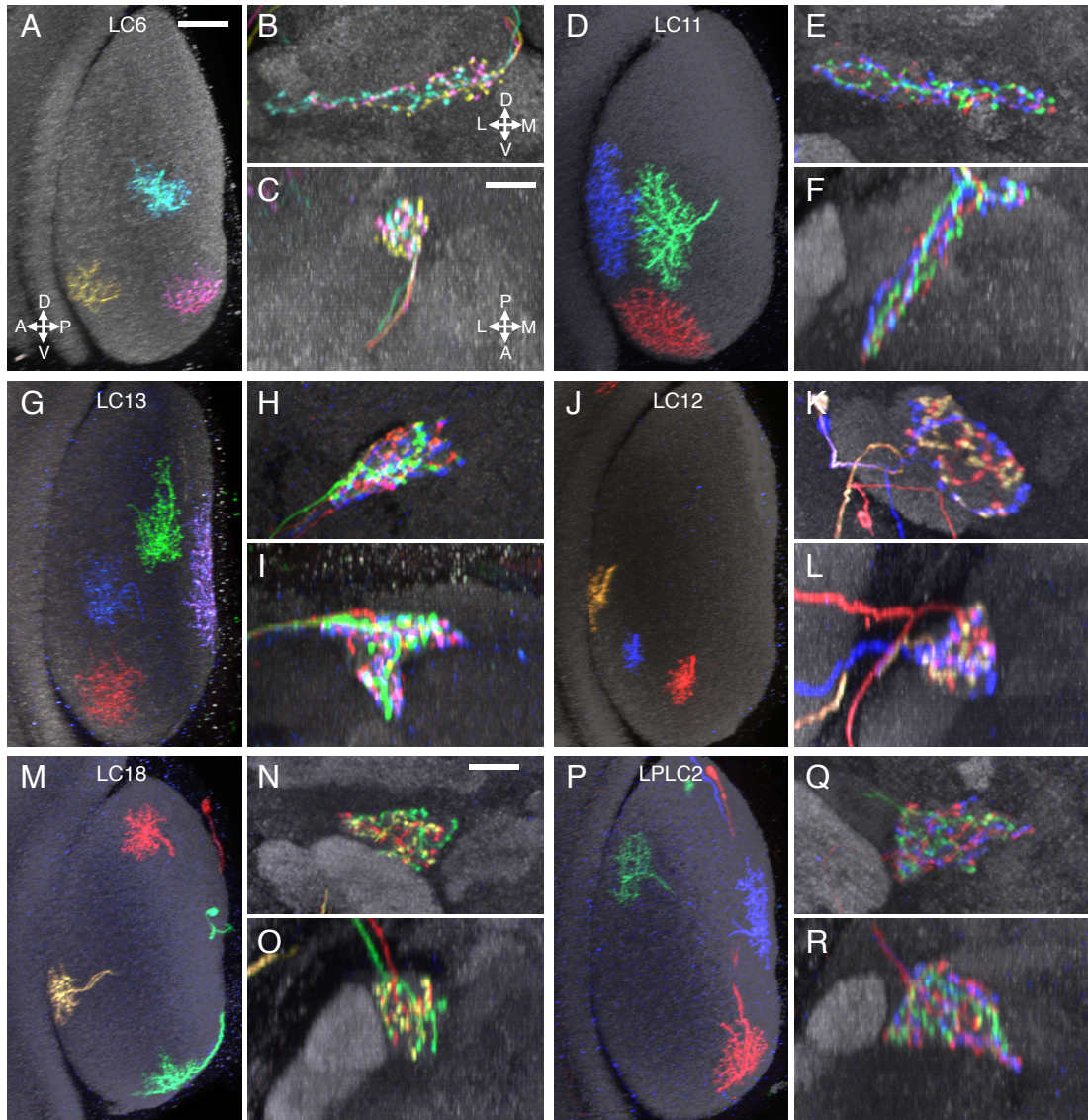


Figure 5

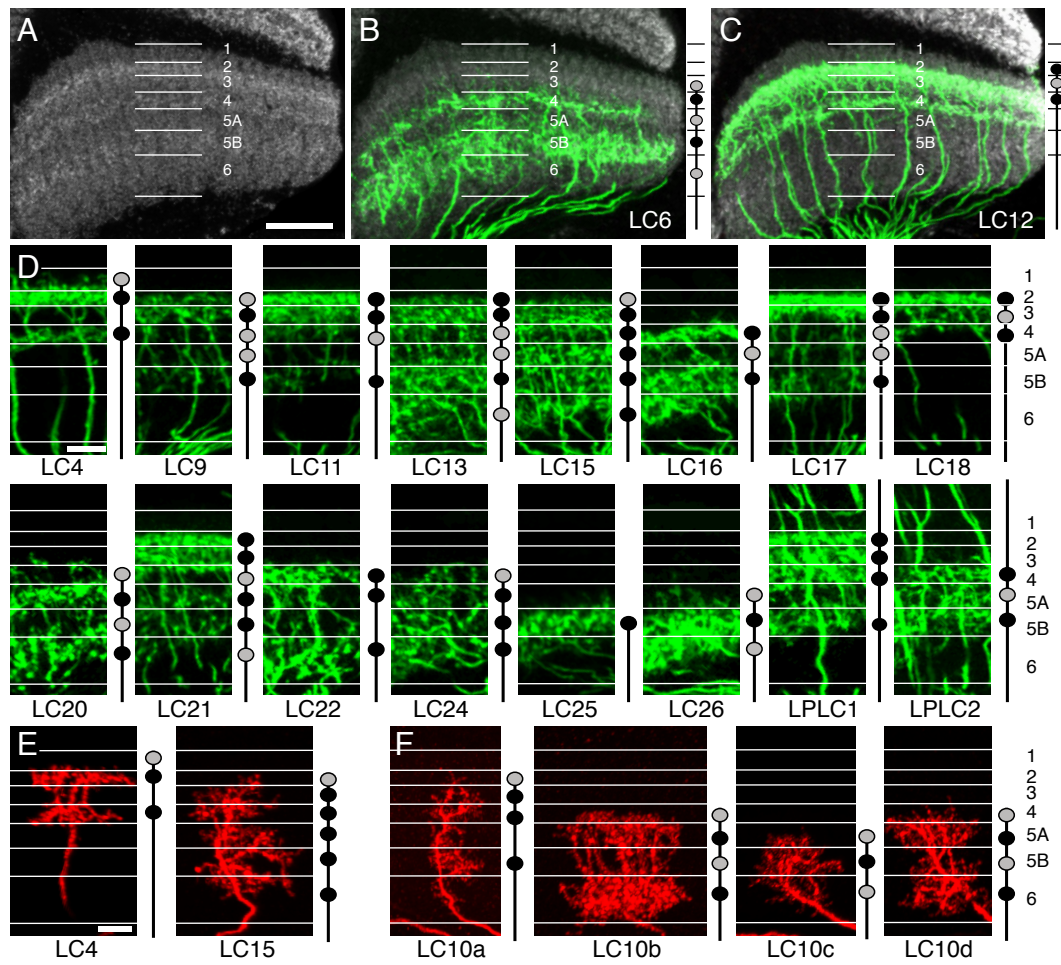


Figure 5 - figure supplement 1

A

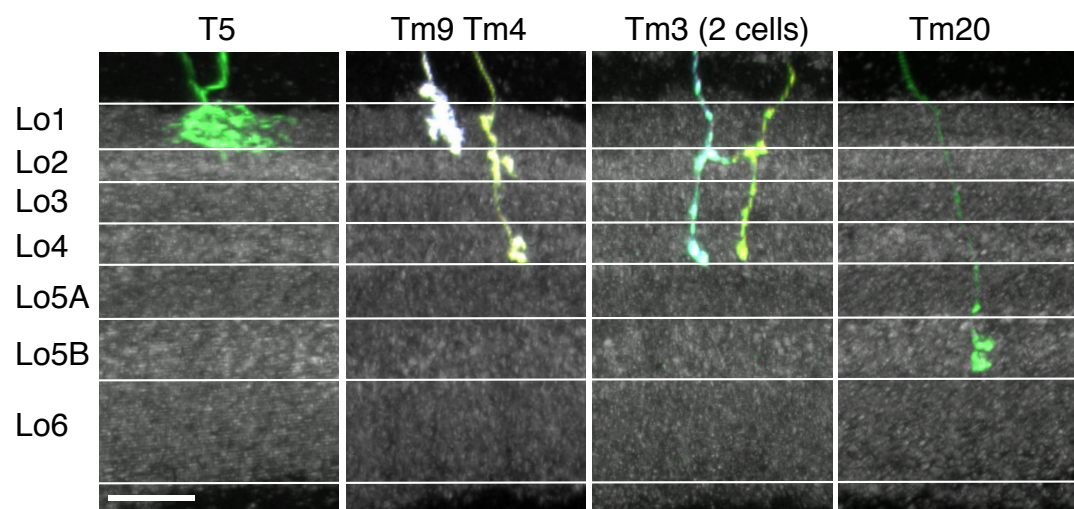


Figure 5 - figure supplement 2

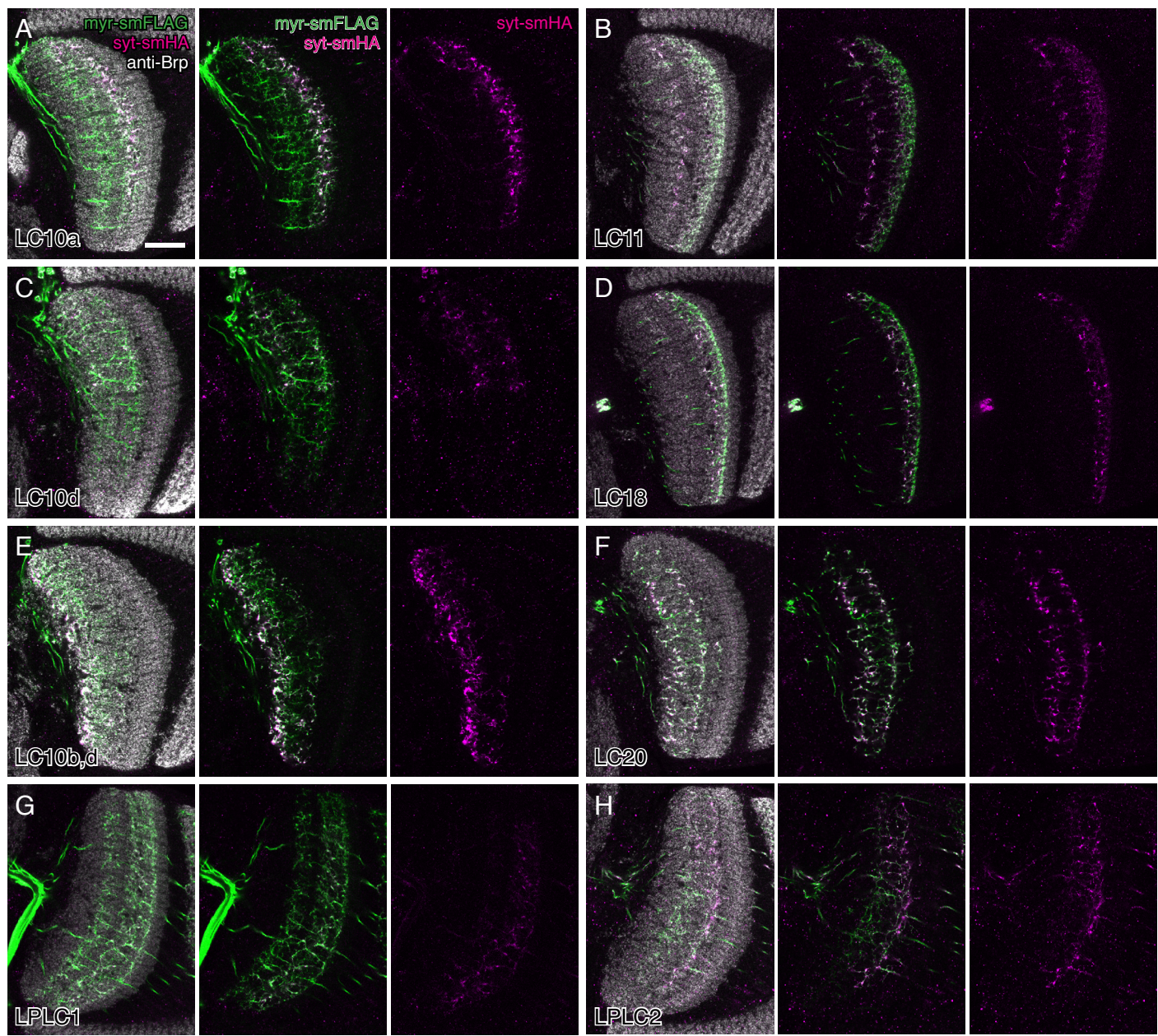


Figure 6

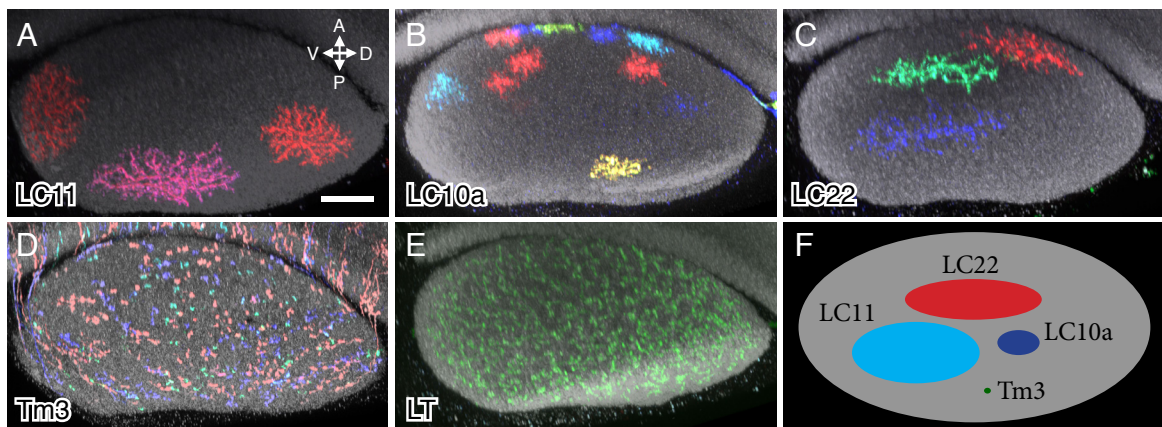


Figure 6 - figure supplement 1

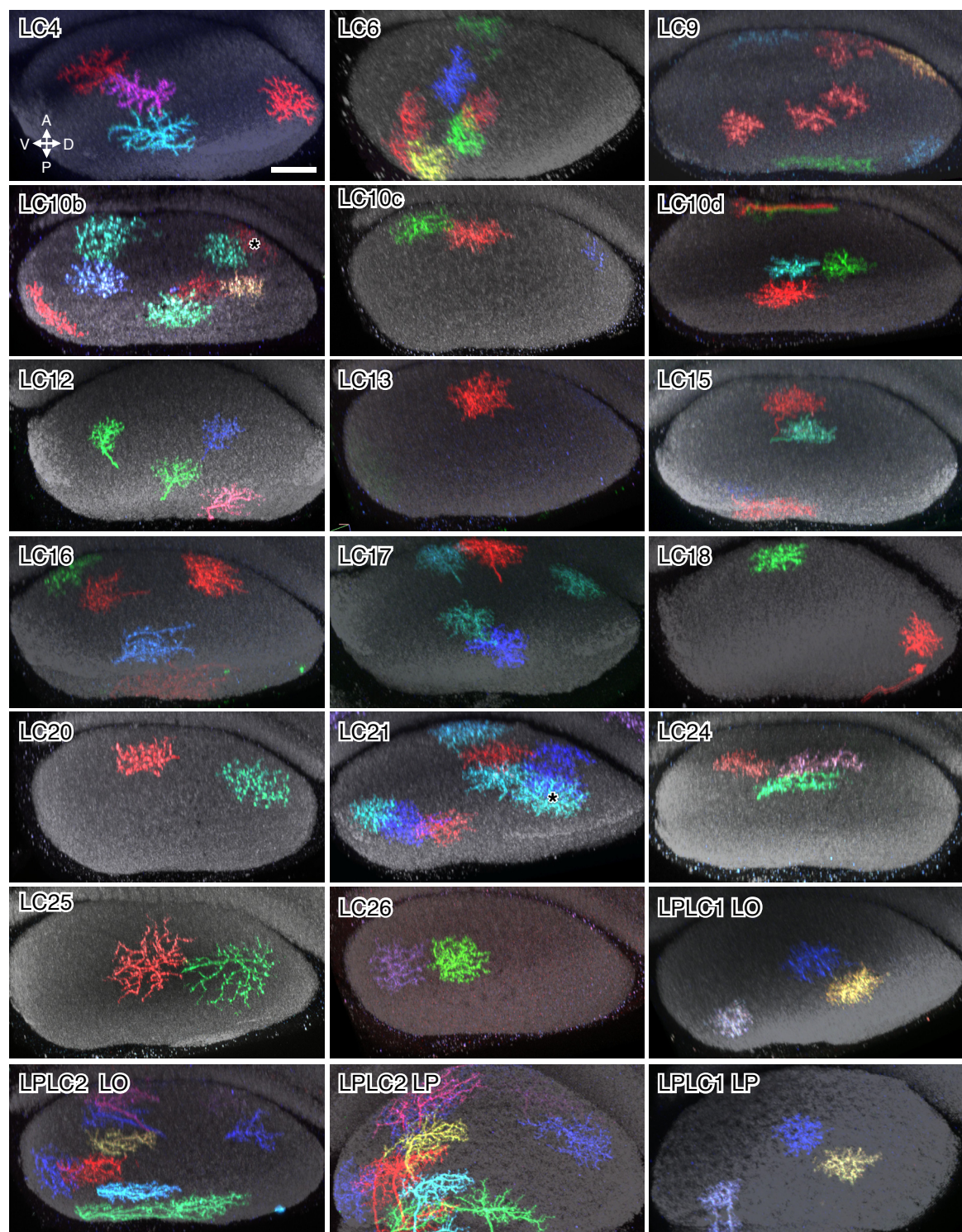


Figure 7

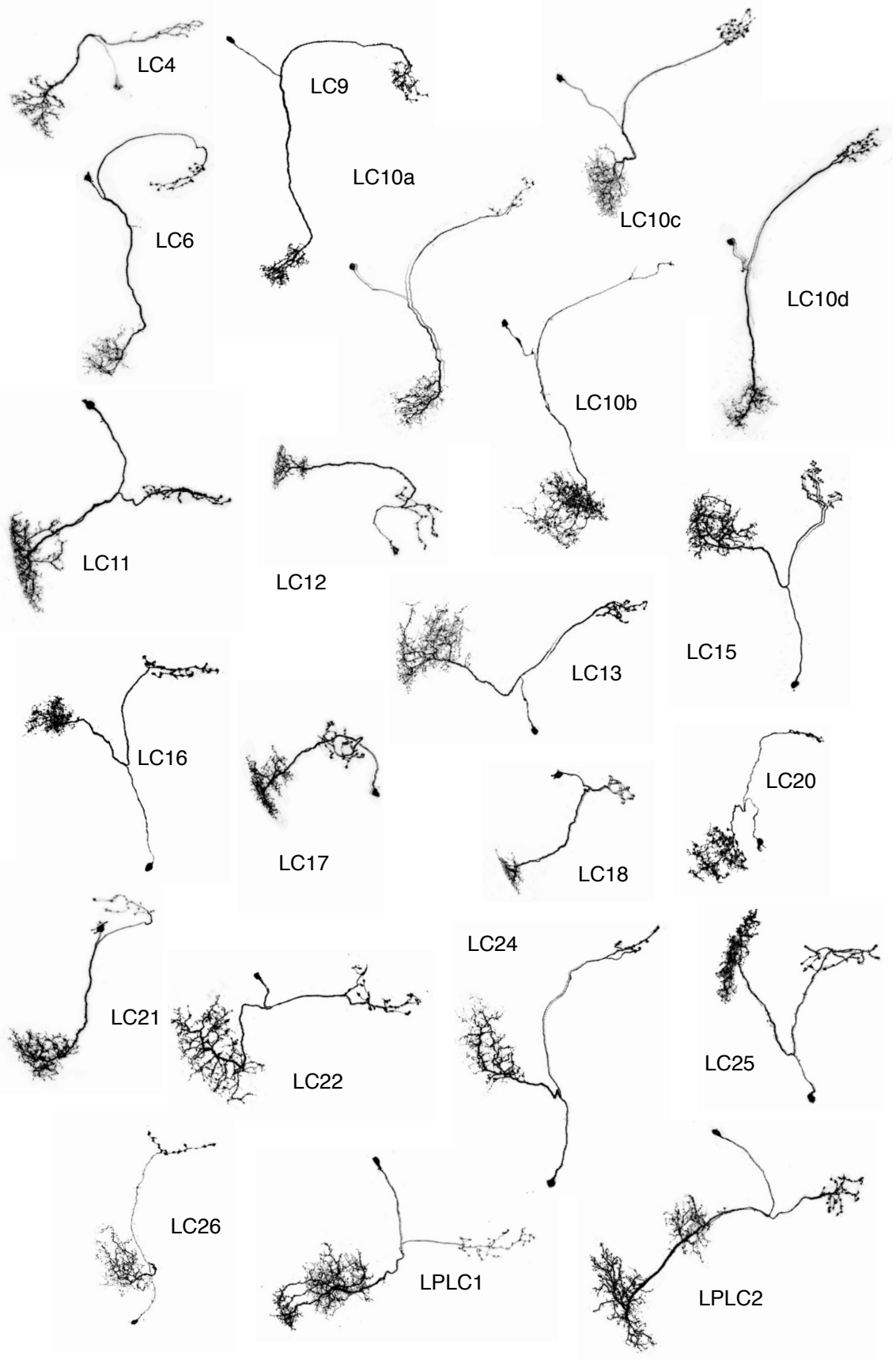


Figure 7 - figure supplement 1

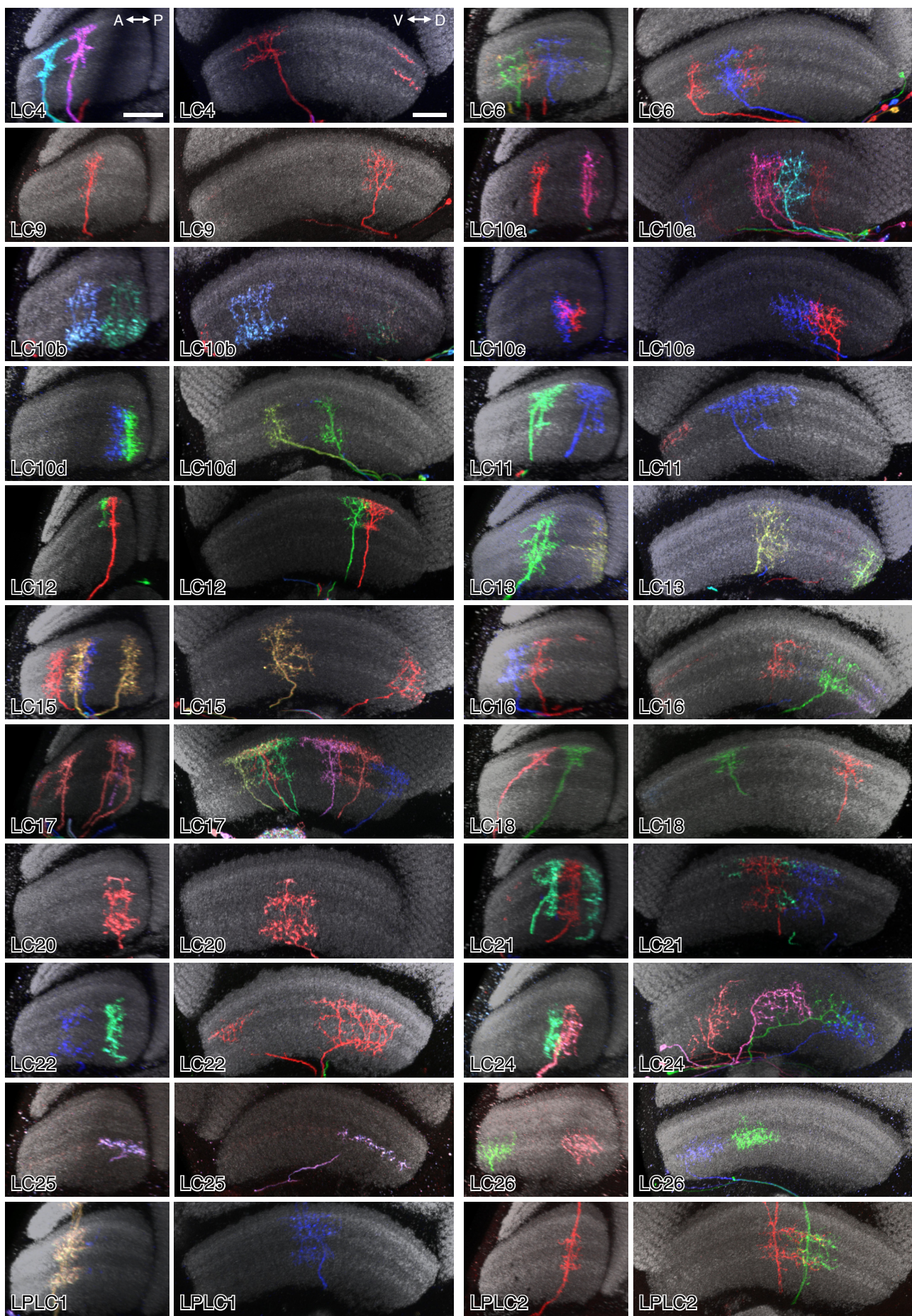


Figure 7- figure supplement 2

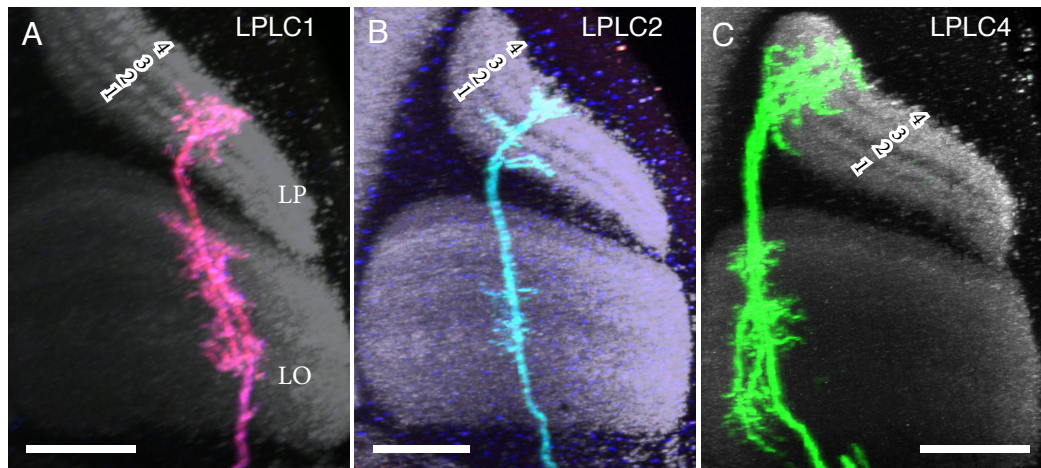


Figure 8

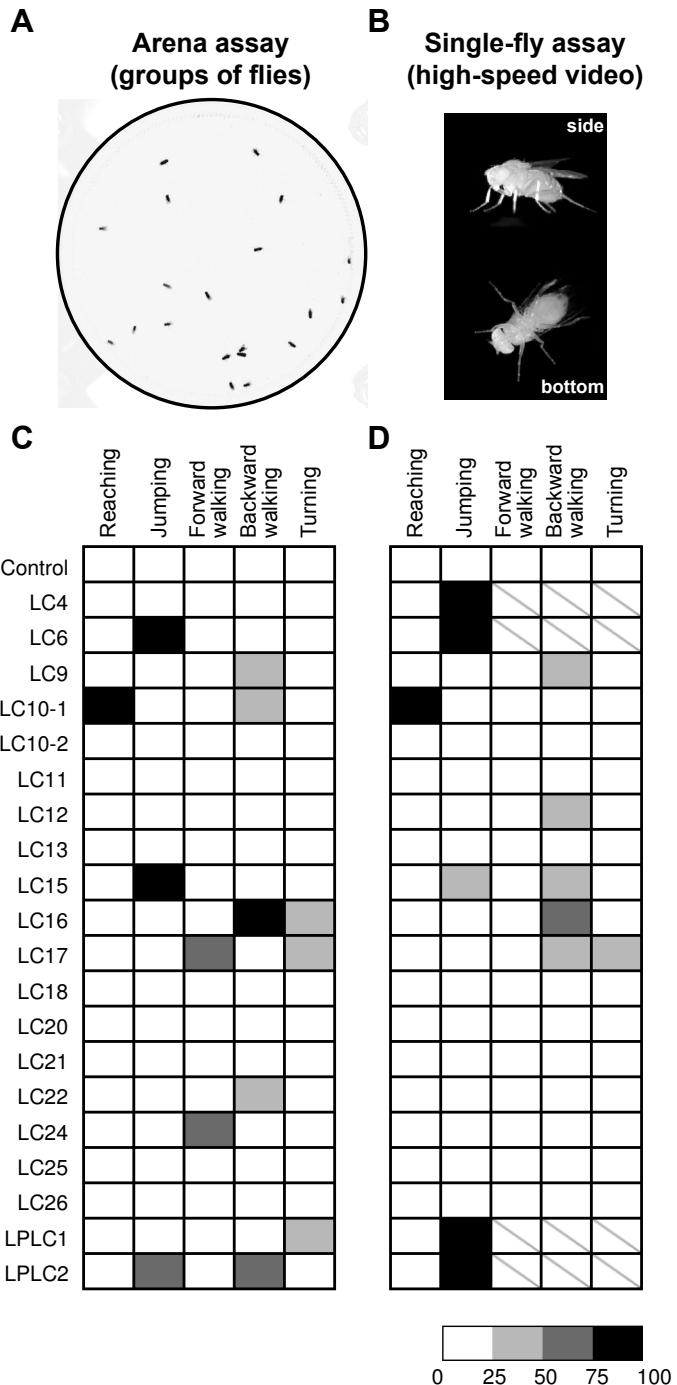


Figure 8 - figure supplement 1

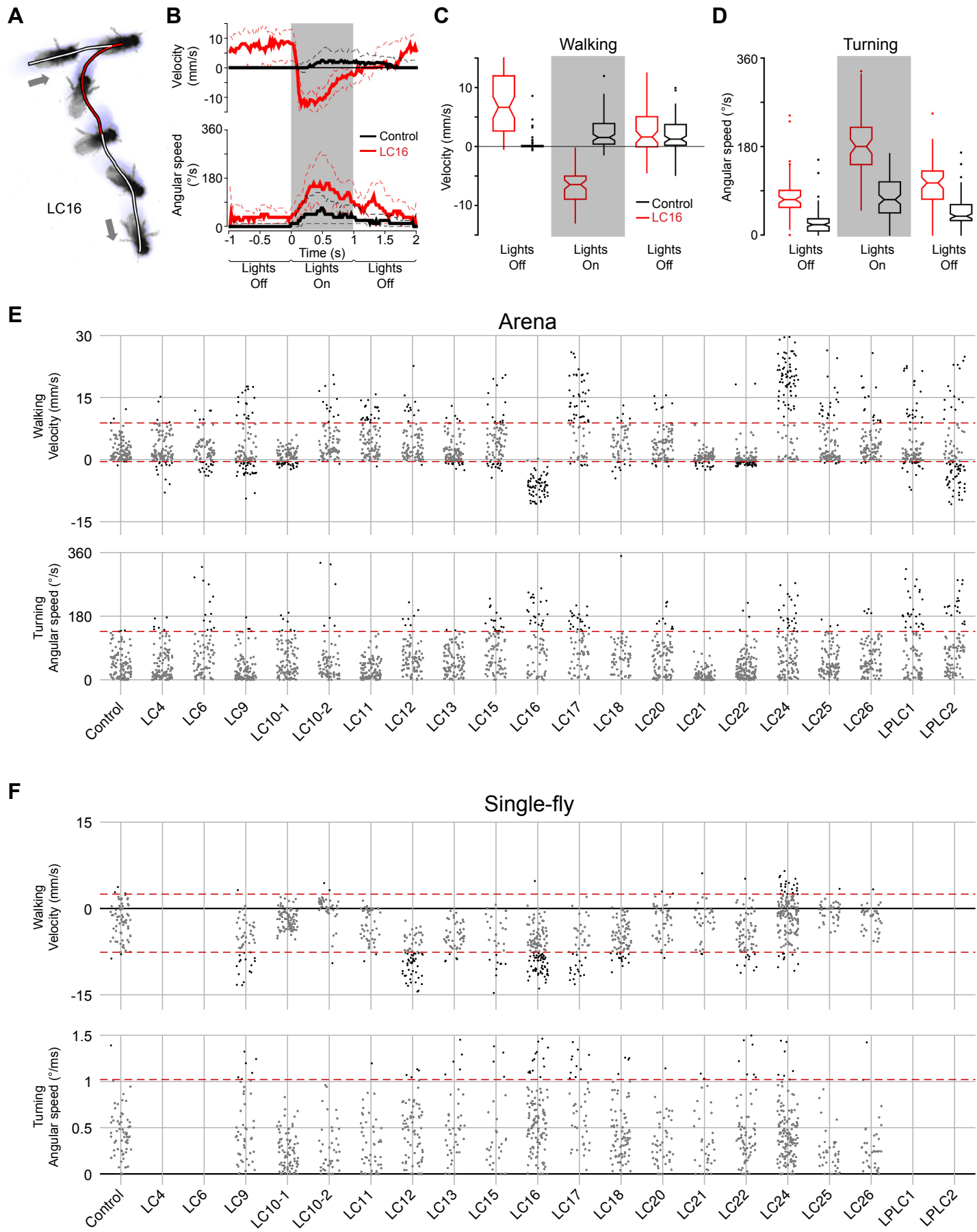


Figure 8 - figure supplement 2

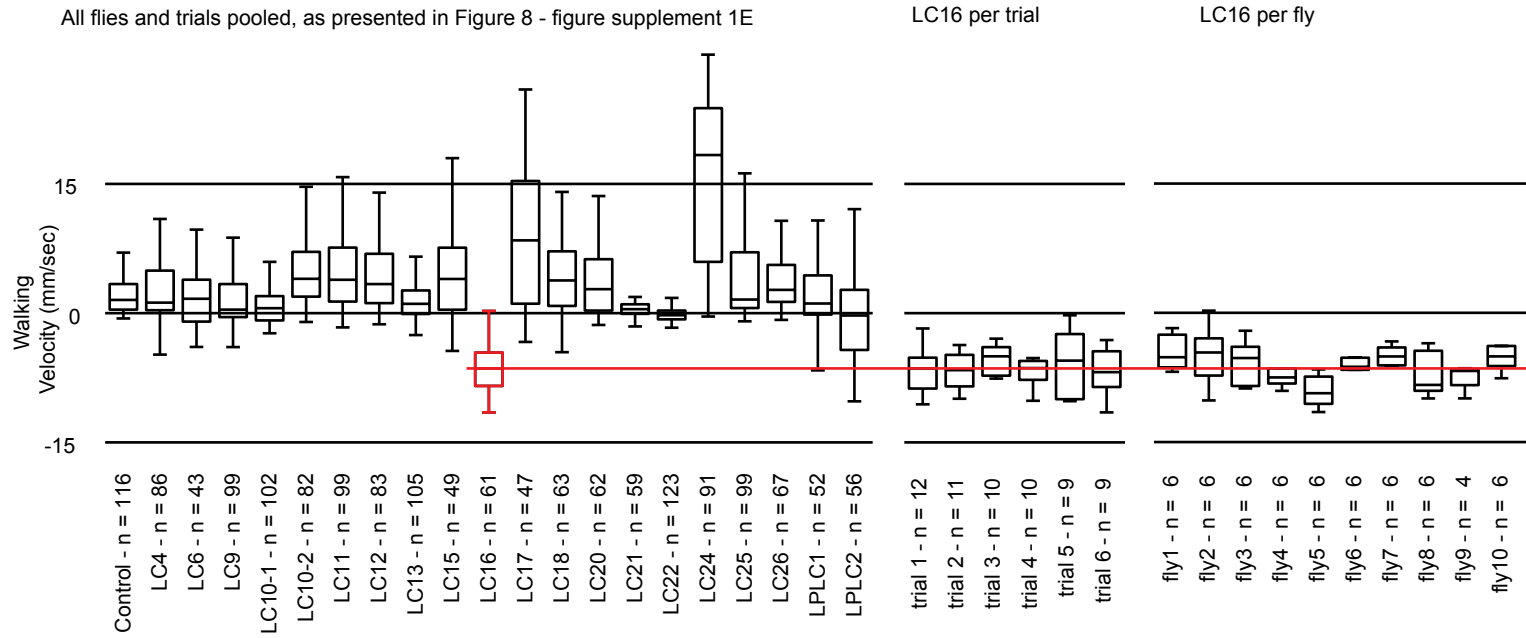


Figure 9

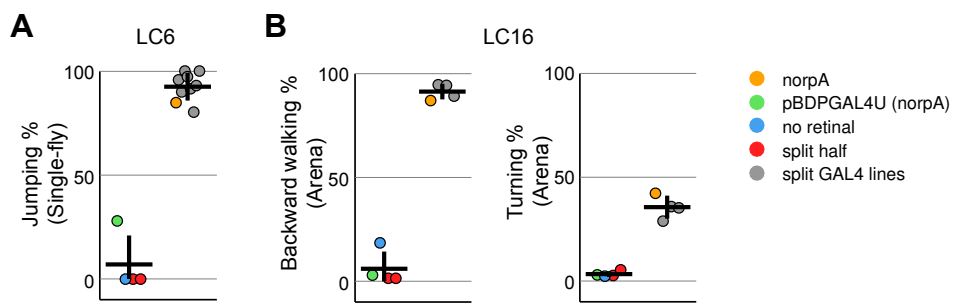


Figure 9 - figure supplement 1

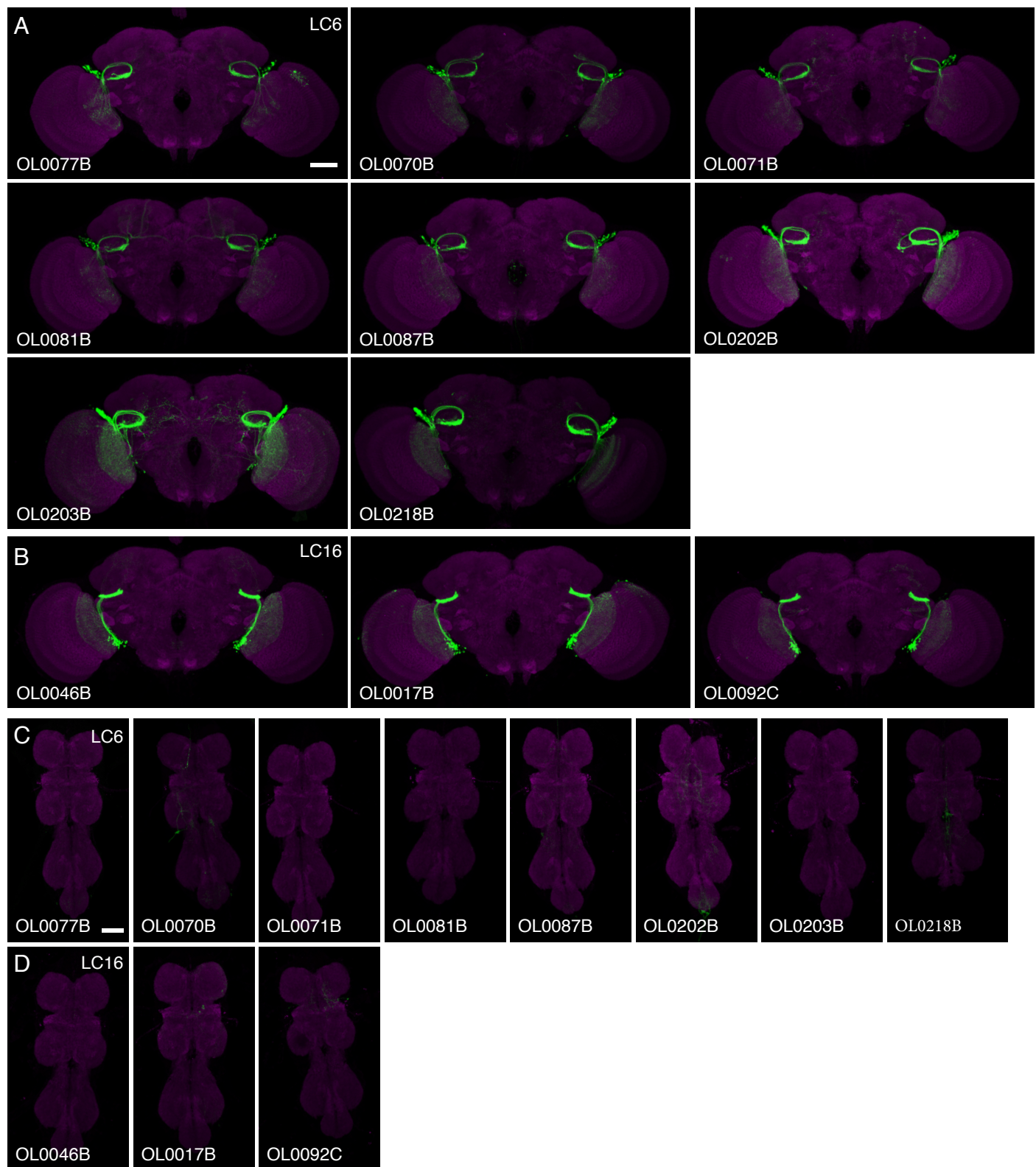


Figure 9 – figure supplement 2

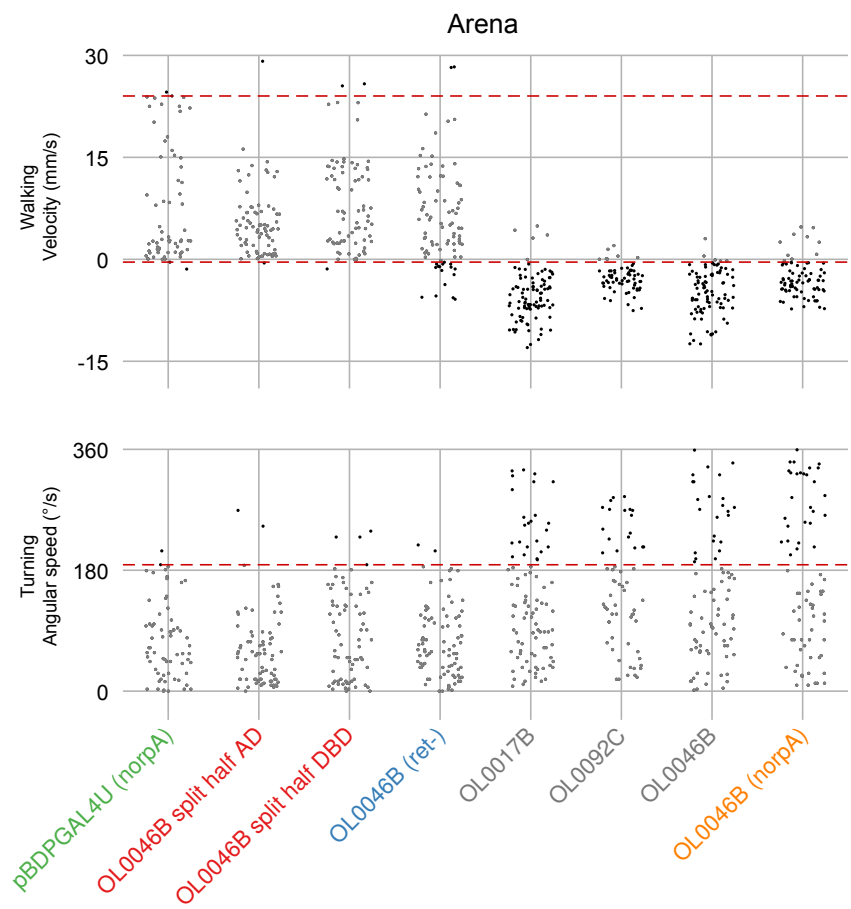


Figure 10

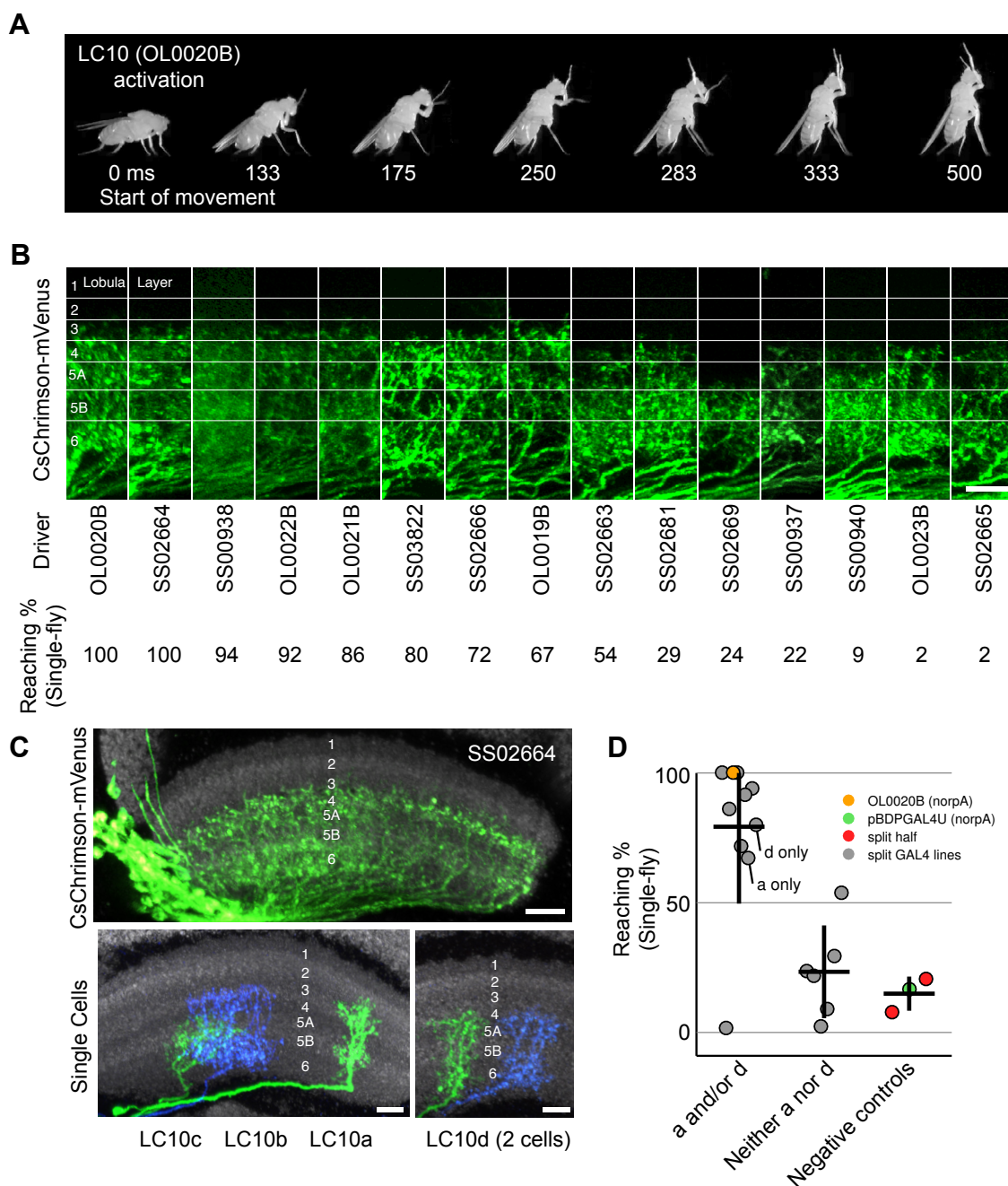


Figure 10 – figure supplement 1

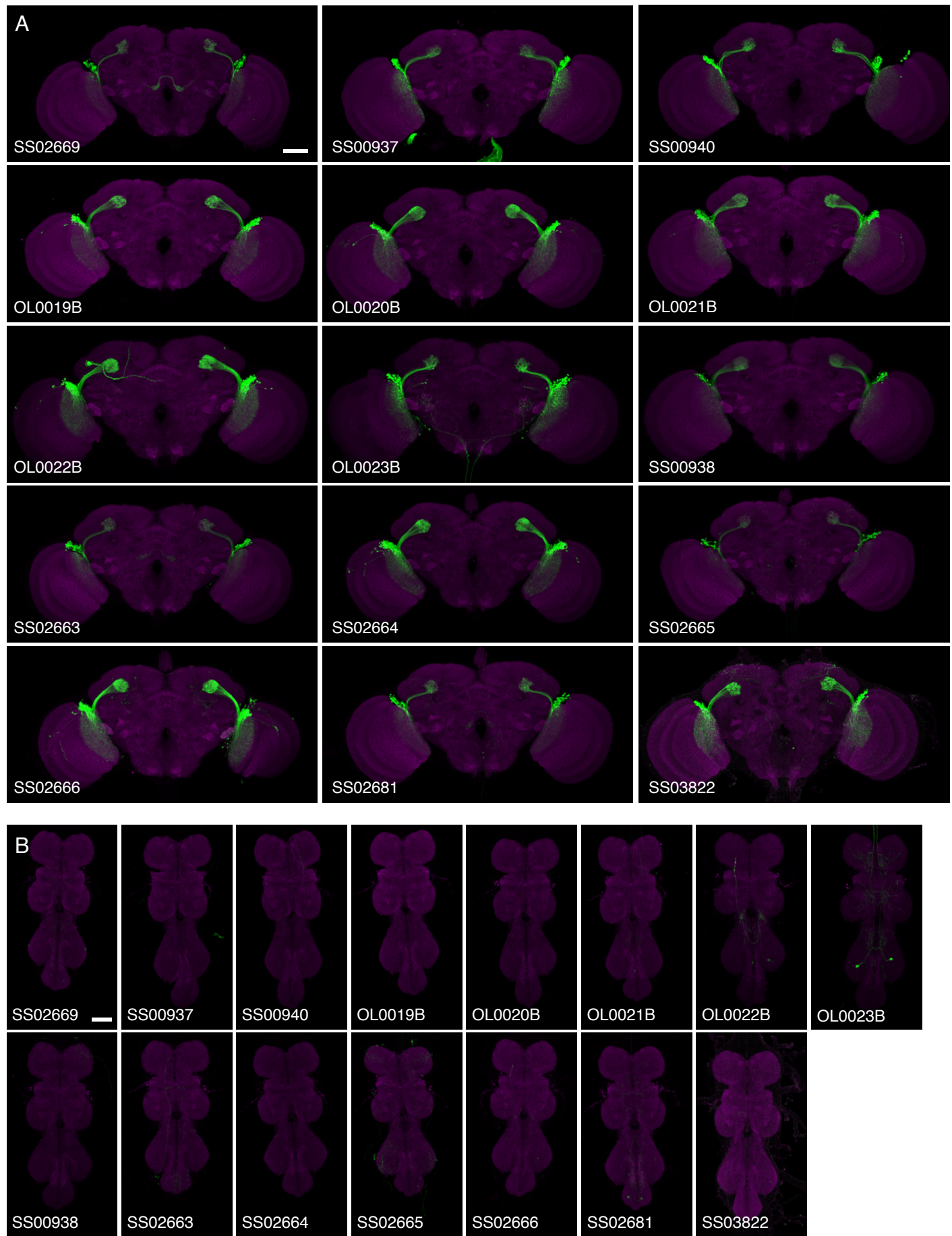
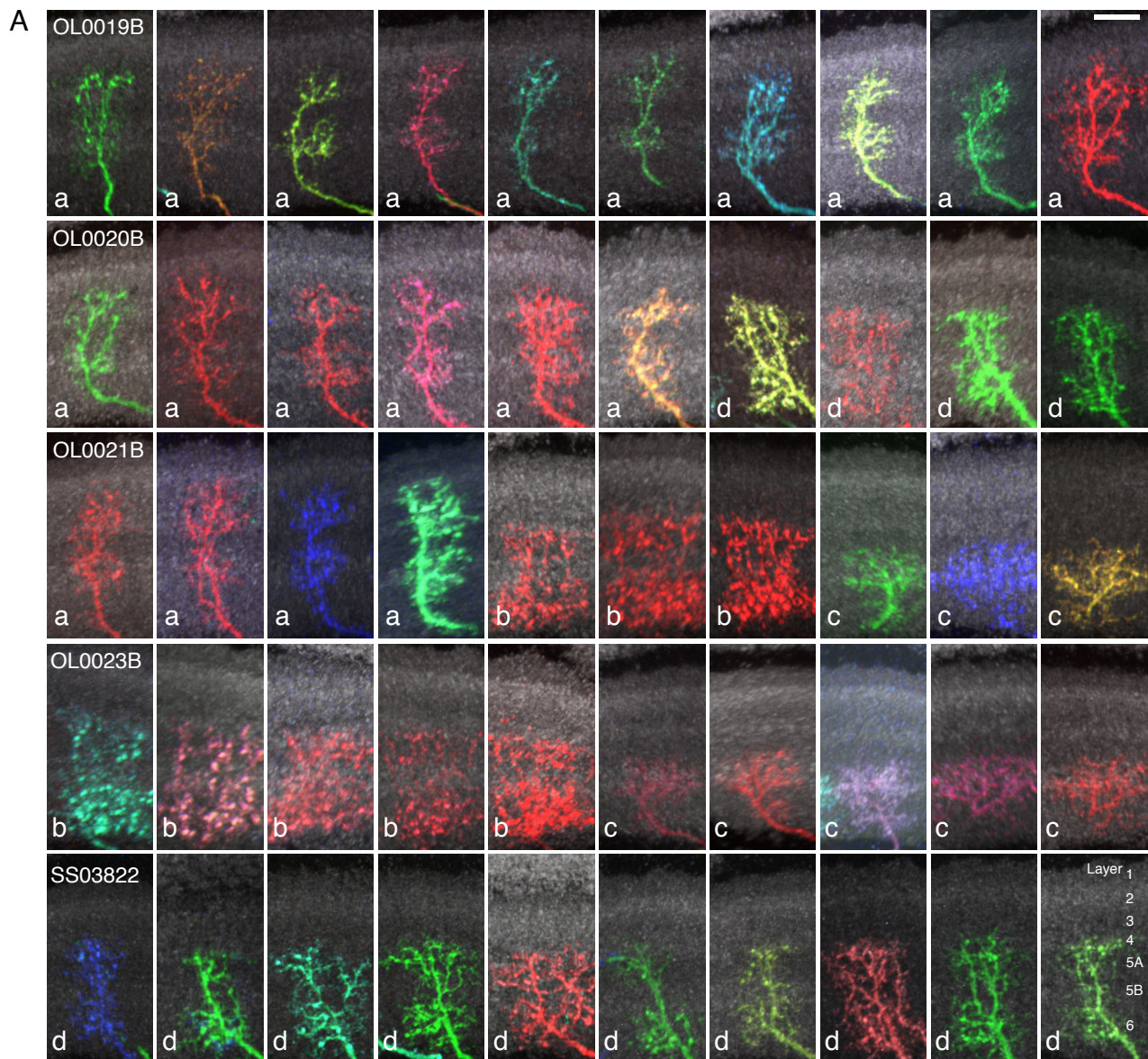


Figure 10 – figure supplement 2



B

Line	Flies	Total cells	LC10a	LC10b	LC10c	LC10d	Summary
OL0019B	10	120	120	0	0	0	a
OL0020B	5	81	44	0	0	37	a,d
OL0021B	3	62	26	17	9	0	a,b,c
OL0022B	5	49	30	0	0	19	a,d
OL0023B	8	77	0	42	35	0	b,c
SS00937	4	38	0	29	9	0	b,c
SS00938	6	47	5	24	8	10	a,b,c,d
SS00940	6	68	1	21	46	0	(a),b,c
SS02663	14	128	0	59	69	0	b,c
SS02664	8	24	9	4	5	6	a,b,c,d
SS02665	7	13	0	4	6	3	b,c,d
SS02666	4	18	9	1	1	7	a,(b),(c),d
SS02669	4	8	0	2	6	0	b,c
SS02681	6	14	0	9	5	0	b,c
SS03822	7	52	0	0	0	52	d

Figure 11

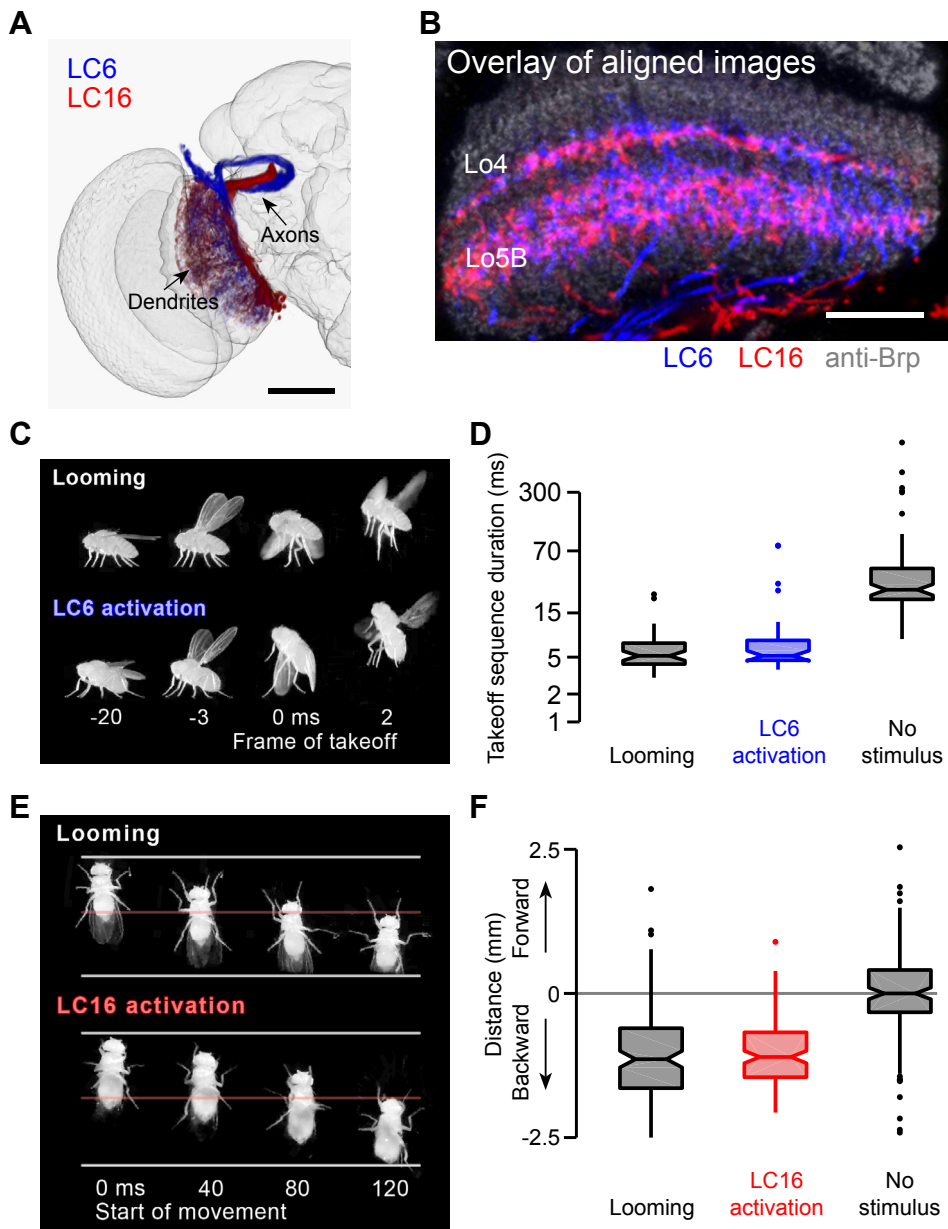


Figure 11-figure supplement 1

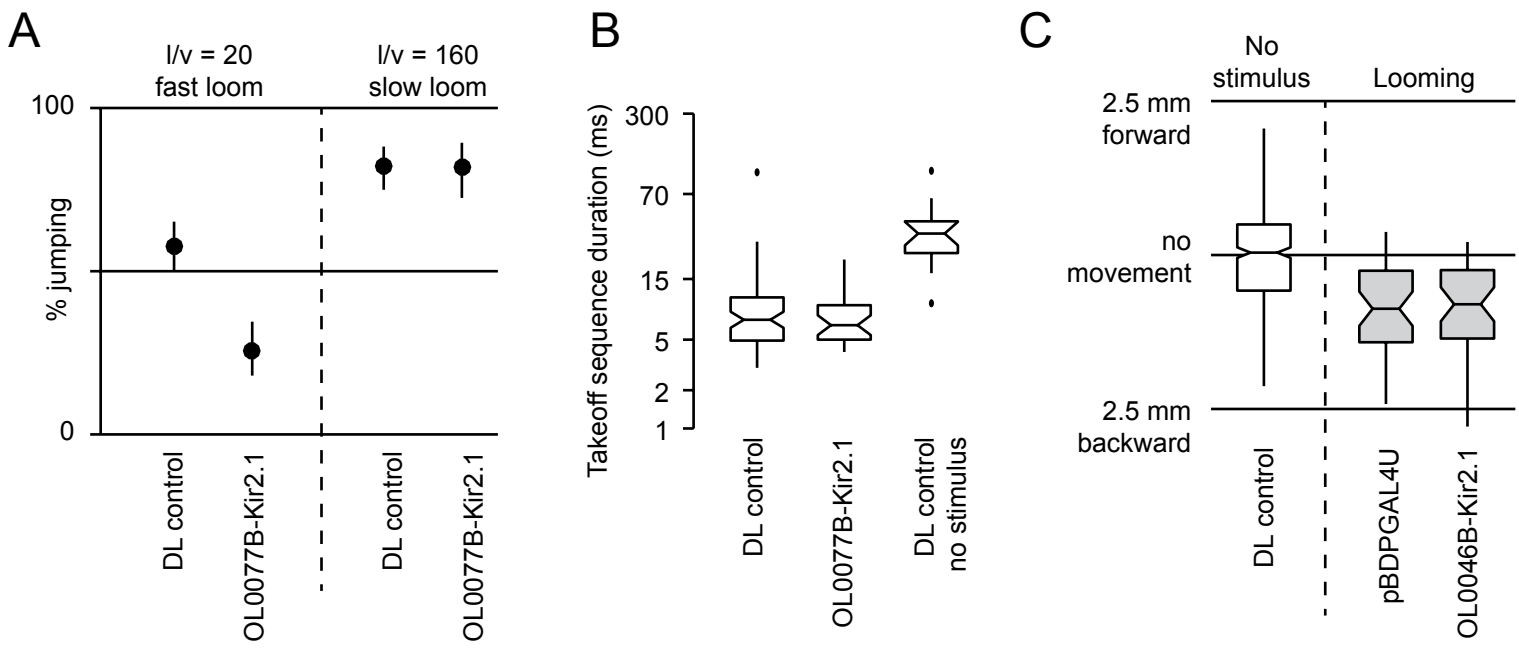


Figure 12

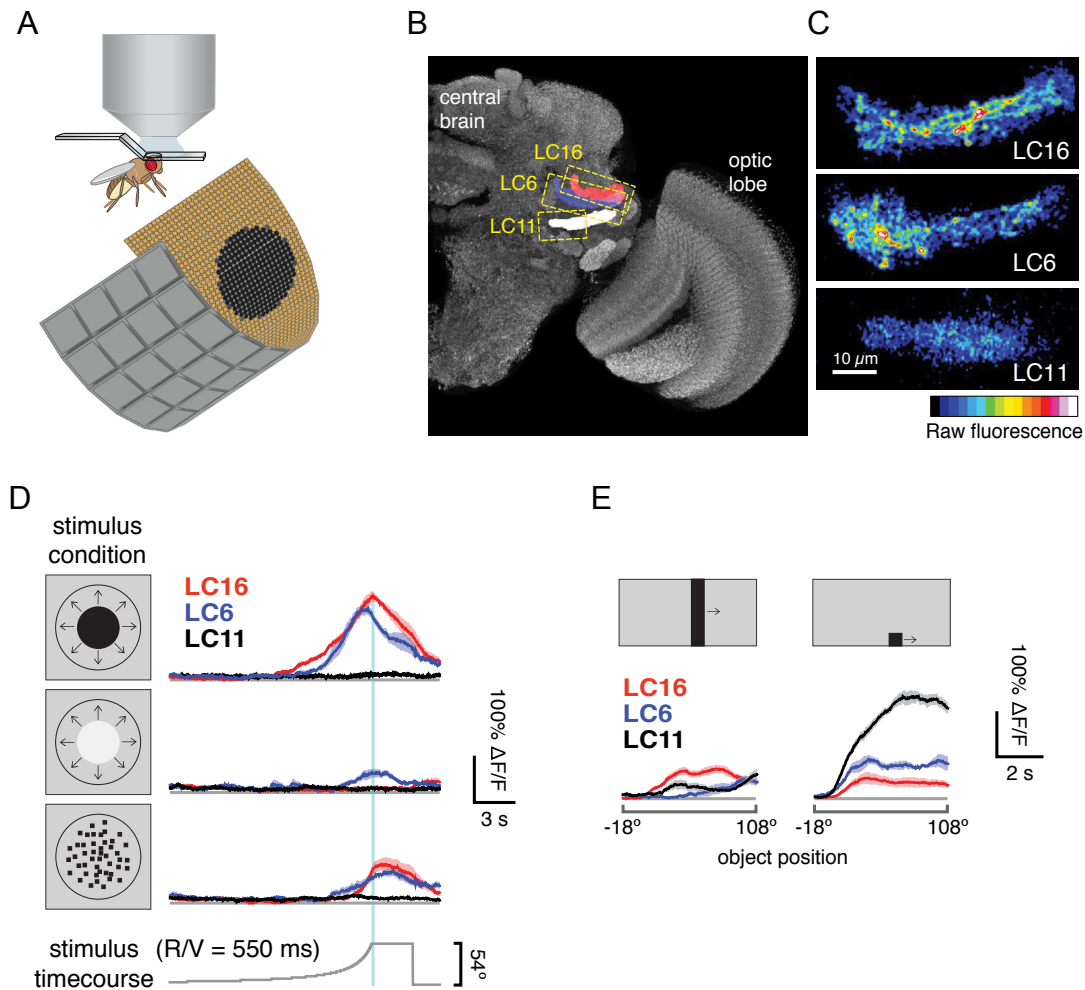


Figure 12 – figure supplement 1

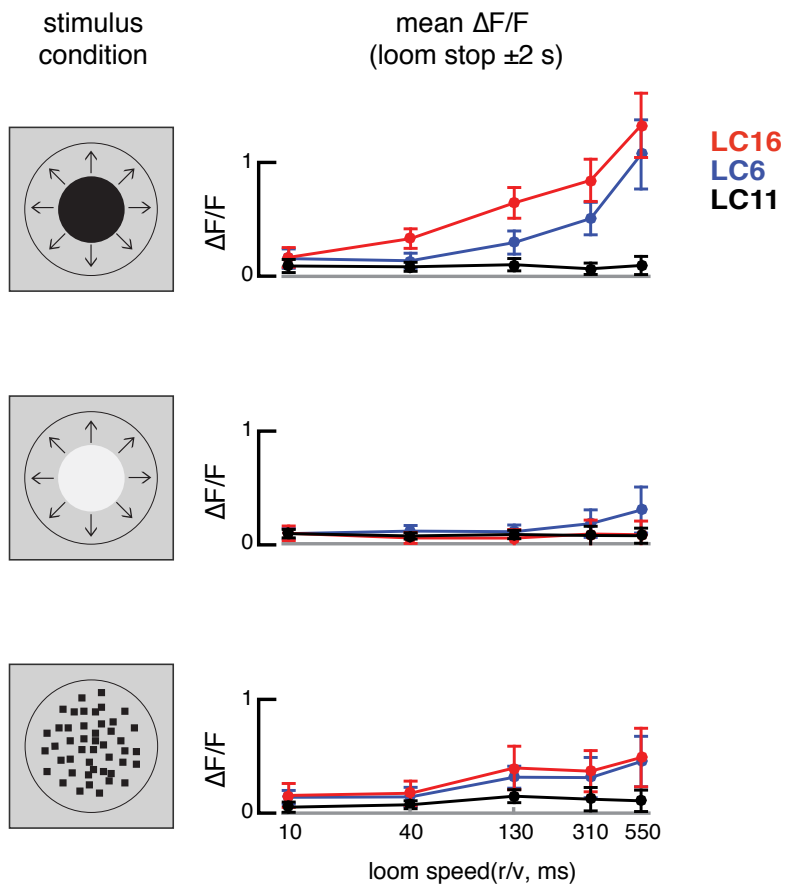


Figure 13

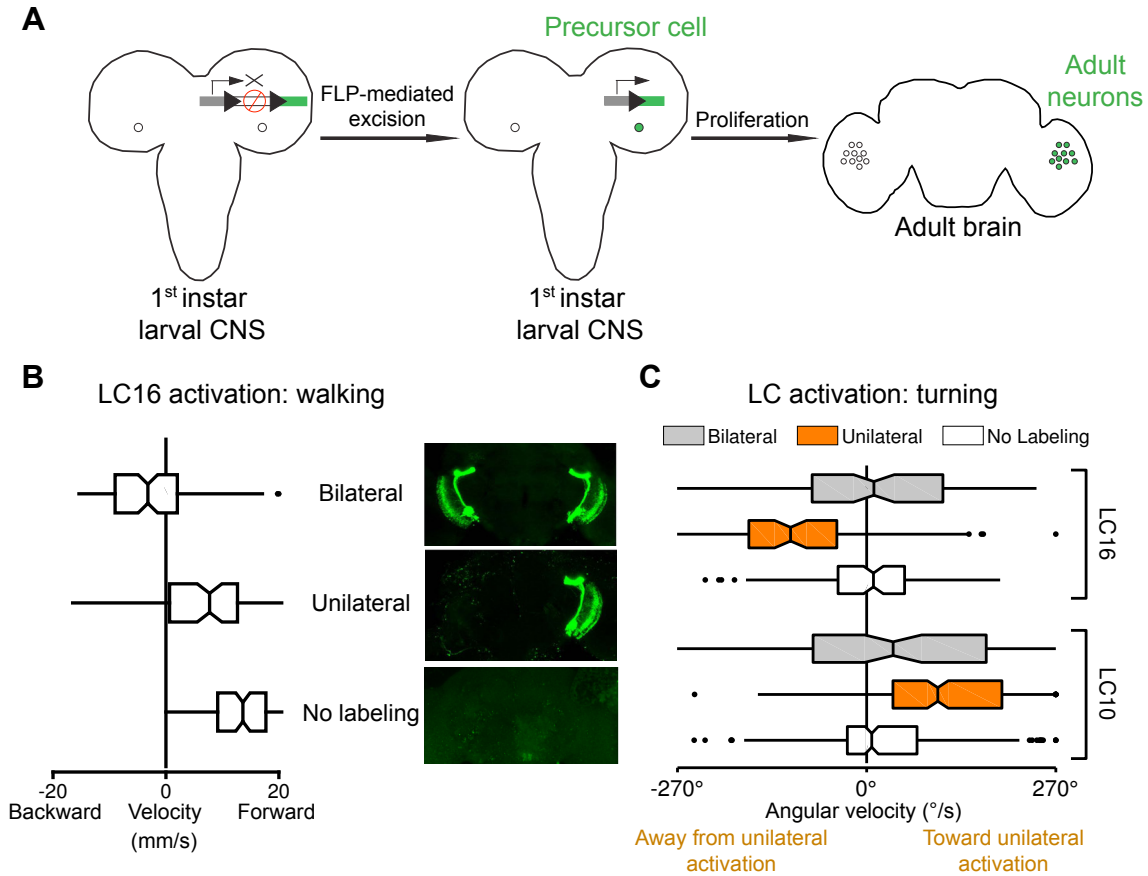


Figure 13 – figure supplement 1

